
Doctoral

Science

2010-11

Development of Acrylamide Based Photopolymer for Full Colour Display Holography

Chakrapani Meka
Technological University Dublin

Follow this and additional works at: <https://arrow.tudublin.ie/sciendoc>



Part of the [Engineering Physics Commons](#), and the [Optics Commons](#)

Recommended Citation

Meka, C. (2010). *Development of Acrylamide Based Photopolymer for Full Colour Display Holography*. Doctoral Thesis. Technological University Dublin. doi:10.21427/D7XK5B

This Theses, Ph.D is brought to you for free and open access by the Science at ARROW@TU Dublin. It has been accepted for inclusion in Doctoral by an authorized administrator of ARROW@TU Dublin. For more information, please contact arrow.admin@tudublin.ie, aisling.coyne@tudublin.ie, vera.kilshaw@tudublin.ie.

**DEVELOPMENT OF ACRYLAMIDE BASED
PHOTOPOLYMER FOR
FULL COLOUR DISPLAY HOLOGRAPHY**

Chakrapani Meka M.Sc (Tech)

**A thesis submitted for the degree of Doctor of Philosophy to
the Dublin Institute of Technology**



Supervisors

**Dr.R.Jallapuram, Prof. V.Toal, Dr. I. Naydenova,
Dr. S. Martin**

**Center for Industrial and Engineering Optics
School of Physics
Dublin Institute of Technology
Kevin Street, Dublin 8, Ireland**

ABSTRACT

Holography is a firmly established discipline that can be used as a tool for scientific and engineering studies and as a display medium as well. Until now both silver halide photographic emulsions (SHPE) and dichromated gelatine (DCG) have been the most common materials used for high efficiency full colour reflection hologram recording. However, these materials require wet chemical processing for developing the holograms which is laborious and costly from the point of view of commercial applications.

Self-developing photopolymers such as acrylamide based photopolymer (ABP) which do not require development are the ideal choice for real-time recording and reconstruction of holograms. This thesis reports on the development of an acrylamide based photopolymer system for full colour reflection holographic display.

Firstly ABP was dye sensitised separately at 633 nm and 473 nm using methylene-blue and acriflavine respectively to record holographic reflection gratings and the corresponding diffraction efficiencies were measured. Following this, the ABP material which had already been sensitised at 532 nm at the IEO centre by using erythrosine B as a dye, a panchromatic ABP was developed at IEO sensitised at all three selected primary wavelengths which were available, namely 633 nm, 473 nm and 532 nm. The Bidirectional Scattering Distribution Function (BSDF) was measured for the ABP and scattering obtained was relatively low compared with that of air and glass in the visible region.

Reflection holographic gratings were recorded at 633 nm, 532 nm, and 473 nm wavelengths to evaluate the diffraction efficiencies at spatial frequencies of 4200 lines/mm, 5000 lines/mm and 5700 lines/mm respectively. An optical setup was established to record multicolour holograms by combining three selected laser beams (at 633 nm, 532 nm, and 473 nm). Further multicolour reflection holographic gratings were recorded using a combined single RGB beam so that all wavelengths illuminated the same spot. Spectral characterisation was carried out on the multicolour reflection holographic gratings and the Bragg peaks of the diffracted beam were monitored and compared with the recording wavelengths to reveal the shifts which were considered due to the dimensional changes inside the photopolymer. These spectral shifts in the photopolymer response were minimised by using zeolite nanoparticles (Si-MFI 30nm).

Reflection holograms of objects were successfully recorded at all three primary wavelengths, and also using a combined RGB beam. The results provided a strong confirmation that this acrylamide based photopolymer can be used as a panchromatic recording material and can be employed in future commercial holographic applications.

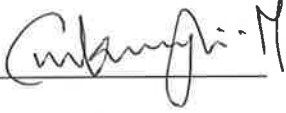
Declaration

I certify that this thesis which I now submit for examination for the award of Doctor of Philosophy, is entirely my own work and has not been taken from the work of others save and to the extent that such work has been cited and acknowledged within the text of my work.

This thesis was prepared according to the regulations for postgraduate study by research of the Dublin Institute of Technology and has not been submitted in whole or in part for an award in any other Institute or University.

The work reported on in this thesis conforms to the principles and requirements of the Institute's guidelines for ethics in research.

The Institute has permission to keep, to lend or to copy this thesis in whole or in part, on condition that any such use of the material of the thesis be duly acknowledged.

Signature 
Candidate

Date 19/11/2010

ACKNOWLEDGMENTS

First of all I would like to thank Prof. Vincent Toal for giving me an opportunity to do my PhD at the CIEO. I am very thankful to all my supervisors Dr. Raghavendra Jallapuram, Prof. Vincent Toal, Dr. Izabela Naydenova and Dr. Suzanne Martin for their guidance, valuable suggestions and encouragement throughout my PhD work.

I would like to thank Prof. V. Sainov, Asst. Prof. E. Stoykova (Bulgarian Academy of Sciences, Bulgaria) for inviting me to their lab and giving me an opportunity to learn more about recording holograms in silver halide materials. I would like to thank Dr. Lian Nedelchev for his company and hospitality during my stay in Bulgaria.

I would like to thank Prof. Hugh Byrne, Dr. Mary Mc Namara, FOCAS facilities, HEA Technology Sector, Strand 1 and Dublin Institute of Technology for funding the project and graduate studies.

I would like to thank Prof. S. Mintova (University of Haute Alsace, France) for providing Si-MFI zeolite nanoparticles for my experiments.

I would like to thank Dennis Bade, Elsa Leite for their help with LabView programs and scattering measurements respectively.

Finally I am thankful to all my group members Dr. Mihaylova, Dr. Svetanka, Dr. Pavani, Elsa, Dennis, Mohesh, Mahmood, Viswanath for their continuous help and support throughout my project.

Thanks to Joe Keogh, Andrew and Anne for technical support and all the people with whom I shared my office space.

I would like thank Pavani for taking special care right from day I arrived to Dublin. Thank you so much Pavani. Viswanath and Deepa, thank you for your consistent company during the Tea time and for all the discussion and gossips we enjoyed...

thanks to you guys...😊😊😊 ... thanks to the small Indian Focas thotti gang....for making my stay so lively ... and Deepa thank you for all the week end get- together.

Last but not least I would like to thank my parents, brother, wife and all my family members for the encouragement and support throughout my PhD.

Table of Contents

CHAPTER 1	1
INTRODUCTION	1
1.1 Genesis of Holography	2
1.2 Brief history of colour holography	8
1.3 Motivation for the Project.....	10
1.4 Objectives	10
1.5 Research summary	11
1.6 Thesis Outline	13
References.....	14
CHAPTER 2	17
COLOUR HOLOGAPHY	17
2.1 Introduction to colour holography	17
2.2 Types of holograms.....	18
2.2.1. Transmission holograms	18
2.2.2 Reflection holograms	19
2.2.3 Rainbow holograms	21
2.2.4 Other types of holograms.....	22
2.3 Coupled wave theory of volume holograms	24
2.4 Choice of laser wavelength.....	35
2.5 Recording set-up	38
2.6 Recording material.....	40

References.....	46
CHAPTER 3	50
ACRYLAMIDE BASED PHOTOPOLYMER: RECORDING MECHANISM AND MODELS.....	50
3.1 Introduction.....	50
3.2 Background.....	51
3.3 Recording mechanism.....	54
3.3.1 Photo polymerization	54
3.3.2 Hologram formation mechanism (refractive index modulation)	57
3.3.3 Diffusion model	60
3.4 Scattering in the material	68
References.....	72
CHAPTER 4.....	78
HOLOGRAPHIC RECORDING AT 633 NM IN AN ACRYLAMIDE BASED PHOTOPOLYMER.....	78
4.1 Introduction.....	78
4.2 Sample preparation	79
4.3 Recording of transmission gratings at 633 nm	80
4.4 Reflection gratings recorded at 633 nm	82
4.5 Doping with nanoparticles	86
4.6 Spectral characterisation	89
4.7 Reflection holograms	90
4.8 Conclusion	91

References	93
CHAPTER 5	95
HOLOGRAPHIC RECORDING AT 473 NM IN AN ACRYLAMIDE BASED PHOTOPOLYMER.....	95
5.1 Introduction.....	95
5.2 Recording transmission gratings at 473 nm.....	95
5.3 Reflection gratings at 473 nm	100
5.4 Optimizing dye concentration at 473 nm.....	104
5.5 Doping with nanoparticles	106
5.6 Spectral characterisation	107
5.7 Reflection holograms	108
5.8 Conclusion	109
CHAPTER 6.....	111
HOLOGRAPHIC RECORDING IN PANCHROMATIC ACRYLAMIDE BASED PHOTOPOLYMER	111
6.1 Introduction.....	111
6.2 Recording material and experimental setup.....	112
6.3 Recording reflection gratings.....	114
6.4 Optimization of dye composition.....	115
6.4.1 Recording at wavelength 633nm	116
6.4.2 Recording at wavelength 532nm	118
6.4.3 Recording at wavelength 473 nm	120
6.5 Reflection gratings in nanoparticle doped material	121

6.6 Spectral characterisation	125
6.6.1 Spectral characterization of reflection gratings recorded at 633 nm	125
6.8.2 Spectral characterization of reflection gratings recorded at 532nm	127
6.8.3 Spectral characterization of reflection gratings recorded at 473nm	128
6.8.4 Spectral characterization of multicolour reflection gratings.....	129
6.7 Transmission holograms	130
6.8 Reflection holograms	132
6.9 Conclusion	134
CHAPTER 7	136
CONCLUSION	136

List of Figures

Figure 1.1 Gabor holography setup.....	3
Figure 1.2 Formation of the twin images in in-line hologram.....	4
Figure 1.3 Off axis holography setup.....	6
Figure 1.4 Reconstruction of off axis hologram.....	7
Figure 2.1 Transmission hologram recording setup.....	18
Figure 2.2 Reflection hologram recording setup.....	19
Figure 2.3 Single beam Denisyuk recording setup.....	20
Figure 2.4 Two-step rainbow holography.....	22
Figure 2.5 Recording geometry for recording 360° hologram.....	23
Figure 2.6 Recording geometry for edge lit hologram.....	24
Figure 2.7 Basic geometry of thick holographic grating with slanted fringes.....	27
Figure 2.8 Transmission holograms-angular and wavelength selectivity of a phase grating showing the normalized diffraction efficiency (η/η_0) as a function of the parameter ζ	31
Figure 2.9 Volume reflection gratings.....	33
Figure 2.10 Reflection holograms-shows the angular and wavelength sensitivity of a lossless dielectric grating with the normalised efficiency η/η_0 as a function of ξ_r	34
Figure 2.11 CIE chromaticity diagram.....	35
Figure 2.12 Multicolour hologram recording set up.....	39
Figure 3.1 Grating formation in a photopolymer.....	58
Figure 3.2 Scatterometer set up to measure BSDF.....	68
Figure 3.3 BSDF data for the air, glass and uniformly polymerised layer measured at 473nm.....	69
Figure 3.4 Shows the BSDF of the uniformly polymerised photopolymer layer measured at 633nm and 473nm.....	70

Figure 4.1 Absorption spectrum of dry photopolymer layer sensitized to record at 633 nm.....	80
Figure 4.2 Experimental setup for recording transmission gratings.....	81
Figure 4.3 Diffraction efficiency as a function of exposure time for transmission gratings recorded at 1000 lines/mm and 2000 lines/mm spatial frequency for 633 nm.....	82
Figure 4.4 Experimental setup for recording reflection grating.....	83
Figure 4.5 Recording geometry (cross section view) of reflection gratings.....	83
Figure 4.6 Diffraction efficiency (%) of reflection gratings (4200 lines/mm) as a function of exposure time (sec) for layer thickness of 60 μm at two intensities (3 mW/cm^2 and 1.5 mW/cm^2).....	85
Figure 4.7 Diffraction efficiency (%) of reflection gratings (4200 lines/mm) as a function of exposure time (sec) for a of 30 μm thick layer at two recording intensities (3 mW/cm^2 and 1.5 mW/cm^2).....	85
Figure 4.8 Schematic representation of Si-MFI nanoparticle.....	87
Figure 4.9 Comparison of diffraction efficiency growth profiles for the reflection gratings recorded at 633nm for four different concentrations of zeolite nanoparticles (Si-MFI) using	88
Figure 4.10 Experimental setup used for spectral characterisation of the reflection gratings.....	89
Figure 4.11 Bragg peak wavelengths as function of nanoparticle concentration for the gratings recorded at 633nm wavelength.....	90
Figure 4.12 Photographs of white light holographic reconstructions after recording with a red laser at 633nm.....	91
Figure 5.1 Absorption spectrum of dry photopolymer layer sensitized with acriflavine	96
Figure 5.2 Experimental setup for recording transmission grating and to measure the diffraction efficiency in real time.....	97
Figure 5.3 Diffraction efficiency (%) of transmission gratings (2000lines/mm) as a function of exposure time (sec) recorded at 473 nm for layer thickness 15 μm at three different intensities (1.5 mW/cm^2 , 3 mW/cm^2 and 6 mW/cm^2).....	98
Figure 5.4 Diffraction efficiency (%) of transmission gratings (2000 lines/mm) as a function of exposure time (sec) recorded at 473 nm, for layer thickness 30 μm at three intensities (1.5 mW/cm^2 , 3 mW/cm^2 and 6 mW/cm^2).....	98

Figure 5.5 Diffraction efficiency (%) of transmission gratings (2000 lines/mm) as a function of exposure time (sec) recorded at 473 nm, for layer thickness 60µm at three intensities (1.5 mW/cm ² , 3 mW/cm ² and 6 mW/cm ²).....	99
Figure 5.6 Diffraction efficiency (%) of reflection gratings (5700 lines/mm) as a function of exposure time (sec) recorded at 473nm for layer thickness of 30 µm at two intensities (3 mW/cm ² and 6 mW/cm ²).....	101
Figure 5.7 Diffraction efficiency (%) of reflection gratings (5700 lines/mm) as a function of exposure time (sec) recorded at 473 nm for a layer thickness 60 µm at two intensities (3 mW/cm ² and 6 mW/cm ²).....	102
Figure 5.8 Diffraction efficiency (%) of reflection gratings (5700 lines/mm) as a function of exposure time (sec) recorded at 473 nm for a layer thickness 15 µm at 6 mW/cm ² intensity.....	103
Figure 5.9 Absorption spectra of four different concentrations of the acriflavine dye.....	105
Figure 5.10 Comparison of diffraction efficiency growth profiles for the gratings recorded (473 nm) with different concentrations of the acriflavine dye.....	105
Figure 5.11 Diffraction efficiency growth profiles for the reflection gratings recorded at 473nm for four different concentrations of Si-MFI zeolite nanoparticles.....	107
Figure 5.12 Shows the wavelength of the Bragg peak for a recorded grating at 473 nm as a function of concentration of nanoparticles in the photopolymer.....	108
Figure 5.13 Photograph of white light holographic reconstructions recorded with a blue laser at 473nm	109
Figure 6.1 Normalised absorption spectrum of panchromatic acrylamide based photopolymer recording material.....	112
Figure 6.2 Experimental setup for recording multicolour reflection holographic grating.....	113
Figure 6.3 Diffraction efficiency (%) as a function of time of exposure for the reflection gratings recorded at red, green and blue wavelengths in a 60 µm thick photopolymer layer.....	114
Figure 6.4 Absorption spectra of panchromatic acrylamide based photopolymer recording material for two different thicknesses (30 µm and 60 µm).....	116
Figure 6.5 Diffraction efficiency of reflection gratings recorded at 4200 lines/mm spatial frequency as a function of exposure time (sec) in a 30 µm layers for 3 mW/cm ² and 1.5 mW/cm ² recording intensities) at 633nm.....	117

Figure 6.6 Diffraction efficiency of reflection gratings recorded at 4200 lines/mm spatial frequency as a function of exposure time (sec) in a 60 μm layers for 3 mW/cm^2 and 1.5 mW/cm^2 recording intensities at 633nm.....	117
Figure 6.7 Diffraction efficiency (%) of reflection gratings recorded in 30 μm layers (5000 lines/mm) as a function of exposure time (sec) for 3 mW/cm^2 and 1.5 mW/cm^2 recording intensities at 532 nm.....	119
Figure 6.8 Diffraction efficiencies (%) of reflection gratings (5000 lines/mm) recorded in 60 μm layers as a function of exposure of time (sec) for 3 mW/cm^2 and 1.5 mW/cm^2 recording intensities at 532 nm.....	119
Figure 6.9 Diffraction efficiency (%) of reflection gratings (5700 lines/mm) as a function of exposure time (sec) recorded in 30 μm layers for intensities 3 mW/cm^2 and 6 mW/cm^2 at 473nm	120
Figure 6.10 Diffraction efficiency (%) of reflection gratings (5700 lines/mm) as a function of exposure time (sec) recorded in 60 μm layers for intensities 3 mW/cm^2 and 6 mW/cm^2 at 473 nm.....	121
Figure 6.11 Diffraction efficiency (%) of reflection gratings (4200 lines/mm, $\lambda=633\text{nm}$) as a function of exposure time (sec) recorded in layers of thickness 30 μm at an intensity of 4.5 mW/cm^2	122
Figure 6.12 Diffraction efficiencies (%) of reflection gratings (5000 lines/mm, $\lambda=532\text{nm}$) as a function of exposure time (sec) recorded in layers of thickness 30 μm at an intensity of 4.5 mW/cm^2	123
Figure 6.13 Diffraction efficiency (%) of reflection gratings (5700 lines/mm, $\lambda=473\text{nm}$) as a function of exposure time (sec) recorded in layers of thickness 30 μm at an intensity of 7.5 mW/cm^2	124
Figure 6.14 Bragg spectral selectivity curve of the reflection grating recorded at 633nm in panchromatic photopolymer.....	126
Figure 6.15 Peak wavelength of the Bragg spectral selectivity curve for the gratings recorded at 633nm plotted against nanoparticle concentration in the photopolymer.....	126
Figure 6.16 Bragg spectral selectivity curve of a reflection grating recorded at 532 nm in panchromatic photopolymer.....	127
Figure 6.17 Peak wavelength of Bragg spectral selectivity curves of gratings recorded at 532nm as a function of nanoparticle concentration in the photopolymer.....	127
Figure 6.18 Spectral response curve of the reflection grating recorded at 473 nm in panchromatic photopolymer.....	128

Figure 6.19 Reconstructed wavelengths of gratings recorded at 473nm as a function of nanoparticle concentration in the photopolymer.....	129
Figure 6.20 Bragg spectral selectivity curves of a reflection grating recorded using combined RGB beams in undoped and 2.5% and 5% nanoparticle doped panchromatic photopolymer composition.....	130
Figure 6.21 Optical setup for recording transmission hologram.....	131
Figure 6.22 Photographic image of holographic reconstruction from the colour transmission hologram in comparison with object.....	131
Figure 6.23 Photograph of white light holographic reconstructions from holograms recorded at the three primary wavelengths. The object used was a 10 euro cent coin.....	132
Figure 6.24 Photograph of (a) object and (b) reconstructed holographic image.....	133
Figure 6.25 shows photographs of the images reconstructed from the holograms with the objects shown in the insets.....	134

CHAPTER 1

INTRODUCTION

After pondering this problem for a long time a solution suddenly dawned on me . . . Why not take a bad electron picture, but one which contains the whole information, and correct it by optical means? It was clear to me for some time that this could be done, if at all, only with coherent electron beams, with electron waves which have a definite phase. But an ordinary photograph loses the phase completely, it records only the intensities. No wonder we lose the phase, if there is nothing to compare it with! Let us see what happens if we add a standard to it, a 'coherent background'.

- Nobel acceptance speech, Dennis Gabor, 1971

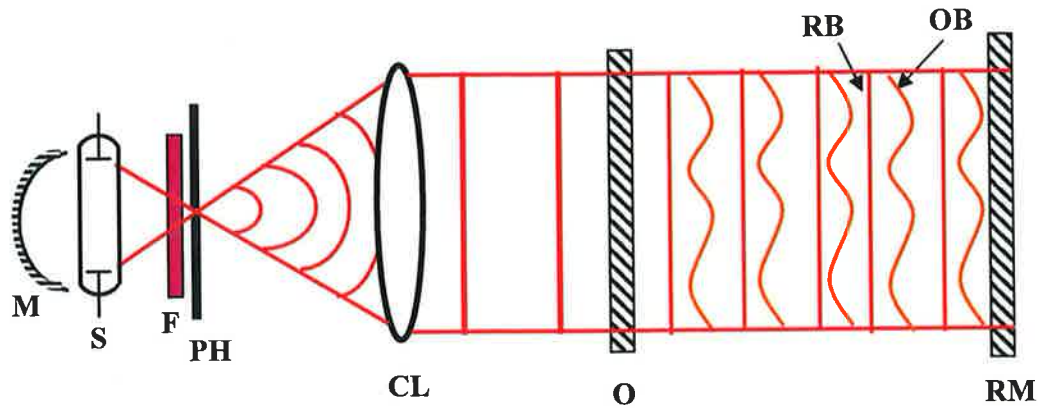
Dennis Gabor, discovered holography and derived the name “hologram” from the Greek words holos, meaning “whole,” and gramma, meaning “message”. Holography is concerned with the production of holograms and their practical applications. Holography is a method for producing a three-dimensional image of an object, by recording the interference pattern formed by two beams namely the reference beam and the object beam on a recording material and then illuminating the recorded pattern either with a laser or with ordinary light. The unique property of holography is that a photosensitive material records an interference pattern containing information about the phase and amplitude of the object, unlike photography which records only the amplitude information of the object. It can be described as an advanced form of photography that allows an image to be recorded in three dimensions. The striking three dimensional properties of holographic images make holograms ideal for display applications which can be used for scientific, educational, medical, artistic and commercial purposes.

1.1 Genesis of Holography

Gabor worked with the British company Thomson-Houston for 15 years from 1933, to improve the resolving power of the electron microscopes. During that time spherical aberration of electron lenses set the theoretical resolution limit of electron microscopes at around 5 \AA [1] while the practical limit achieved was 12 \AA . This resolving power was related to the aperture of the lenses. When the aperture was doubled, it reduced the diffraction error (image being fuzzy) and increased the spherical aberration (sphericity - as though one were looking at the picture through a raindrop) error. Thus the obtained image was fuzzy and had the problem of sphericity. If the fuzziness was improved, the sphericity was made worse and vice-versa.

In 1947 Gabor was able to look at the problem in a different way. His idea was to use this “fuzziness” which was nothing but the diffraction pattern that included all the information about the atomic lattice. So he decided to take an unclear electron picture and then clarify the same by an optical process, which led to the discovery of the new concept called holography [2].

In Gabor’s in-line holography setup (figure 1.1) the object and reference beam were aligned on the same axis, normal to the recording plate. The object was a transparency consisting of a clear background with a few fine opaque lines.



M-mirror, S-mercury lamp, F- green narrow band filter, PH-pinhole, CL-collimating lens, O- object (transparency), RM- recording medium, RB- recording beam and OB-object beam.

Figure 1.1 Gabor holography setup.

When the transparent object is illuminated with a collimated beam from mercury lamp, the incident light on the recording plate consists of two parts. One is the reference beam; its complex amplitude can be represented by a constant r , since its amplitude and phase do not vary across the recording plate. The other one is a weak scattered beam caused by the transmittance variations in the object, represented by complex amplitude $O(x, y)$. The resultant complex amplitude at any point on the recording plate is the sum of these two complex amplitudes. The resultant intensity of the light in the interference pattern is $I(x, y)$ and is written as

$$I(x, y) = |r + O(x, y)|^2$$

$$= r^2 + |O(x, y)|^2 + rO(x, y) + rO^*(x, y)$$

Where $O^*(x, y)$ is the complex conjugate of $O(x, y)$.

If the plate is processed so that the amplitude transmittance is proportional to the original illuminating intensity distribution then the amplitude transmittance of the hologram is written as

$$t(x, y) = t_0 + PT \left[r^2 + |O(x, y)|^2 + rO(x, y) + rO^*(x, y) \right]$$

where T is the exposure time and P is a parameter determined by the recording plate and t_0 is a constant background transmittance.

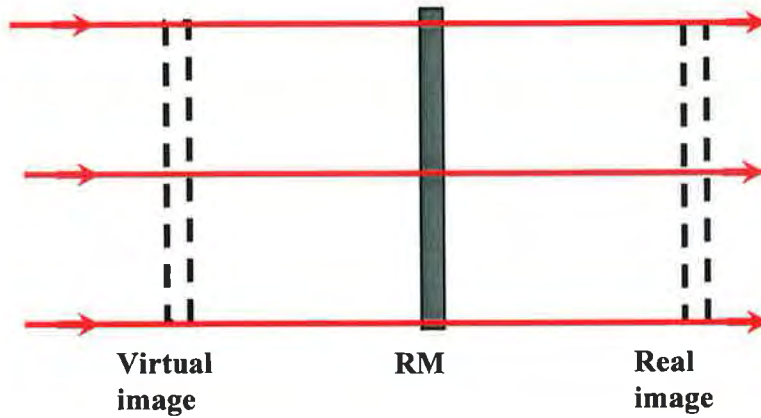


Figure 1.2 Formation of the twin images in in-line hologram.

When the recorded hologram was illuminated with a collimated monochromatic beam one can view the hologram (shown in figure 1.2) and the complex amplitude transmitted by the hologram can be written as

$$u(x, y) = r(t_0 + PTr^2) + PTr|O(x, y)|^2 + PTr^2O(x, y) + PTr^2O^*(x, y).$$

The expression for the transmitted wave contains four terms, which have the following meaning:

$r(t_0 + PTr^2)$ represents a uniform plane wave, corresponds to the directly transmitted beam.

$PTr|O(x, y)|^2$ is extremely small in comparison to the others terms, since $|O(x, y)| \ll r$ and is neglected.

$PTr^2O(x, y)$ except for the constant factor, is identical with the complex amplitude of the scattered wave from the object and represents a virtual image.

$PTr^2O^*(x, y)$ corresponds to a wavefront that resembles the original complex amplitude of object wavefront, except that it has conjugate $O^*(x, y)$ and represents a real image.

The hologram recorded in this setup had two limitations. One was that the object should have high average transmittance and another major limitation was the formation of twin images. Gabor's first holograms used a mercury-vapour lamp as the light source and thus the recorded holograms were difficult to be viewed. With the invention of lasers in 1960, holography started flourishing rapidly.

In 1962 Leith and Upatnieks [3, 4] introduced a very effective method known as the off axis technique for recording and reconstructing an image from a hologram, which made it possible to separate the twin images. In their technique (shown in figure 1.3), the object and reference beams were incident at an offset angle θ to one another to record the hologram. The amplitude due to the object beam at any point (x, y) on the film can be expressed as

$$O(x, y) = |O(x, y)| \exp[-i\phi(x, y)]$$

While due to the reference beam is

$$r(x, y) = r \exp(i2\pi vx)$$

Where $v = \sin \theta / \lambda$

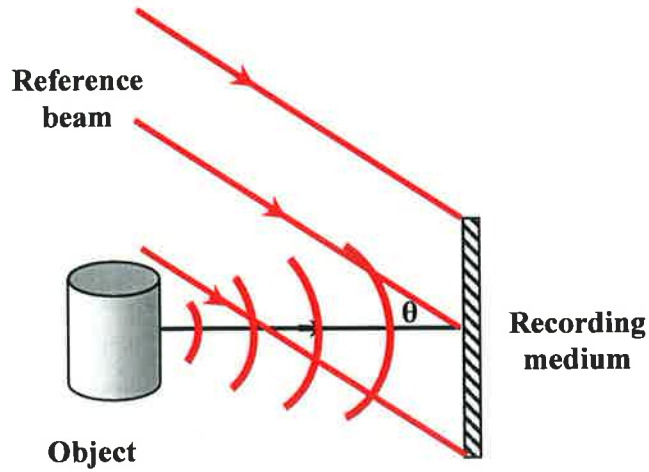


Figure 1.3 Off axis holography setup.

So the resultant intensity at the photographic plate is

$$\begin{aligned}
 I(x, y) &= |r(x, y) + O(x, y)|^2 \\
 &= r^2 + |O(x, y)|^2 + 2r|O(x, y)|\cos[2\pi\nu x + \phi(x, y)].
 \end{aligned}$$

The amplitude and phase of the object wave are therefore encoded as amplitude and phase modulations, respectively, for a set of interference fringes equivalent to a carrier with a spatial frequency of ν .

When the hologram was illuminated with the reference beam, the holographic image of the object was reconstructed at the same offset angle (shown in figure 1.4) and the complex amplitude of the transmitted wave can be written as (similar to in-line hologram),

$$u(x, y) = rt_0 \exp(i2\pi\nu x) + PTr |O(x, y)|^2 \exp(i2\pi\nu x) + PTr^2 O(x, y) + PTr^2 O^*(x, y) \exp(i2\pi\nu x)$$

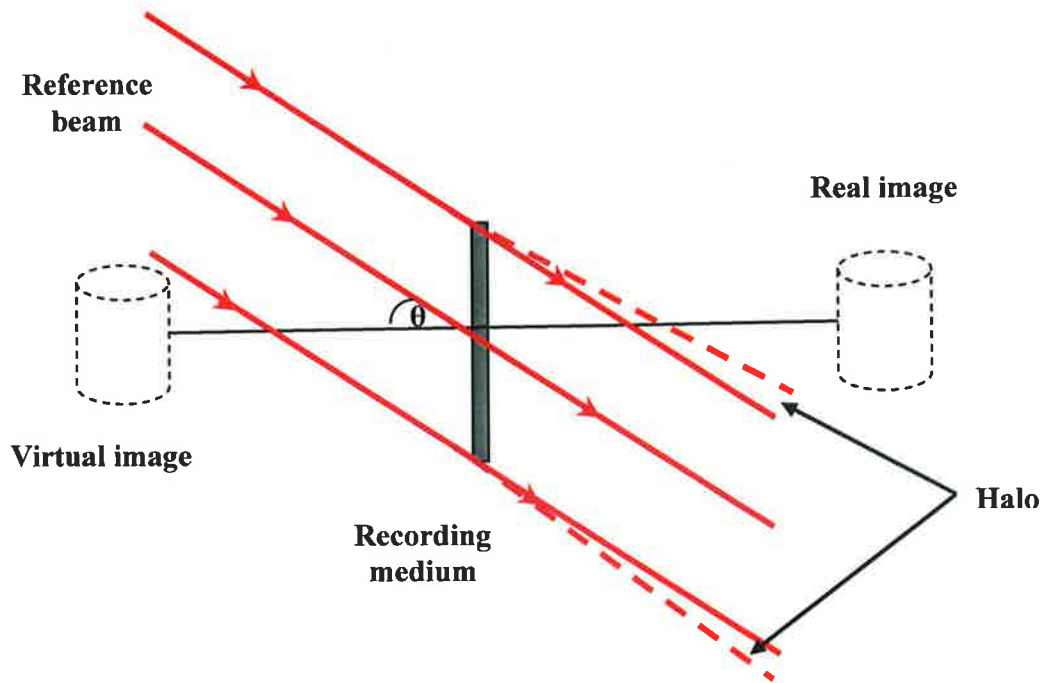


Figure 1.4 Reconstruction of off axis hologram.

The first term in the expression represents a plane wave directly transmitted through the hologram. The second term corresponds to the halo around the direct beam. The third term represents the virtual image of the object in its original position. Similarly the fourth term gives rise to the conjugate image.

After this introduction of off axis method, holography has been widely used for range of applications such as holographic displays, non destructive testing, optical data storage, holographic optical elements etc. As this thesis is dedicated to full colour holography the next section gives a brief history of the development of colour holography.

1.2 Brief history of colour holography

In 1964 Leith and Upatneiks [5] first proposed multicolour wavefront reconstruction using laser light. They explained that a multi colour hologram can be obtained by superposition of three holographic diffraction patterns using three additive primary colours. When the hologram was illuminated with the three reference beams, each beam generated three images, resulting in nine virtual images. Out of these nine images, three of them exactly coincided to produce a full colour reconstructed virtual image of the object. Angular separation of the desired image from the undesired ones was obtained by illuminating the recording material (by reference beams) at different angles. Mandel [6] then showed that the problem of spurious images can be minimized by restricting the field of view of the reconstructed image. The reference beams of the three colours need not be at different angles. Pennington and Lin [7] recognised the inherent potential of thick emulsions (15 μ m) Kodak 649F to suppress the unwanted diffraction even when the reference beam angles were identical and recorded the first transmission two-colour hologram using an Ar⁺ ion laser at 488 nm and a He-Ne laser at 633 nm. Friesem and Fedorowicz [8], in their method, showed that there was dominant interaction between the spectral wavelengths that were close to each other such as 488 nm and 514.5 nm and this resulted in unwanted images. They suggested that this problem can be reduced by increasing the thickness of the recording material. These earliest methods were concerned mainly with transmission holograms recorded with different wavelengths from one or more lasers and with different reference beam directions. In spite of the availability of high quality colour holograms, complications and cost involved in making the reconstruction setup prevented this technique (recording transmission hologram) from becoming more popular.

Reflection holography was invented by Denisjuk [9] based on interference colour photography developed by Lippmann [10]. Lin et al., [11] first made white light viewable multi colour holograms of a 2-dimensional object using two wavelengths (633 nm and 488 nm). Later Upatneiks et al., [12] made colour holograms by using three wavelengths (633 nm, 514.5 nm and 488 nm) and a 3-dimensional object.

Noguchi [13] attempted the first quantitative study of colour fidelity in multicolour holograms on the basis of colorimetry. He performed colour reproduction by comparing the original colour patches with the aid of a colour computer and the human eye. Kubota and Ose [14] made a high quality full colour reflection hologram by using dichromated gelatin (DCG) sensitized to red wavelength using methylene blue photosensitive dye. Hariharan [15] developed a method using a two layer sandwich of Agfa 8E75 silver halide emulsion sensitized at 633 nm and 8E56 emulsion sensitized at both 515 nm and 488 nm and also improved the image brightness by using a one step, limited aperture, image plane geometry. Kubota [16] used this sandwich technique with a combination of DCG (for 514.5 nm and 488 nm) and silver halide (for 633 nm) to make full colour holograms. Hubel and Solymar [17] reported theoretical and experimental studies on colour reflection holography and produced reflection holograms using eight recording wavelengths. Finally from the theoretical analysis they found that 460 nm, 530 nm and 615 nm were the optimum recording wavelengths for best colour reproduction. Bjelkhagen et al., [18] used an ultra high resolution single layer panchromatic silver halide material to record colour reflection holograms successfully. Sainov et al., [19] reported high quality multi colour holograms in Bulgarian silver halide materials.

Many researchers have developed high quality colour holograms by introducing novel and improved panchromatic recording materials. Recording materials such as silver halide photographic emulsions (SHPE), dichromated gelatin (DCG) and DuPont photopolymer are being used to record high efficiency holograms.

1.3 Motivation for the Project

However, all these materials that have been mentioned earlier to record high quality reflection and transmission holograms have the major disadvantage of the requirement of wet chemical processing for developing the holograms. From the point of view of commercial applications, the whole process of development is laborious and expensive. Self-developing photopolymers bypass this tedious developing procedure making them the ideal choice for real-time recording and reconstruction of holograms. This thesis explains the development of one such self processing acrylamide based photopolymer to record reflection holograms for full colour display.

1.4 Objectives

The main objectives of this project are to

- Measure the diffraction efficiency of transmission and reflection holographic gratings at 633 nm, in methylene blue dye sensitized self processing acrylamide based photopolymer.
- Sensitize the self processing acrylamide based photopolymer at 473 nm and record transmission and reflection holographic gratings and optimise dye concentration for high diffraction efficiency.
- Sensitize self processing acrylamide based photopolymer at all three primary wavelengths to record reflection holographic gratings.

- Study the influence of the Si-MFI zeolite nanoparticle dopants on the diffraction efficiency of the reflection holographic gratings (633 nm, 473 nm and multi colour).
- Perform spectral characterization for both doped and undoped photopolymers by recording reflection holographic gratings.
- Record full colour transmission and reflection holograms.

1.5 Research summary

This project, as mentioned before is dedicated to the development of self processing acrylamide based photopolymer to record full colour reflection holograms for display applications. It is very important to mention that a considerable amount of work has been done by Feely on red sensitised acrylamide based photopolymer [20] and Martin and Jallapuram on green sensitized photopolymer [21, 22] and the work discussed in this thesis is a continuation, to reach the goal of recording full colour holograms by sensitizing the photopolymer for blue wavelength and optimising the photopolymer for full colour holographic recording.

The acrylamide based photopolymer sensitised at 532 nm was well optimised for recording reflection holograms. Therefore as a first step in this project, acrylamide based photopolymer that was photosensitised at 633 nm using methylene blue dye to record high spatial frequency (4200 lines/mm) reflection holographic gratings and measure their diffraction efficiencies. This study was undertaken so as to determine the material's capability for recording reflection holograms at this wavelength.

The photopolymer was sensitised to record at 473 nm using acriflavine photosensitive dye. Transmission and reflection gratings were recorded at 473 nm and the diffraction

efficiencies were measured in order to study the material's capability for recording reflection holograms. In the second stage, the influence of zeolite nanoparticles (Si-MFI) dopant on the diffraction efficiency of the photopolymer material was studied in an effort to improve the holographic recording capability. The spectral response of recorded reflection gratings was measured in nanoparticle doped photopolymer, and compared with the undoped photopolymer in order to see if better control over the reconstruction wavelength could be obtained.

The knowledge gained from the preliminary work that was carried out to sensitise the photopolymer at all three primary wavelengths separately, was used to further sensitise the photopolymer at all three primary wavelengths red (633 nm), green (532 nm) and blue (473 nm) together. Therefore the next set of experiments was aimed at using the panchromatic acrylamide based photopolymer material to record white light viewable full colour holograms. For this purpose reflection holographic gratings were recorded in photopolymer layers of different thicknesses at different intensities and the corresponding diffraction efficiency was measured at each recording wavelength. Further the photopolymer material was doped with zeolite nanoparticles (Si-MFI) to improve the diffraction efficiency of the reflection gratings. Spectral characterisation studies were performed on doped and undoped panchromatic photopolymers to investigate the effect of nanoparticle dopants on the reconstruction wavelengths of the recorded gratings. Finally after all these investigations and optimisations, full colour holograms were successfully recorded in this panchromatic acrylamide based photopolymer developed in the IEO Centre, DIT.

1.6 Thesis Outline

Chapter 2 introduces the reader to hologram types and key issues in colour holography.

Chapter 3 focuses on photopolymer materials and the mechanisms involved in holographic recording using these materials.

Chapter 4 discusses the recording of transmission and reflection holographic gratings at 633 nm in self processing acrylamide based photopolymer. The influence of the Si-MFI zeolite nanoparticle dopants on the diffraction efficiencies of the reflection holographic gratings recorded in the photopolymer was studied. This chapter also discusses the results of spectral characterisation of both undoped and nanoparticle doped photopolymers.

In **Chapter 5** sensitisation of self processing acrylamide based photopolymer at 473 nm to record holographic transmission and reflection gratings is explained. Dye optimization and doping with Si-MFI Zeolite nanoparticles in order to increase the diffraction efficiency of reflection gratings is also discussed. Finally spectral characterization performed on both doped and undoped nanoparticle photopolymers for checking the reconstructed wavelength, is discussed.

Chapter 6 details the procedure undertaken to sensitise acrylamide based photopolymer at three primary wavelengths for recording full colour holograms. The steps taken to improve the diffraction efficiency and wavelength reconstruction are also discussed.

Chapter 7 summarises the achievements and also discusses the future scope of this work.

References

1. R.J.Collier, C.B.Burckhardt, and L.H.Lin, "Optical holography," student edition, Academic press, New York, 1971.
2. D.Gabor, "A new microscopic principle", Nature 161, 777-778 (1948).
3. E.N.Leith and J.Upatnieks, "Reconstructed wavefronts and communication theory," J. Opt. Soc. Am. 52, 1123-1130 (1962).
4. E.N.Leith and J.Upatnieks, "Wavefront reconstruction with continuous-tone objects," J. Opt. Soc. Am. 53, 1377-1381 (1963).
5. E.N.Leith and J.Upatnieks, "Wave-front reconstruction with diffused illumination and three-dimensional objects," J. Opt. Soc. Am. 54, 1295-1301 (1964).
6. L.Mandel, "Color imagery by wavefront reconstruction," J. Opt. Soc. Am. 55, 1697-1698 (1965).
7. K.S.Pennington and L.H.Lin, "Multicolour wavefront reconstruction," Appl. Phys. Lett. 7, 56-57 (1965).
8. A.A.Friesem and R.J.Fedorowicz, "Recent advances in multicolor wavefront reconstruction," Appl. Opt. 5, 1085-1086 (1966).
9. Yu.N.Denisyuk, "Photographic reconstruction of the optical properties of an object in its own scattered radiation field," Sov. Phys, Doklady. 7, 543-545 (1962).
10. G.Lippmann, "Sur la théorie de la photographie des couleurs simples et composées par la méthode interférentielle," J. Physique 3 (3), 97-107 (1894).
11. L.H.Lin, K.S.Pennington, G.W.Stroke, and A.E.labeyrie, "Multicolour holographic image reconstruction with white-light illumination," Bell Syst. Tech. J. 45, 659-661 (1966).

12. J.Upatnieks, J.Marks, and R.Fedorowicz, "Colour holograms for white light reconstruction," *Appl. Phys. Lett.* 8, 286-287 (1966).
13. M.Noguchi, "Color reproduction by multicolour holograms with white-light reconstruction," *Appl. Opt.* 12, 496-499 (1973).
14. T.Kubota and T.Ose, "Lippmann color holograms recorded in methylene-blue sensitized dichromated gelatine," *Opt. Lett.* 1, 8-9 (1979).
15. P.Hariharan, "Improved techniques for multicolour reflection holograms," *J.Opt. (Paris)* 11, 53-55 (1980).
16. T.Kubota, "Recording of high quality color holograms," *Appl. Opt.* 25, 4141-4145 (1986).
17. P.M.Hubel and L.Solymar, "Color reflection holography: theory and experiment," *Appl. Opt.* 30, 4190-4203 (1991).
18. H.I.Bjelkhagen, T.H.Jeong, and D.Vukicevic, "Color reflection holograms recorded in a panchromatic ultrahigh-resolution single-layer silver halide emulsion," *J.Imaging Sci. Technol.* 40, 134-146 (1996).
19. V.Sainov, K.Zdravkov, E.Stoykova, B.Ivanov, D.Nazarova, B.Markova, S.Sainov, T.Petrova, "Multi colour holographic recording," *J. Optoelectr. Adv. Materials*, v.11, 1448-1451 (2009).
20. C.A.Feely, "The development and characterisation of a red sensitised photopolymer holographic recording material" Ph.D thesis University of Dublin (1998).
21. S.Martin, "A new photopolymer recording material for holographic applications: photochemical and holographic studies towards an optimised system" Ph.D thesis University of Dublin (1995).

22. R.Jallapuram, "Optimization of an acrylamide-based photopolymer for reflection holographic recording" Ph.D thesis Dublin Institute of Technology (2005).

CHAPTER 2

COLOUR HOLOGAPHY

2.1 Introduction to colour holography

Colour holography is a technique used for producing a three-dimensional image of a coloured object, whose colour approximates that of the original object when illuminated with an appropriate light source. These holographic images are referred to as full colour or natural colour or true colour holograms. Full colour holography is used to record an interference pattern between reference waves of three primary wavelengths and the light scattered or reflected from a coloured object. This object is illuminated with the chosen primary wavelengths. Upatnieks and Leith [1] first reported that multicolour holographic images could be obtained by superposition of three holograms recorded using three additive primary wavelengths (red, green and blue). The recording parameters for full colour reflection holograms mainly depend on the selected primary wavelengths, recording material, and the geometry of recording. This chapter will further address the key technical issues in colour holography.

Holograms are categorised into different types, mainly depending on the geometry of recording, the thickness of the recording material and on the response of the recording material to the interference pattern. Some of them are discussed in section 2.2.

The following sections (from 2.3) are dedicated to the discussion of diffraction efficiency of volume holograms by coupled wave analysis, technical issues such as

the selection of recording wavelength, recording setup and recording material for colour holography.

2.2 Types of holograms

This section discusses different types of holograms, differentiated on the basis of recording geometry.

2.2.1. Transmission holograms

Fig 2.1 shows the basic geometry for the recording of transmission holograms. To make this type of hologram, two laser beams (object beam and reference beam) from the same coherent laser source illuminate the holographic recording material from the same side.

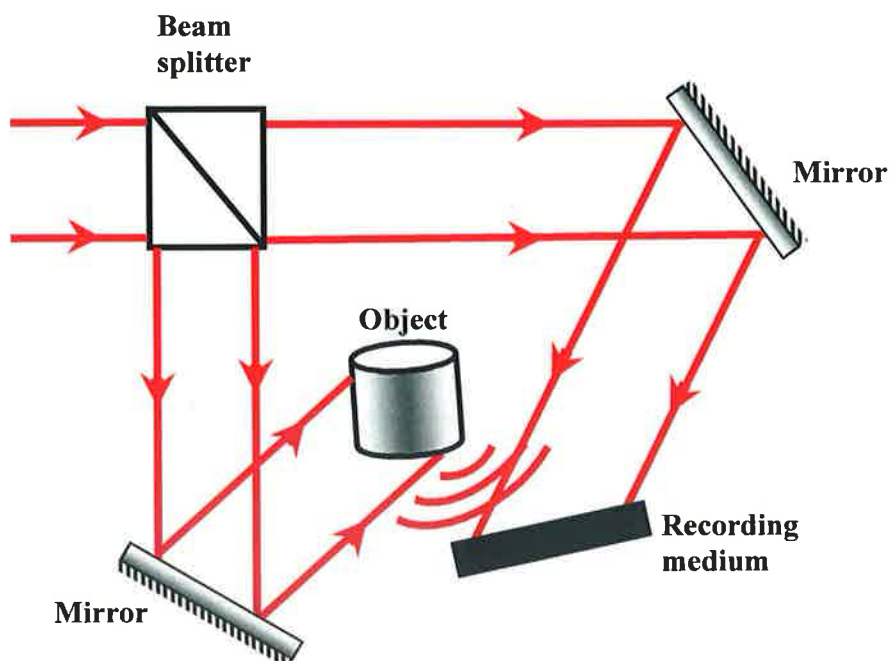


Figure 2.1 Transmission hologram recording setup

An interference pattern is produced in the region of overlap of the two beams and is stored in the holographic recording material as a hologram. To reconstruct the holographic image, the hologram should be illuminated with the reference beam used

in the recording process and the hologram in its original position and at the same angle. Also to view the image the holographic plate and the path of the reference beam should be in their original positions. While looking along the object beam one can observe the virtual image of the object. By shifting the viewpoint, the perspective of the image changes to show the three dimensionality of the original object.

2.2.2 Reflection holograms

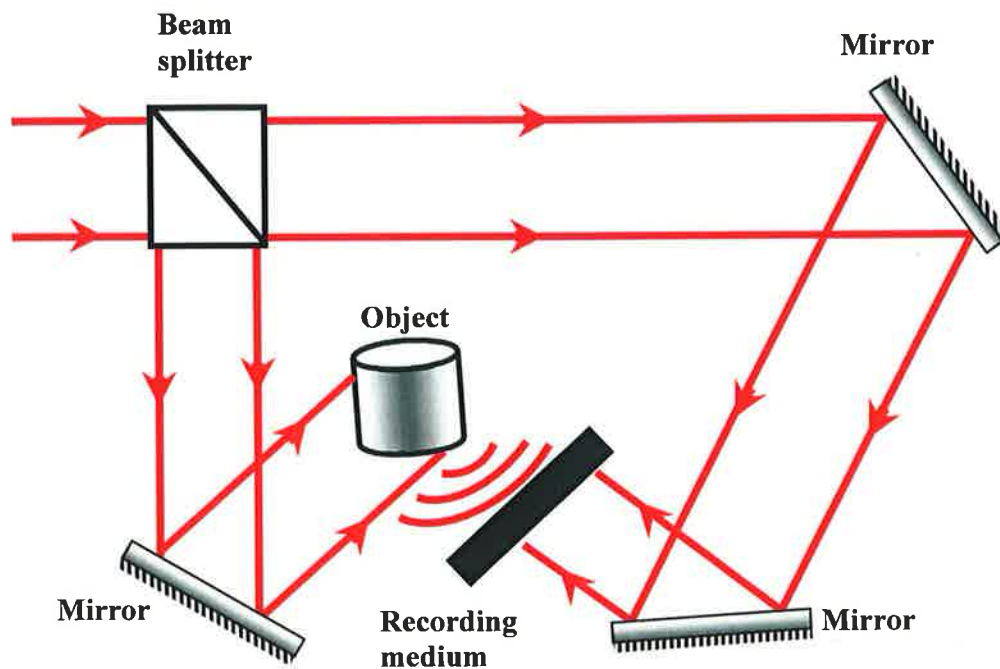


Figure 2.2 Reflection hologram recording setup

Reflection holograms are the most common type of display holograms, also known as white light viewable holograms. This type of hologram is recorded by the two recording beams (object and reference) illuminating the holographic recording material from the opposite sides of the recording material. Figure 2.2 shows a simple geometry for recording a reflection hologram. When the recorded hologram is illuminated with a white light source at the Bragg angle, the holographic image will

be reconstructed at the same wavelength as that of the recording wavelength. In the similar way as in the transmission hologram, one can view the three dimensionality of the image.

Denisyuk [2] developed a simple holographic recording technique for recording reflection hologram which uses a single recording beam. The basic recording geometry is shown in figure 2.3.

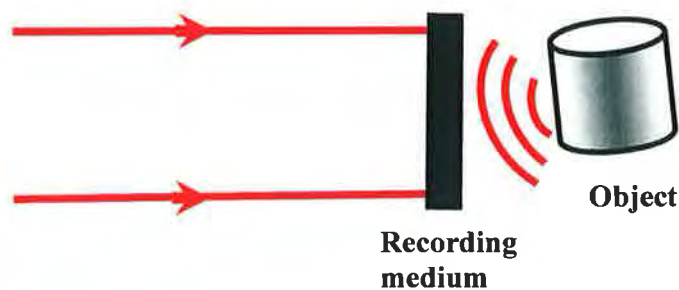


Figure 2.3 Single beam Denisyuk recording setup.

In this technique the recording beam from the coherent laser light source illuminates the holographic recording plate. Some of the light transmitted through the holographic plate illuminates the object, placed behind the holographic recording plate. The light reflected or scattered from the object, illuminates the recording plate from back side and interferes with the reference beam. The interference pattern is thus recorded in the recording material resulting in a hologram. An advantage over the two beam reflection hologram process is that it reduces the complexity of aligning the recording geometry. However, this geometry has a disadvantage of inequality in the intensity of the reference beam and of the object beam, affecting the visibility of interference pattern.

2.2.3 Rainbow holograms

In 1968, Benton [3] invented rainbow holograms, also known as Benton holograms. These rainbow holograms are made by a two step holographic recording process. In the first step, a transmission hologram H_1 is recorded (shown in figure 2.4 (a)) in way similar to that described in section 2.2.1. Later this transmission hologram H_1 , is flipped to form a real inverted image covered by a horizontal slit. This image is used as an object to record the second hologram H_2 as shown in figure 2.4 (b). When the hologram H_2 is illuminated with the conjugate of the reference beam, it forms an image of the object near the hologram (shown in figure 2.4 (c)). In addition, it forms a real image of the slit placed across the hologram H_1 . When the H_2 hologram is illuminated with the white light source, this horizontal slit limits the vertical perspective, leading the viewer to see only one wavelength at a particular angle while maintaining the three dimensionality. If the viewer moves vertically, the colour of the reconstruction image changes and appears in all the rainbow colours. Hence this type of hologram is called a rainbow hologram.

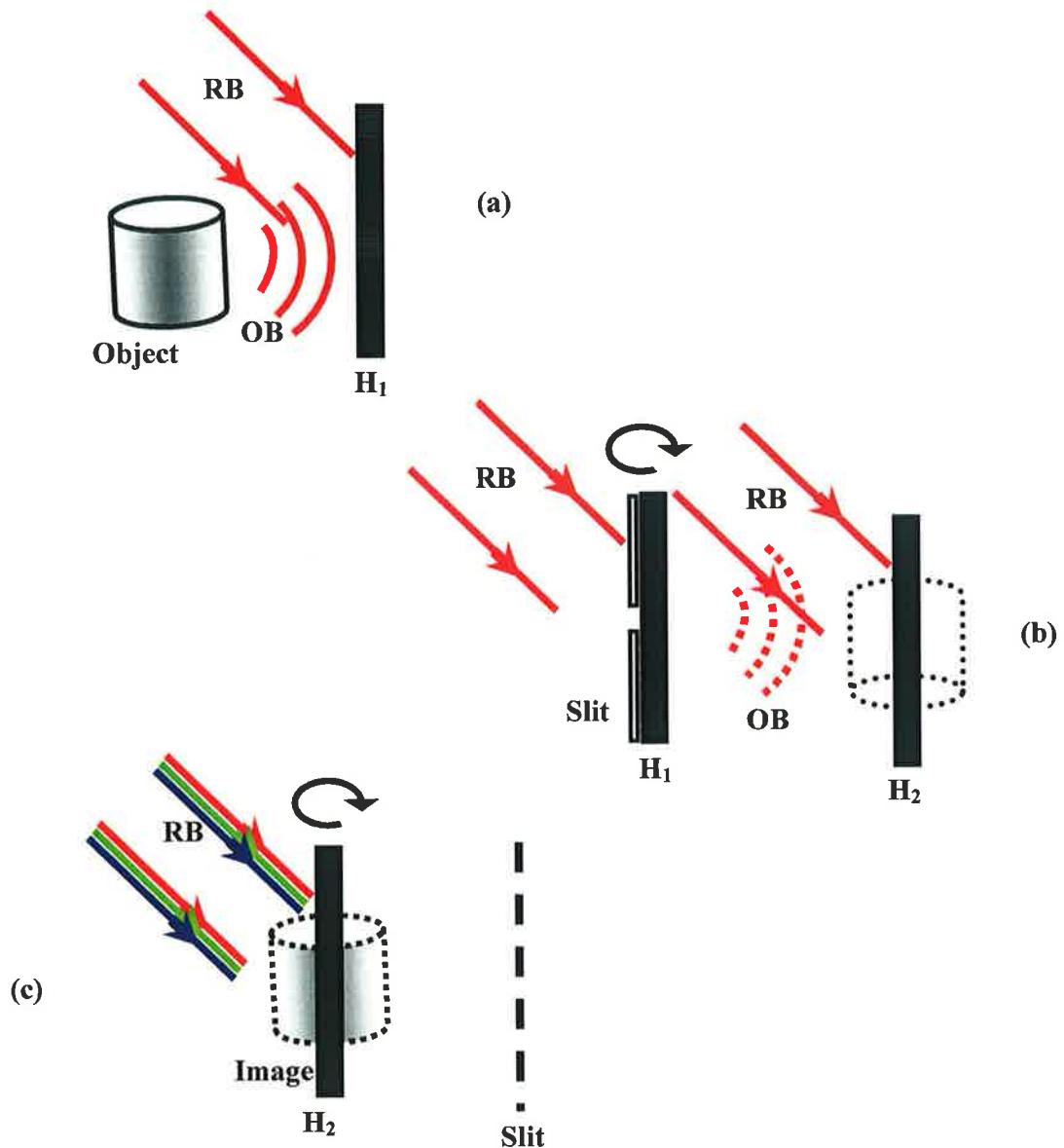


Figure 2.4 Two-step rainbow holography: (a) Recording transmission master hologram H_1 . (b) Recording second transmission hologram H_2 . (c) Reconstruction of H_2 hologram.

2.2.4 Other types of holograms

Holograms that give 360° view of the object can be recorded using either four or more plates or a cylindrical film to surround the object. Figure 2.5 shows the simple optical setup for recording a 360° viewable holograms [4]. In this setup, the center portion of

the expanded laser beam illuminates the object, while the outer portion of the light which falls directly on the film acts as a reference beam. Hence, the interference pattern is recorded on a cylindrical photographic film from all sides of the selected object and the reference beam. During reconstruction the object is removed and the hologram is illuminated with the reference beam. On reconstruction one can view the complete detail of the object, by rotating the hologram or walking around it.

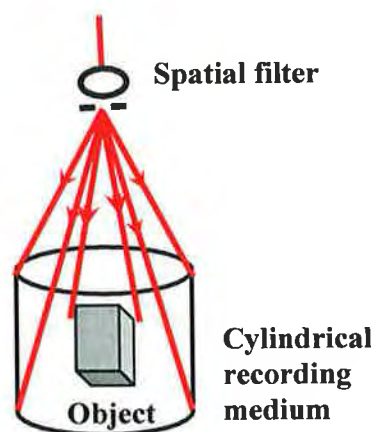


Figure 2.5- Recording geometry for recording 360° hologram

Edge lit holograms [5] are another type of holograms used for compact portable displays. Figure 2.6 shows Upatniek's method for edge illuminated holograms. In this setup the reference beam is brought to a focus on the edge of the cover plate (adjacent to the holographic plate) and expands entirely within it. The object beam enters from the opposite side of the holographic plate and superpose with the reference beam to form the interference pattern. As the reference beam travels parallel to the recording plane at an angle of incidence 90° , it gives maximum tilt to the fringe planes. The image thus formed on the holographic plate can be reconstructed by illuminating with the laser diode placed on the edge of the cover plate at the point where the reference beam was focussed.

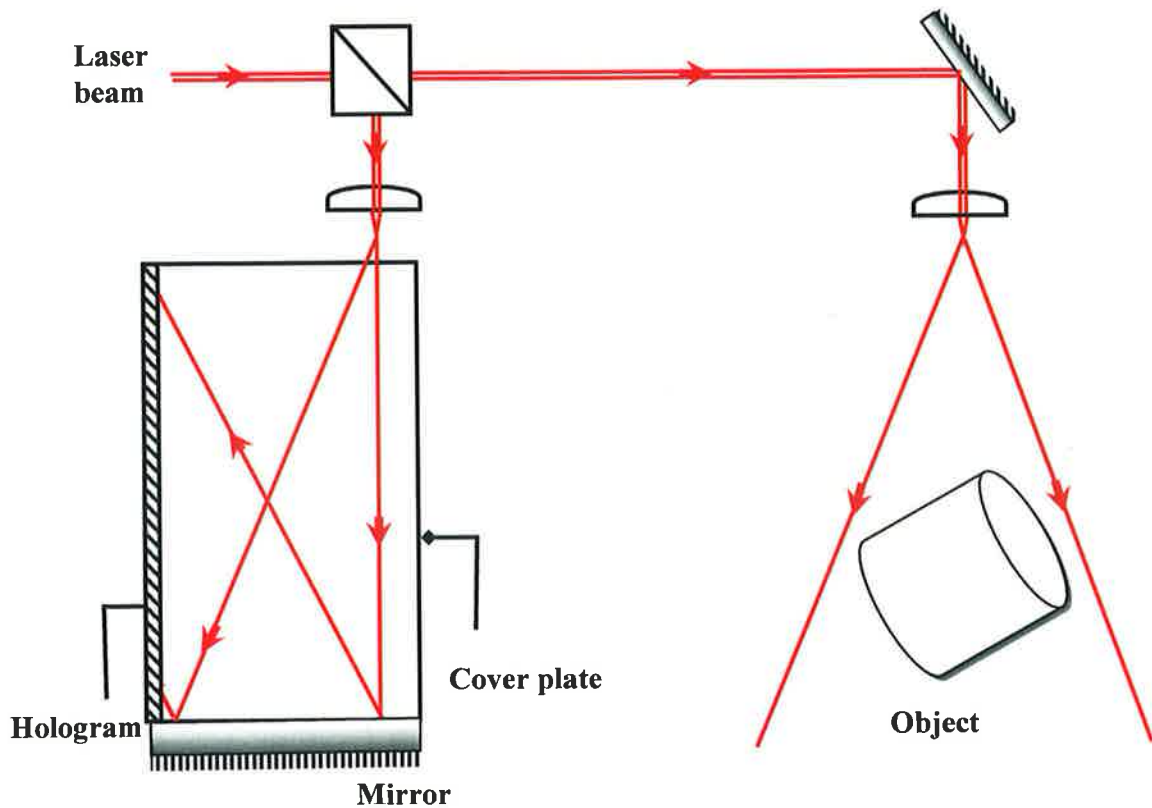


Figure 2.6 Recording geometry for edge lit hologram.

Another method for holographic display is recording holographic stereograms [6], which are hybrids of holography and photography. In this type, a series of two dimensional views of an object are recorded from different angles, in the form of a composite hologram such that the image appears to be in three dimensions. All the images are multiplexed into a single hologram in such a way that for any viewing position the two eyes of the viewer see only the two images appropriate to that viewpoint. By moving the holograms quickly, the entire range of view points appear in such a way that the overall image has full horizontal parallax, or animation, or both.

2.3 Coupled wave theory of volume holograms

On the basis of thickness of the recording materials and the fringe spacing of the recorded gratings, holograms can be classified into thin and thick holograms. In the

case of a thin hologram, the thickness of the recording medium is small compared to the average fringe spacing of the grating. While in a thick hologram, the thickness of the recording medium is much larger in comparison to the average fringe spacing of the grating. This type of hologram is also known as a volume hologram. A parameter called the Q parameter is used for the classification of these holograms and given by equation 2.1

$$Q = \frac{2\pi\lambda T}{nd^2} \quad [2.1]$$

where T is the thickness of the photosensitive recording material, n is the refractive index of the recording material, d is the fringe spacing and λ is the wavelength of the light source.

If the value of $Q > 1$ then the hologram is considered as thick, while if $Q < 1$ the holograms are considered as thin holograms.

Holographic recording in thick media has gained particular interest for holographic data storage, colour holography and white light display holography because of the disadvantages in the thin holograms which require special techniques to minimize or eliminate the cross talk problem that occurs in angular or wavelength multiplexing. Some of the methods that are used to minimize the cross talk in thin holograms are, coded reference beam method and non-overlapping spatial sampling [11]. Reference beam coding is done by varying the amplitude and phase of the reference beam using a ground glass. Non-overlapping spatial sampling uses a series of thin red, green and blue colour strips over the hologram in order to avoid the overlapping of the

interference patterns formed by different colours. However all these methods have limitations like restriction in image viewing direction and low signal to noise ratio. In volume holograms the cross talk problem is eliminated by using thick recording medium. The interference fringe pattern recorded in a thick hologram is usually in the form of a spatial modulation of the absorption or refractive index or both. The maximum diffraction efficiency of these thick holograms is obtained when the illuminating beam satisfies the Bragg's law shown in equation 2.2.

$$2nd \sin \theta = \lambda \quad [2.2]$$

where θ is the Bragg angle defined as the angle that the incident beam makes with the fringe plane in the recording medium.

The diffraction efficiency of volume holograms can be analysed using coupled wave theory [7-9] which was developed by Kogelnik [10]. This theory predicts the maximum diffraction efficiency that can be obtained for different types of gratings. The coupled wave theory assumes that the hologram or grating is illuminated with a monochromatic light source at or near the Bragg angle and the incident light is polarized perpendicular to the plane of incidence.

Figure 2.7 shows the geometry used for the diffraction efficiency analysis of volume holograms. The z-axis is chosen perpendicular to the surface of the medium, the x-axis is the plane of incidence and parallel to the recording medium boundaries and the y-axis is perpendicular to the plane of the paper. Fringe planes are oriented perpendicular to the plane of incidence and slanted with respect to the medium

boundaries ($z=0$ and $z=T$) at an angle Φ . The grating vector \mathbf{K} with magnitude

$K = |\mathbf{K}| = \frac{2\pi}{d}$ is normal to the fringe planes.

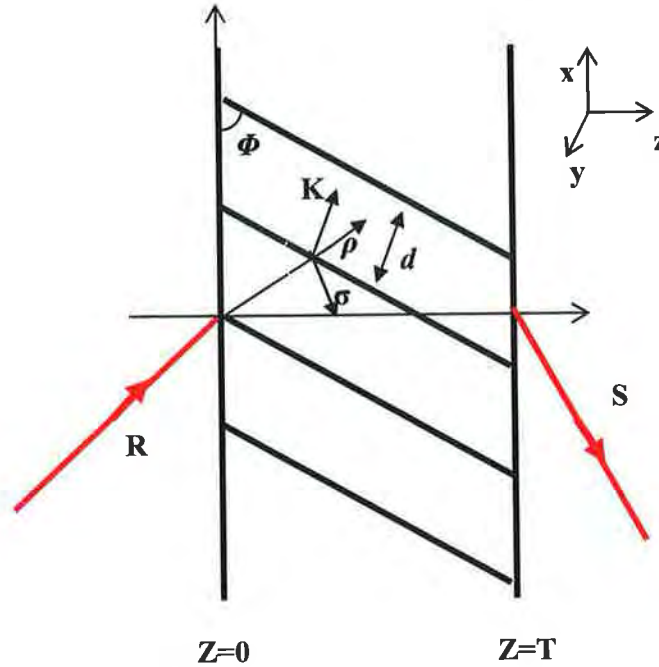


Figure-2.7 Basic geometry of thick hologram with slanted fringes.

Wave propagation in the medium can be described by the scalar wave equation

$$\nabla^2 E(x, z) + \left(\frac{\omega^2}{c^2} \varepsilon - j\omega\mu\sigma \right) E(x, z) = 0 \quad [2.3]$$

where $E(x, z)$ is the complex amplitude of the electric field with an angular frequency ω , c is the velocity of light in free space, μ is the permeability of the medium, ε is dielectric constant and σ is conductivity of the medium. The holographic grating is represented by a spatial modulation of ε or σ , expressed as

$$\varepsilon = \varepsilon_0 + \varepsilon_1 \cos \vec{K} \cdot \vec{r} \quad [2.4]$$

$$\sigma = \sigma_0 + \sigma_1 \cos \vec{K} \cdot \vec{r} \quad [2.5]$$

where $\vec{r} = \vec{i}x + \vec{j}y + \vec{k}z$ is a vector, ε_1 and σ_1 are amplitudes of spatial modulation, ε_0 is average dielectric constant, σ_0 is average conductivity.

Substituting ε and σ from equation 2.4 and 2.5 in equation (2.3), the wave equation can be written as

$$\nabla^2 E(x, z) + \left(\beta^2 - 2j\alpha\beta + 4\chi\beta \cos \vec{k} \cdot \vec{r} \right) E(x, z) = 0 \quad [2.6]$$

where β is the average propagation constant and α is the average absorption constant;

$$\beta = \frac{2\pi(\varepsilon_0)^{1/2}}{\lambda}; \quad \alpha = \frac{c\mu\sigma_0}{2(\varepsilon_0)^{1/2}}, \quad [2.7]$$

and the coupling constant χ is defined as

$$\chi = \frac{1}{4} \left(\frac{2\pi}{\lambda} \frac{\varepsilon_1}{(\varepsilon_0)^{1/2}} - j \frac{\mu c \sigma_1}{(\varepsilon_0)^{1/2}} \right) \quad [2.8]$$

The optical properties of the material are characterized by its refractive index (n) and absorption constant (α). Assuming that the absorption per wavelength as well as relative variation in refractive index of the medium are small, so that

$$\alpha_0 \ll 2\pi n_0 / \lambda \quad [2.9]$$

$$\alpha_1 \ll 2\pi n_0 / \lambda \quad [2.10]$$

$$n_1 \ll n_0 \quad [2.11]$$

Here n_0 is average refractive index, n_1 and α_1 are the amplitudes of the spatial modulations of refractive index and the absorption constant respectively. Under above assumptions, equation (2.7 and 2.8) can be written as

$$\beta = \frac{2\pi}{\lambda} n; \quad \chi = (\pi n_1 / \lambda) - j\alpha_1 / 2 \quad [2.12]$$

In the equation 2.12 the coupling constant χ describes the coupling of the light between the reference wave (R) and diffracted wave (S). If $\chi=0$ there is no energy exchange between them, hence no diffraction.

The propagation of two coupled waves through the grating can be described by their complex amplitudes $R(z)$ and $S(z)$ which vary along the z axis. The total electric field E in the grating is due to the sum of these two waves ($R(z)$ and $S(z)$) is:

$$E = R(z)e^{-i\vec{\rho}\cdot\vec{r}} + S(z)e^{-i\vec{\sigma}\cdot\vec{r}} \quad [2.13]$$

where propagation vectors $\vec{\rho}$ and $\vec{\sigma}$ are defined by the propagation constants and the direction of the propagation of R and S . The relationship between the incident and diffracted wave propagation vectors with the grating vector is expressed as

$$\vec{\sigma} = \vec{\rho} - \vec{K} \quad [2.14]$$

The coupled wave equations are derived by inserting equation 2.13 and 2.14 in equation 2.6. By comparing the terms with equal exponentials $e^{-j\rho\cdot r}$ and $e^{-j\sigma\cdot r}$, the following equations can be obtained

$$R'' - 2j\rho_z R' - 2j\alpha\beta R + 2\chi\beta S = 0 \quad [2.15]$$

$$S'' - 2j\sigma_z S' - 2j\alpha\beta S + 2\chi\beta R = 0 \quad [2.16]$$

The primes denote the differentiation with respect to z . By assuming that the energy interchange between $R(z)$ and $S(z)$ and also energy absorption in the medium is slow, the second differentials (R'' and S'') are neglected and the equations 2.15 and 2.16 can be rewritten as;

$$c_R R' + \alpha R = -j\chi S \quad [2.17]$$

$$c_S S' + (\alpha + j\Gamma)S = -j\chi R \quad [2.18]$$

Where

$$c_R = \rho_z / \beta = \cos \varphi, \quad c_S = \sigma_z / \beta, \quad \Gamma = \beta \delta \sin 2\theta_0$$

The coupled wave equations 2.17 and 2.18 show that the changes in the complex amplitudes $R(z)$ or $S(z)$ along z -axis are either caused by absorption (αR and αS) or by coupling to the other wave (χR and χS). The term $j\Gamma S$ in the equation 2.16 indicates that a deviation of small angle δ of the incident wave from the Bragg's condition by small angle δ , results in a decrease in the interaction between the incident and diffraction wave.

The introduced boundary conditions for the coupled wave analysis for transmission holograms are $R(0)=1, S(0)=0$, and for the reflection holograms $R(0)=1, S(0)=1$.

For transmission holograms, in the case of a lossless phase hologram where $\alpha=\alpha_I=0$, the amplitude of the diffracted wave at $z=T$ is given by

$$S(T) = -j \frac{\exp(-i\xi) \sin(\xi^2 + \nu^2)^{1/2}}{\left(1 + \frac{\xi^2}{\nu^2}\right)^{1/2}} \quad [2.19]$$

where

$$\xi = \frac{\Gamma T}{2 \cos \theta_0} \quad \nu = \frac{\pi n_1 T}{\lambda_a \cos \theta_0}$$

When light is incident exactly at the Bragg angle, then $\delta=0$ so that $\xi=0$. Now the diffraction efficiency of the hologram can be written as

$$\eta = |S(T)|^2 / |R(0)|^2 = |S(T)|^2 = \sin^2 \nu \quad [2.20]$$

The efficiency is 100% when the parameter $\nu = \pi/2$. Beyond this point if ν increases, the energy couples back in to the incident wave, resulting in the decrease of the efficiency.

When the incident wave angle deviates from the Bragg condition, the diffraction efficiency drops to

$$\eta = \frac{\sin^2(\xi^2 + \nu^2)^{1/2}}{\left(1 + \frac{\xi^2}{\nu^2}\right)} \quad [2.21]$$

$$\xi = \delta KT / 2 \quad \text{or} \quad \xi = \Delta\lambda K^2 T / 8\pi n_0 \cos\theta_0 \quad [2.22]$$

From the above equations 2.19 and 2.20, it is clear that the efficiency of the hologram is influenced by angular deviation δ and wavelength deviation $\Delta\lambda$ through the parameter ξ .

Figure 2.8 shows the normalized diffraction efficiency (η_0 is the maximum value of the diffraction efficiency) of the lossless transmission phase holograms as a function of the parameter ξ for three values of the parameter ν . The diffraction efficiency of the hologram with $\nu = \pi/2$ is 100%, with $\nu = \pi/4$ and $3\pi/4$ will be 50%. It can be observed that for a fixed value of ξ the diffraction efficiency drops to zero if there is slight deviation from the Bragg condition.

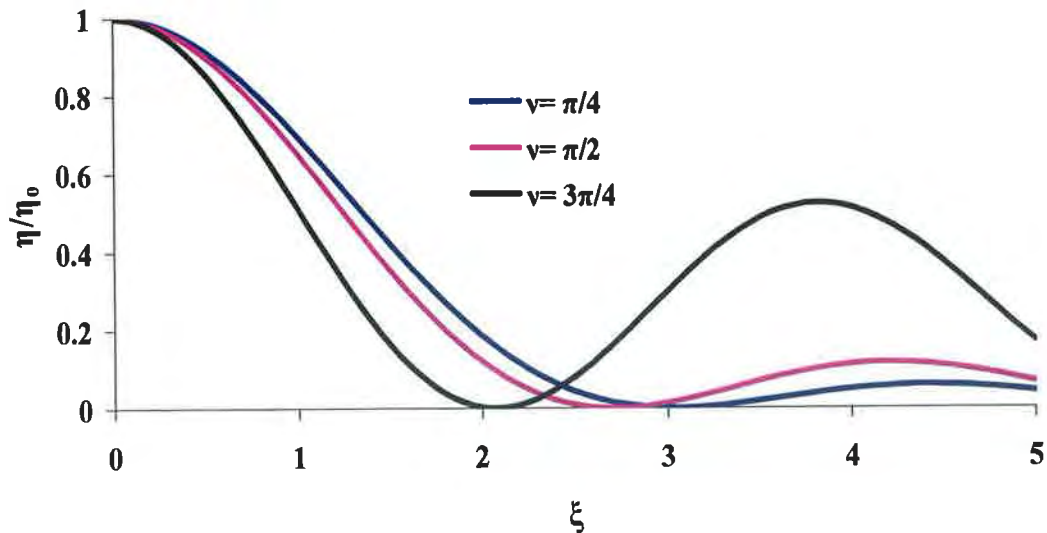


Figure 2.8 Transmission holograms-angular and wavelength selectivity of a phase hologram showing the normalized diffraction efficiency (η/η_0) as a function of the parameter ξ for various values of the parameter ν .

In the case of an absorption transmission hologram, formed by the spatial modulation of absorption constant (α_l) with no refractive index modulation ($n_l=0$) the coupling constant is defined as $\chi = -j\alpha_l/2$, $\nu_a = \alpha_l T/2 \cos \theta_0$ and the amplitude of the diffracted wave is

$$S(T) = -\exp\left(-\frac{\alpha T}{\cos \theta_0}\right) \exp(-j\xi) \frac{\sinh(\nu_a^2 - \xi^2)^{1/2}}{\left(1 - \xi^2/\nu_a^2\right)^{1/2}} [2.23]$$

For Bragg incidence ($\xi=0$), diffraction efficiency for an absorption grating obtained from the above equation 2.23 for an the absorption grating is

$$\eta = \exp\left(-2\alpha T/\cos \theta_0\right) \sinh^2\left(\alpha_l T/2 \cos \theta_0\right) [2.24]$$

The maximum possible diffraction efficiency is 3.7% obtained when $\alpha_l = \alpha$. Since $\alpha_l \leq \alpha$ the negative absorption (gain) in the medium can be excluded.

In unslanted reflection holograms, the recorded fringe pattern is parallel to the surface of the recording medium. When the hologram is illuminated with an incident wave from the left, the diffracted wave thus obtained gains in amplitude as it propagates towards the left of the recording material as shown in the figure (2.9).

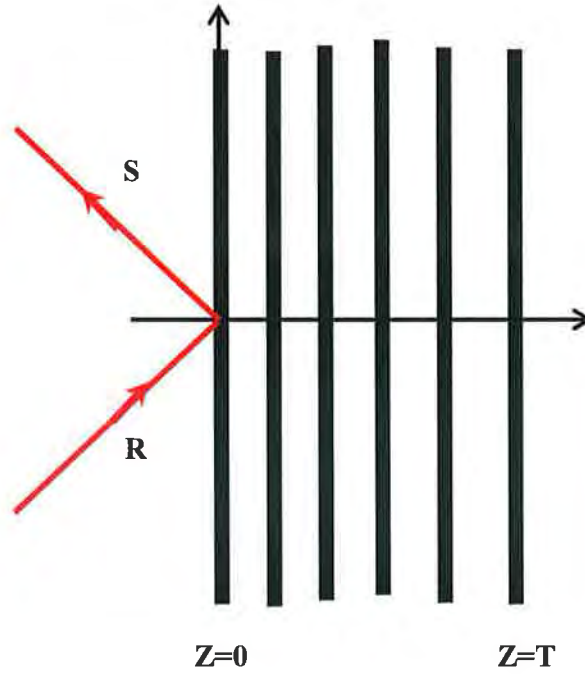


Figure 2.9 Volume reflection hologram

In a lossless phase hologram $\alpha = \alpha_1 = 0$ and $\chi = -j\alpha_1 / 2$, the amplitude of the diffracted wave $S(0)$ emerging from the hologram at $z=0$ is given by

$$S(0) = -j[(j\xi_r / \nu_r) + (1 - (\xi_r / \nu_r)^2)^{1/2} \coth(\nu_r^2 - \xi_r^2)^{1/2}]^{-1} \quad [2.25]$$

where

$$\xi_r = \frac{\Gamma T}{2 \cos \psi_0} \qquad \nu_r = \frac{\pi n_1 T}{\lambda_a \cos \psi_0}$$

$$\eta = [1 + (1 - (\xi_r / \nu_r)^2) / \sinh^2(\nu_r^2 - \xi_r^2)^{1/2}]^{-1} \quad [2.26]$$

When the grating is illuminated with the reference wave at the Bragg angle ($\xi_r = 0$), the equation to calculate the diffraction efficiency of the reflection hologram can be simplified and represented by $\eta = \tanh^2(\nu_r)$. The diffraction efficiency of the reflection hologram increases asymptotically to 100% with respect to ν_r . Figure 2.10 shows the normalized diffraction efficiency of the lossless phase holograms as a

function of the ξ_r , for the values of $v = \pi/4, \pi/2$ and $3\pi/4$. The diffraction efficiency drops to zero in all cases when $\xi_r \approx 3.5$.

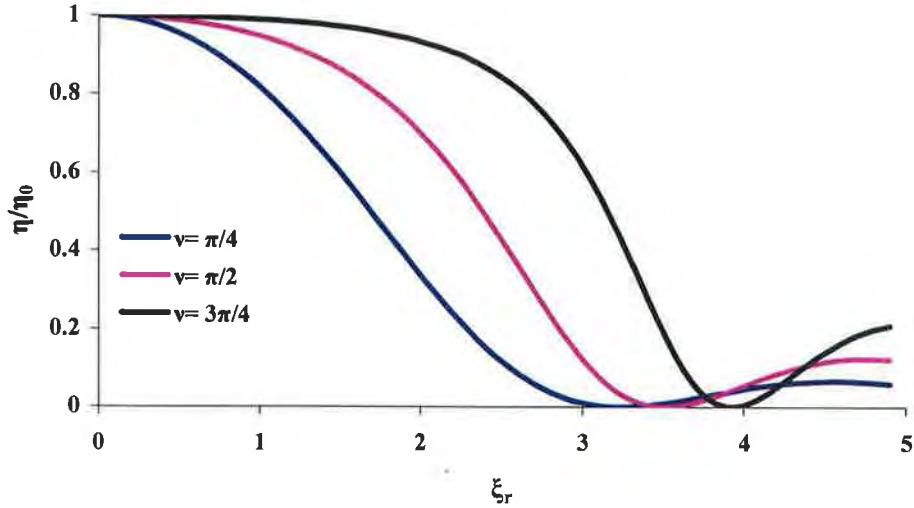


Figure 2.10 Reflection holograms shows the angular and wavelength sensitivity of a lossless dielectric grating with the normalised efficiency η/η_0 as a function of ξ_r .

In the case of an absorption reflection holograms, where $n_l=0$ while α and α_l remain finite, the diffracted wave amplitude emerging from the hologram can be represented as

$$S(0) = - \left\{ \frac{\xi_{ra}}{v_{ra}} + \left[\left(\frac{\xi_{ra}}{v_{ra}} \right)^2 - 1 \right]^{1/2} \coth(\xi_{ra}^2 - v_{ra}^2)^{1/2} \right\}^{-1} \quad [2.27]$$

where

$$v_{ra} = \frac{\alpha_l T}{2 \cos \psi_0} \quad \xi_{ra} = \frac{\alpha T}{\cos \psi_0} - j \frac{\Gamma T}{2 \cos \psi_0}$$

At Bragg incidence, $\Gamma=0$, the maximum diffraction efficiency that is possible when α_l takes on its maximum value $\alpha_l = \alpha$, is 7.2%.

Having summarised the coupled wave theory, the next section gives a brief description of colorimetric concepts relevant to colour holography.

2.4 Choice of laser wavelength

The CIE (International Commission on Illumination) diagram plays an important role in selecting the appropriate of laser wavelengths (colours) for recording full holograms. The CIE based on the chromaticity diagram (Figure-2.11) has set up a standard method for predicting the chromaticity of any colour that can be matched by additively mixing a set of primary colours.

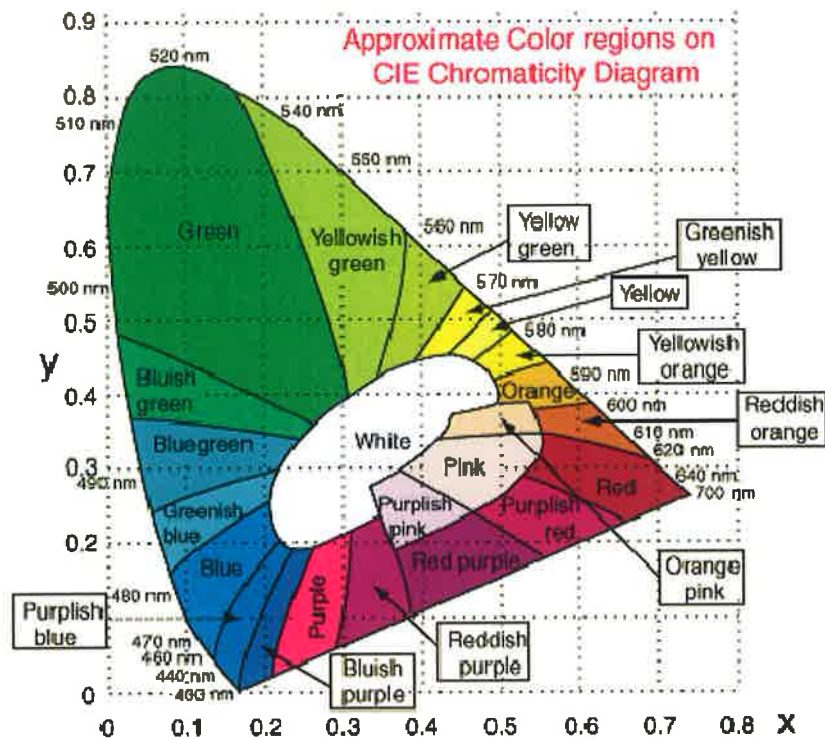


Figure 2.11 CIE chromaticity diagram [12].

The gamut of all visible colours on the CIE diagram has a tongue shape with all the colours of the visible spectrum on the curved edge and non spectral shades of purple on the straight edge. Less saturated colours appear in the interior with white at the centre. This colour space is based on direct measurements of human visual perception which in turn is associated with so called tristimulus values. These tristimulus values are the amounts of three primary colours in a three component colour model [12].

For full colour holography, it is essential to choose the recording wavelengths which can reproduce colours approximating to the colour of the object during reconstruction. These recording wavelengths are chosen based on the CIE chromaticity diagram which predicts the colours that can be reproduced. The chromaticity diagram provides a simple geometrical method to define the range of colours reproduced by additively mixing different spectral wavelengths. If three spectral wavelengths are used during recording, then all the colours that can be reproduced will be within the boundary of a triangle formed by joining the corresponding spectral wavelengths on the CIE diagram. A wide spectral range of colours means a large area on the CIE diagram would be covered by this triangle. A greater area on the CIE diagram can be covered by a polygon or any other irregular shape formed by the selection of a greater number of spectral wavelengths. However, the use of more spectral wavelengths complicates the holographic recording and is also subject to the availability of lasers and the recording materials.

In 1971 Thornton [13] showed the importance of wavelengths (while studying artificial lighting) near 450 nm, 540 nm, and 610 nm to give high luminous efficiency with maximum colour rendering index. These wavelengths can be used for recording holograms of reflective objects. Kubota and Nishimura [14] found 466 nm, 540.9 nm, and 606.6 nm as the optimum recording wavelengths, based on a reconstructing light source of 3400 K, for a 6 μm thick emulsion with a refractive index of 1.63 and an angle of 30° between the reference and object beam. By using these wavelengths they obtained exact reproduction of colours of the Macbeth Color Checker chart recorded as a hologram. Hubel and Solymar [15] did the theoretical and experimental analysis

on finding the ideal wavelengths for recording colour holograms. They suggested that, in practice the optimum wavelengths for recording full colour holography are 460 nm, 530 nm and 615 nm. Peercy and Hesselink [16] discussed wavelength selection based on the sampling nature of the holographic process. During the recording of a colour hologram, the chosen wavelength points sample the surface reflectance functions of the object. This sampling of colour can be studied by the tristimulus values of points in the reconstructed image, which is mathematically equivalent to the approximation of the tristimulus integrals. They used Gaussian quadrature and Riemann summation analysis, and found the wavelengths 437 nm, 547 nm and 665 nm from the former method and 475 nm, 550 nm and 625 nm from the later. Their sampling approach suggests that in order to record the object's spectral information accurately, four or five laser wavelengths are required.

Another factor that may influence the choice of the recording wavelengths is the availability of lasers for holographic recording, e.g., Argon ion, Krypton ion, Diode Pumped Solid State (DPSS) frequency doubled Nd:YAG, Helium Neon, and Helium Cadmium lasers. Recent progress in DPSS laser technology has brought both red and blue DPSS Lasers to the market. These lasers are small, air cooled and each laser requires less than a hundred watts of electric power to operate. Most likely, a set of three DPSS lasers will be the best choice of lasers for continuous wave colour holography in the future [17]. Bjelkhagen and Mirlis determined the error in colour rendition for different numbers of wavelengths and found that more than seven laser wavelengths produced a minimum error of 0.0026, while four or five laser sources should be optimum for recording high quality colour holograms [18].

However, in this project we used a 473 nm DPSS laser, a 532 nm Verdi laser and a 633 nm He-Ne laser to record full colour holograms in an acrylamide based photopolymer developed in the CIEO (Centre for Industrial and Engineering Optics) research laboratories.

2.5 Recording set-up

Single-beam Denisyuk geometry is the most promising arrangement to record reflection holograms for its simplicity and requiring no extra optical components such as beam splitters, mirrors after spatial filtering. However for this Denisyuk geometry, the recording material used should have high transmittivity or low optical density in order to have reasonably good beam ratio between the object and the reference beam. In this set-up the laser beam passes through the holographic recording medium and illuminates the object. The light reflected or scattered from the object illuminates the recording medium from behind and interferes with the incoming reference beam to record an interference pattern in the material. Figure-2.12 shows the basic set-up to record full colour reflection holograms based on Denisyuk geometry.

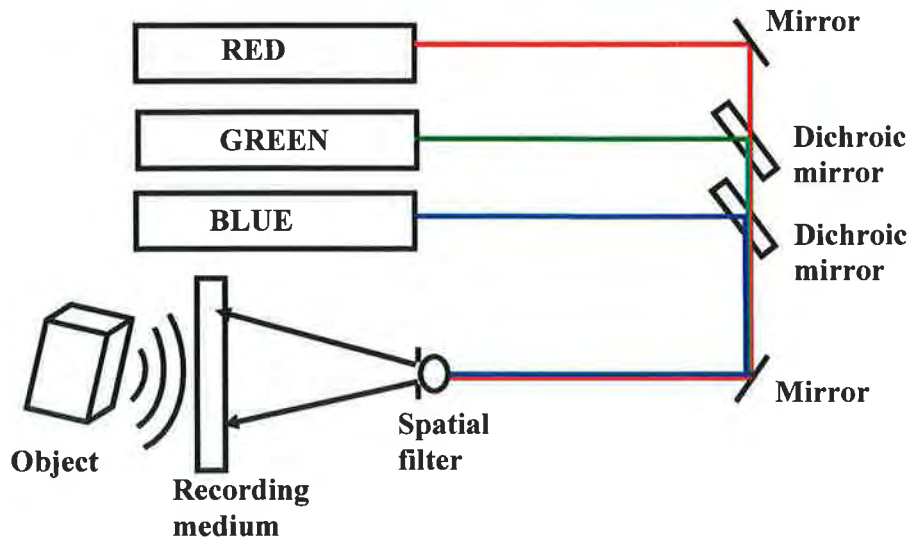


Figure 2.12 Multicolour hologram recording setup

In this arrangement three primary laser beams of red, green and blue wavelengths are combined using two dichroic filters. The combined laser beams pass through a spatial filter and illuminate the object through the holographic recording medium. The use of dichroic mirrors has advantages over movable mirrors as it simplifies the experimental set up and allows simultaneous recording at all wavelengths. The light intensity from the three lasers (red, green and blue) can be varied by using neutral density filters, and thus the overall exposure energy is controlled by varying the exposure time. It is essential during reflection holographic recording that the optical table is free from any vibration. So the whole set-up was arranged on a vibration free optical table. In the evaluation of the colour holographic reproduction process, it is also necessary to analyze the holographic image spectral distribution. A standard coloured object such as Munsell colour checker chart, recommended by the 1973 CIE Commission on colour rendering is used as an ideal object for colour characterization studies.

2.6 Recording material

An ideal recording material for most holographic applications should have high spatial frequency response, high diffraction efficiency, low scattering and high sensitivity. For commercial purposes the material should be recyclable, have long shelf life and be low cost. Several holographic recording materials are currently available in the market. Of these, silver halide photographic emulsion (SHPE) and red wavelength sensitive dichromated gelatin (DCG) are successful materials for recording of high efficiency full colour reflection holograms. The development and application of various panchromatic recording media for holographic recording is discussed below.

Silver halide emulsion is the best known holographic recording material for colour holography. Lin et al., [19] and Upatnieks et al., [20] were the first to record multicolour reflection holograms of two dimensional and three dimensional objects respectively. Lin and LoBianco [21] discussed techniques to solve the problems related to fringe visibility, emulsion shrinkage and low diffraction efficiency in recording colour holograms using Kodak 649F emulsion. They showed that increasing the laser coherence length (using an etalon) improved the fringe visibility. The shrinkage of the emulsion during recording was corrected by swelling the emulsion using triethanolamine after processing the hologram. They also showed that the diffraction efficiency of the holograms improved by reducing the silver halide concentration. Optical density improved due to the reduction of silver halide concentration in the emulsion leading to increase in absorption of the incident light which in turn increases the diffraction efficiency [21].

Hariharan et al., [22] introduced sandwich recording technique to improve image luminance/efficiency, using two different emulsions sensitive to different wavelengths. A hologram was recorded on Agfa 10E75 emulsion, sensitive at 633 nm. Blue and green holograms were recorded on Agfa 10E56 emulsion sensitive at 515 nm and 488 nm. The two holograms were then sandwiched together.

Silver halide photographic emulsions are the most popular materials for holographic recording. Although they are high sensitive materials, they have the limitation of scattering at shorter wavelengths. In 1979 Kubota and Ose [23] presented methylene blue sensitized dichromated gelatin which is essentially grainless material for recording colour holograms. Diffraction efficiency measured in this material was greater than 80% at blue (458 nm and 488 nm), and green (514.5 nm) wavelengths and about 60 % for red wavelength (633 nm). A laser power of 4 mW was used for recording at blue and green wavelengths, while 50 mW laser power was used for recording at red wavelength, since the material absorbs 75 % of light.

Kubota [24] used the technique of sandwiching two different photosensitive recording materials (DCG sensitive at 514.5 nm and 488 nm, and Agfa 8E75 sensitive at 633 nm) to record a full colour hologram. By recording simple holographic gratings at each wavelength separately, Kubota discussed the methods and processing procedures to improve the diffraction efficiency and the reconstructed wavelength in these materials. The transmittance of DCG varied from 75 % to 25 % for concentrations containing ammonium dichromate between 5 % and 23 % respectively. For 488 nm wavelength a maximum diffraction efficiency of 80 % was obtained for 5 % concentration. A similar result was obtained for 514.5 nm wavelength. A method for

controlling the reconstruction wavelength was by heating the hologram at around 100° C. For silver halide plate, isopropyl alcohol treatment was proposed for controlling the reconstruction wavelength. On the basis of these results a three dimensional colour object was successfully recorded in DCG and silver halide plates separately and the plates were then sandwiched together to get a full colour hologram.

Based on Hariharan's [22] sandwich technique, Hubel and Ward [25] used commercially available silver halide emulsions from Ilford. IlfordSP672T for blue and green and IlfordSP673T for red, and recorded full colour reflection holograms at 458 nm, 528 nm and 647 nm.

Jeong and Wesly [29] reported on the recording of the true colour holography in different recording materials such as silver halide, dichromated gelatin, DuPont photopolymer materials, and different sandwich combinations like Agfa-DuPont. The recording wavelengths that were used are 633 nm, 514 nm and 476 nm. Bjelkhagen and Vukicevic [30] introduced SLAVICH single layer panchromatic silver halide photo emulsion (Russian PFG-03). This was used to record colour hologram of test objects including the 1931CIE diagram and a ceramic mask of size 4" X 5". The holograms were recorded sequentially starting from blue wavelength at 488 nm, followed by green at 532 nm and red wavelength at 633 nm. The second and third exposures were calculated from the formula given by Johnson et al. [31]. Bjelkhagen and Huang [32] recorded large format holograms of a Chinese vase (12" X 16") in the SLAVICH material in the HOLOS colour holography facility. They also discussed the advantages of using dichroic filters to minimize the number of optical components to

simplify the recording geometry and more importantly simultaneous recording at all the wavelengths.

Bjelkhagen et al., [33] performed colorimetric evaluation of holograms recorded in SLAVICH emulsion in which recordings were made at 633 nm, 531 nm and 476 nm. A Macbeth Colour Checker chart was used as an object. The holograms were evaluated using a 12 Volt 50 Watt Phillips type 6438 GBJ halogen lamp to reconstruct the hologram. The 1931 CIE x, y coordinates were calculated for both the actual target and the holographic image of the target. Later in 2002, Bjelkhagen [34] recorded holograms of a French house and Peking masks (of size 4" X 5") with recording wavelengths of 476 nm, 532 nm and 647 nm in SLAVICH material. In that paper the author discussed the two imaging techniques used to record colour images. One was the colour holography which provides full parallax three dimensional colour images with a large field of view. The other one was Lippmann photography which was an old photographic technique.

Zhu et al., [35] reported on spectral response, photosensitivity and spectral selectivity of single layer panchromatic dichromated gelatin material for colour holography. They introduced methylene blue and rhodamine 6G (R6G) into photo crosslinking gelatin system as red and blue-green sensitizers to develop a new DCG material. Methylene blue is liable to separate out from the solution in an acidic state, and in alkaline state ammonium dichromate (ADC) have low sensitivity at green-blue region. Since R6G has good compatibility with methylene blue the authors [35] replaced ammonium dichromate with R6G to improve the sensitivity in the blue-green region. Using this combination maximum diffraction efficiency of 80 % was achieved for the

transmission gratings recorded at spatial frequency 1600 lines/mm, recorded at 633 nm, 514.5 nm, 488 nm, and 442 nm. The spectral characterization studies showed that the central peaks of spectral response curves of reflection gratings were very close to the original recording wavelength. The authors also reported a successful colour hologram recorded in a 7 X 7cm² DCG plate using three laser wavelengths 633 nm, 514.5 nm and 488 nm.

Sainov et al., [36] presented HP-P sensitive at blue, green and red wavelength regions. The average grain size of the ultra fine silver halide emulsion was less than 10 nm. The maximum diffraction efficiency of gratings recorded in the emulsion at 442 nm, 532 nm and 633 nm was 40 %, 50 % and 60 % respectively. They recorded multicolour holograms by using 442 nm, 532 nm and 633 nm wavelengths.

As mentioned above both silver halide photographic emulsions and DCG although record incredible holograms, still require wet chemical processing after recording and often is a limitation, For this reason photopolymers seem to be the most promising recording media for recording full colour holograms and other holographic applications due to their unique property of self-development. Thus panchromatic photopolymer recording materials are an alternative to photographic emulsions and DCG. DuPont's photopolymer film is one of the commercially available recording materials for making colour holograms [26]. Gambogi et al., [27] and Trout et al., [28] studied the performance of DuPont photopolymer material at three wavelengths 647 nm, 532 nm and 476 nm, and reported the diffraction efficiency ≥ 95 %. To achieve this diffraction efficiency, the material has to undergo UV cure and heat treatment

which in turn shows that the material is not completely self developing. Moreover, DuPont's photopolymer films are proprietary and available to licensees only.

Recently [37] a new photopolymer material (Bayfol HX) from Bayer Material Science for colour holographic recording has been introduced. The material is highly sensitive at 633 nm. This photopolymer material was based on cross linked matrix, with holographic gratings formed by photo polymerization.

The next chapter discusses the acrylamide based photopolymer that has been used to record full colour holograms in this project.

References

1. E.N.Leith and J.Upatnieks, "Wave-front reconstruction with diffused illumination and three-dimensional objects," J. Opt. Soc. Am. 54, 1295-1301 (1964).
2. Yu.N.Denisyuk, "Photographic reconstruction of the optical properties of an object in its own scattered radiation field," Sov. Phys, Doklady. 7, 543-545 (1962).
3. S.A.Benton, "Hologram reconstructions with extended incoherent sources," JOSA, 59, 1545- 1546 (1969).
4. T.H.Jeong, "Cyndrical holography and some proposed applications," JOSA, 57, 1396-1398 (1967).
5. J.Upatnieks, "Edge illuminated holograms," Applied optics, 31, 1048-1052 (1992).
6. J.T.McCrickered and N.George, "Holographic stereogram from sequential component photographs," Applied physics Letters, 12, 10-12 (1968).
7. R.J.Collier, C.B.Burckhardt, and L.H.Lin, "Optical holography," Academic Press, New York, 1971.
8. P.Hariharan, "Optical holography," Cambridge University Press, Cambridge, UK, 1986.
9. R.R.A.Syms, "Practical Volume holography," Clarendon press, Oxford, 1990.
10. H.Kogelnik, "Coupled wave theory for thick hologram grating," The Bell System Technical Journal 48, (2909-2947)1969.
11. R.J.Collier and K.S.Pennigton, "Multicolor imaging from holograms formed on two-dimensional media," Appl.Opt.6, 1091-1095 (1967).
12. <http://hyperphysics.phy-astr.gsu.edu/hbase/vision/cie.html#c2>.

13. W.A.Thornton, "Luminosity and color-rendering capability of white light," JOSA, 61, 1155-1163 (1971).
14. T.Kubota and M.Nishimura, "Recording and demonstration of cultural assets by color holography (II) - recording method of hologram for optimizing the color reproduction," J.Soc.Photogr.Sci.Tech.Jpn. 53, 297-302 (1990).
15. P.M.Hubel and L.Solymer, "Color reflection holography: theory and experiment," Appl. Opt. 30, 4190-4203 (1991).
16. M.S.Peercy and L.Hesselink, "Wavelength selection for true-color holography," Appl.Opt. 33, 6811-6817 (1994).
17. J.E.Ludman, H.J.Caulfield, J.Riccobono, "Holography for the new millennium," Springer, 2002.
18. H.I.Bjelkhagen and E.Mirlis, "Color holography to produce highly realistic three-dimensional images" Appl.Opt. 47, A123-A133 (2008).
19. L.H.Lin, K.S.Pennington, G.W.Stroke, and A.E. Labeyrie, "Multicolour holographic image reconstruction with white-light illumination," Bell Syst. Tech. J. 45, 659-661 (1966).
20. J.Upatnieks, J.Marks, and R.Fedorowicz, "Colour holograms for white light reconstruction," Appl. Phys. Lett. 8, 286-287 (1966).
21. L.H.Lin and C.V.LoBianco, "Experimental technique in making multicolour white light reconstructed holograms," Appl. Opt. 6, 1255-1258 (1967).
22. P.Hariharan, W.H.Steel, and Z.S.Hegedus, "Multicolor holographic imaging with a white-light source," Opt. Lett 1, 8- 9 (1977).
23. T.Kubota and T.Ose, "Lippmann color holograms recorded in methylene-blue sensitized dichromated gelatine," Opt. Lett. 4, 289-291 (1979).

24. T.Kubota, "Recording of high quality color holograms," Appl. Opt. 25, 4141-4145 (1986).
25. P.M.Hubel and A.A.Ward, "Color reflection holography," in Practical Holography III, S.A.Benton, ed., Proc. Soc. Photo- Opt. Instrum. Eng. 1051, 18-24 (1989).
26. W.K.Smothers, B.M.A.M.Weber, D.E.Keys, "Photopolymers for holography", Proc. SPIE 1212, 20-29 (1990).
27. W.J.Gambogi, W.K.Smothers, K.W.Steijn, S.H.Stevenson and A.M.Weber, "Color holography using DuPont holographic recording films," Proc. SPIE, vol. 2405, 62-73 (1995).
28. T.J.Trout, W.J.Gambogi and S.H.Stevenson, "Photopolymer materials for color holography," Proc. SPIE, vol. 2577, 94-105 (1995).
29. T.H.Jeong and E.Wesly, "Progress in true color holography," in Practical Holography IV, S. A. Benton, ed., Proc. SPIE. 1212, 183-190 (1990).
30. H.I.Bjelkhagen and D.Vukicevic, "Lippmann color holography in a single layer silver halide emulsion," in 5th Int. Symp. on Display holography, T.H.Jeong, ed., Proc. SPIE 2333, 34-38 (1995).
31. K.M.Johnson, L.Hesselink, J.W.Goodman, "Holographic reciprocity law failure," Appl. Opt. 23, 218-227 (1984).
32. H.I.Bjelkhagen and Q.Huang, "Largeformat color holograms recorded on ultra-high resolution silver-halideemulsion," Proc. SPIE, vol. 2866, 227-234 (1996).
33. H.I.Bjelkhagen, Q.Huang, and T.H.Jeong, "Progress in color reflection holography" Sixth Int. Symp. on Display Holography, T.H.Jeong, ed., Proc. SPIE 3358, 104-113(1998).

34. H.I.Bjelkhagen, "Super-realistic imaging based on color holography and lippmann photography", Proc. SPIE Vol. 4737, 131-141 (2002).
35. J.Zhu, Y.Zhang, G.Dong, Y.Guo and L.Guo, "Single layer panchromatic dichromated gelatin material for lippmann color holography," J. Optic. Comm. 241, 17-21 (2004).
36. V.Sainov, K.Zdravkov, E.Stoykova, B.Ivanov, D.Nazarova, B.Markova, S.Sainov, T.Petrova, " Multi colour holographic recording," J. Optoelectr. Adv. Materials, v.11, 1448-1451 (2009).
37. F.K.Bruder, F.Deuber, T.Facke, R.Hagen, D.Honel, D.Jurberg, M.Kogure, T.Rolle and M.Weiser, "Full-Color Self-processing Holographic Photopolymers with High Sensitivity in Red - The First Class of Instant Holographic Photopolymers," J.Photopoly. Sci. and Tech 22, 257-260 (2009).

CHAPTER 3

ACRYLAMIDE BASED PHOTOPOLYMER: RECORDING MECHANISM AND MODELS

3.1 Introduction

Photopolymers are volume phase holographic recording materials which basically consist of one or more photosensitive dyes, monomers, binder and free radical generator (electron donor). The most attractive feature of the photopolymer recording material used here is that it is completely self developing and no further processing is required after exposure. These types of photopolymers find application in holographic interferometry, holographic optical elements, holographic data storage and holographic displays. The first part in this chapter briefly describes the progress made in the acrylamide based photopolymer since late 1960s. The basic recording mechanism in this material is that, when an interference pattern of dark and bright regions is incident on the medium, the dye molecule absorbs a photon in the bright region and enters into a singlet excited state. This singlet excited dye molecule enters into a triplet excited state through intersystem crossing. The dye molecule in the excited state reacts with the electron donor to generate a free radical. This free radical in the presence of monomer initiates the polymerization reaction. As a result, a spatial density redistribution of material occurs. This redistribution of the material results in the refractive index modulation corresponding to the dark and bright region of the incident interference pattern. The following sections are aimed at explaining in detail the recording processes such as photo polymerisation, diffusion and refractive index modulation that occur during holographic recording.

3.2 Background

In 1969 Close et al., [1] were the first to use photopolymer as a recording material. Their photopolymer consisted of a monomer, a photosensitive dye and an initiator. In addition, dry photopolymers contained a polymeric binder. The photopolymer reported by Close et al., consisted of a polymeric solution formed using acrylamide, barium acrylate and lead acrylate as monomers and methylene blue, 4-nitrophenylacetic acid sodium salt and p-toluenesulfonic acid sodium salt as initiators. The holograms were made using a ruby laser operating at wavelength 694 nm and a diffraction efficiency of 45 % was obtained for exposure energy of approximately 300 mJ/cm². Jenney [2] optimised Close's photopolymer system and improved the sensitivity by adding lead or barium acrylate. The exposure energy required to achieve a diffraction efficiency of 45 % at 3000 lines/mm spatial frequency was 0.6 mJ/cm². Van Renesse [3] improved this acrylamide based photopolymer by adding N N'methylene-bis-acrylamide which served as a cross-linker to the main polymer network. In this way more stable holograms were recorded. However, the drawbacks of this system included lack of adhesion to the substrate and surface crystallisation of chemicals on the layers. Later Sugawara et al., [4] developed a photopolymer system consisting of acrylamide, NN'methylene-bis-acrylamide and a photo-reductant such as acetyl acetone or triethanolamine (TEA). They achieved a diffraction efficiency of 65 % for exposure energy of 50 mJ/cm². Sadlej and Smolinska [5] improved the shelf life of photopolymer system proposed by Jenny [2] by introducing polyvinylalcohol binder into the system. Polyvinylalcohol also helped to obtain dry photopolymer layers. Though this greatly improved the shelf life of the material, they achieved diffraction efficiency of 4.5 %. Jeudy and Robillard [6] made an interesting composition using a photochrome (indolino-spiropyran) as sensitiser and

polyvinylalcohol as binder. The interesting thing was that the sensitiser shifted its absorption band when excited with UV light to allow recording at 633 nm. (This sensitizing action takes place only when the material is irradiated with UV light). Diffraction efficiency of 80 % was achieved with exposure energy of 100 mJ/cm².

Calixto [7] extended the work on acrylamide based photopolymer systems by introducing a photopolymer composition that included acrylamide monomer, triethanolamine as electron donor, methylene blue dye as a sensitizer and polyvinylalcohol as binder. Diffraction efficiency of 10 % was achieved with exposure energy of 94 mJ/cm². Fimia et al., [8] increased the sensitivity of an acrylamide based photopolymer by reducing the inhibition time caused by the presence of oxygen. The photopolymer system that Fimia et al., used contained two photosensitive dyes, methylene blue sensitive at 633 nm and Rose bengal sensitive at 546 nm. Initially the photosensitive layer was uniformly exposed at 546 nm wavelength. The Rose Bengal dye absorbs the photon and excites into an excited state and reacts with the electron donor to generate free radicals. These generated free radicals react with the oxygen contained in the photopolymer layer and consumes it. Then a 633 nm red laser wavelength was used to polymerise the monomer for holographic recording. Diffraction efficiency of 40 % was achieved with exposure energy of 3 mJ/cm² at a spatial frequency of 1000 lines/mm.

Martin et al., [9] characterized Calixto's photopolymer composition using five different xanthene sensitising dyes to record at 514 nm wavelength. The shelf life of the recorded gratings was improved by the addition of a cross-linking monomer NN'-methylene-bis-acrylamide. Jallapuram [10] and Naydenova et al., [11] continued

the work carried out by Martin [9] and studied the diffusion processes that occurred immediately after an exposure of short duration. Transmission gratings were recorded at different spatial frequencies using exposure times of a fraction of a second. The growth of the diffraction efficiency was studied in real time by measuring the intensity in the first order from the recorded gratings. It was observed that two diffusion processes occurred in the material [12], monomer diffusion from the unexposed regions to the exposed regions and a second diffusion process involving short terminated and unterminated polymer chains diffusing from exposed regions to unexposed regions. It was also found that a PVA binder of lower percentage hydrolysis slows down both diffusion processes and improved the spatial resolution. The photopolymer composition was optimized to make reflection holograms at 532 nm. Diffraction efficiency of greater than 30 % was achieved in the reflection mode for recording at 4500 lines/mm spatial frequency [13].

In this work the acrylamide based photopolymer composition that was already optimised for recording in the green region [13] is used. The same photopolymer is further sensitized for recording at red and blue wavelengths to enable the photopolymer to be used for recording full colour reflection holograms. The next section explains the photochemical reactions that occur when the photopolymer recording material is exposed to light and the mechanism that occur during grating recording.

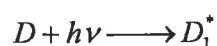
3.3 Recording mechanism

3.3.1 Photo polymerization

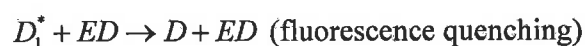
The photo polymerization process is light induced chemical phenomenon that occurs in photopolymer system, can be divided into three simple steps, initiation, propagation and termination [14] as discussed below.

Initiation

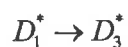
When the dye molecule D absorbs light of a particular wavelength within its absorption band, it is excited to a singlet state D_1^* .



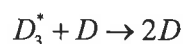
This excited singlet state is very unstable and returns to the ground state either by the emission of a photon (fluorescence) or by transferring non radiative energy to another molecule (electron donor- ED) and the process is called fluorescence quenching.



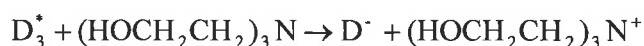
The excited singlet state dye molecule may undergo intersystem crossing into the triplet excited state where the life time of the dye molecules is longer.



The excited triplet state dye molecules may revert to the ground state by non radiative decay (triplet quenching) or by delayed emission of photons. At high dye concentrations, concentration quenching can also occur.



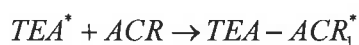
However formation of a free radical when light is incident onto the material is an important process. Triethanolamine (TEA) (HOCH₂CH₂)₃N is used as an electron donor in this photopolymer system. TEA donates an electron to the excited triplet state dye molecule D_3^* leaving the latter with one unpaired electron and an overall negative charge.



The TEA radical cation then loses a proton and becomes an uncharged free radical.



These free radicals in the presence of monomer initiate the polymerization reaction. The initiating free radical breaks the carbon-carbon double bond of the monomer and shares the free electron with one of the π electrons of the carbon atom in the double bond leaving behind the other carbon bond with an unpaired electron. The monomer in this case is acrylamide represented by ACR , while ACR_1^* denotes the primary monomer radical.



These free radicals will also react with dye radicals resulting in dye bleaching to form a transparent dihydro dye (or leuco dye). The bleaching rate in the presence of monomer could be less than in the absence of monomer. Bleaching of dye is also an important process in the making of holograms.

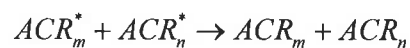
Propagation

The free radical generated in the initiation reaction attacks another monomer in a similar manner by breaking the carbon-carbon double bond. Each time the free radical attacks a monomer, the number of molecules in the polymer chain increases by one. This process continues until either all the monomer is consumed or a termination reaction occurs



Termination

Termination in a free radical polymerization process occurs either by disproportionation or combination. The disproportionation reaction occurs when a hydrogen atom is abstracted from one of the growing polymer chains by another, which finally leads to double bond formation on the first chain.



Termination also occurs by combination, when two free radicals meet and share their single odd free electrons forming a covalent bond resulting in single long polymer chain.



As a result of this polymerization mechanism each carbon double bond is converted into a carbon-carbon single bond lowering the molar refractivity. However, this is accompanied by an increase in density leading to a change in refractive index between polymerized regions and unpolymerized regions. The next section gives a more detailed explanation of the refractive index modulation during hologram formation.

3.3.2 Hologram formation mechanism (refractive index modulation)

When a photopolymer recording material is illuminated with an interference pattern of light, polymerization takes place in the bright region as explained in section 3.3.1 and as shown in figure 3.1.

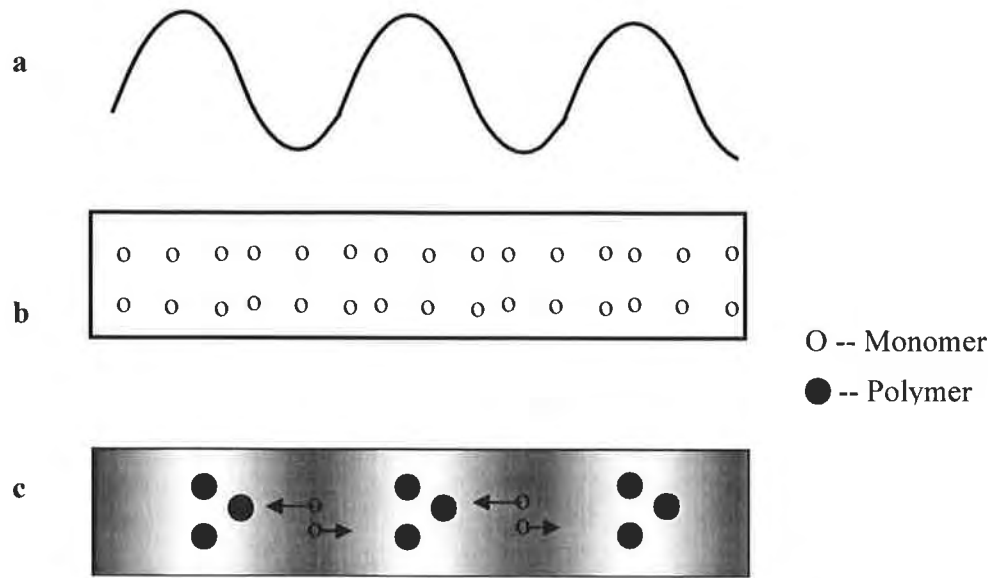


Figure 3.1 shows grating formation in a photopolymer; a- the intensity distribution, b- photopolymer before recording, and c- photopolymer during recording.

On polymerization, each double bond is replaced by two single bonds. This results in depletion of monomer in bright regions and a concentration gradient of the monomer resulting in the diffusion of monomer from the dark unexposed regions to the bright exposed regions. But the overall refractive index is higher in the polymerized region than the unpolymerized region due to the increased density. Holograms recorded by this mechanism are known as phase holograms. The diffraction efficiency of the hologram depends on the extent of refractive index modulation which in turn depends on the rates of polymerization and diffusion within the material. In a multi-component system, the exact mechanism of the change of the refractive index modulation is quite complex and depends on many physical and chemical factors and the composition of the photopolymer system itself. Tomlinson and Chandross [16] gave a detailed explanation of the change in the refractive index of the material that occurs as a result of polymerization. The refractive index modulation depends on the local composition of the material, that is the volume fractions of the concentrations of monomer (ϕ^m),

polymer (ϕ^p) and the binder (ϕ^b). Their sum is assumed to remain conserved at any point and at all times.

$$\phi^m + \phi^p + \phi^b = 1$$

The Lorentz-Lorenz equation shows the relation between refractive index n and the optical polarizability per unit volume P [16].

$$\frac{n^2 - 1}{n^2 + 2} = \frac{4}{3} \pi P$$

The polarizability per unit volume P for a pure substance is equal to the polarizability per molecule α , times the number density of molecules and we have

$$\frac{n^2 - 1}{n^2 + 2} = \frac{4\pi\rho N\alpha}{3M} = \frac{\rho R}{M}$$

where M is the molecular weight, ρ is the density of the substance, N is Avogadro number and R is the molar refractivity.

The molar refractivity of the photopolymer composition can be approximately related to the molar refractivities of its individual components and is given by

$$R = N_m R_m + N_p R_p + N_b R_b$$

where, N_m , N_p and N_b are the number of molecules of monomer, polymer and binder per unit volume respectively.

Aubrecht et al., [17] assumed that each particular density is proportional to the corresponding concentration and is given by

$$N_m = \frac{\phi^m \rho_m N}{M_m}, \quad N_p = \frac{\phi^p \rho_p N}{M_p}, \quad N_b = \frac{\phi^b \rho_b N}{M_b}$$

Where ρ_m , ρ_p , ρ_b are the specific gravities and M_m , M_p and M_b are the molar mass of the monomer, polymer and binder respectively.

The refractive index modulation is considered to be a linear function of the refractive indices and the concentrations of monomer and polymer and can be written as

$$\Delta n \sim \Delta\phi^m \left[\frac{n_m^2 - 1}{n_m^2 + 2} - \frac{n_b^2 - 1}{n_b^2 + 2} \right] + \Delta\phi^p \left[\frac{n_p^2 - 1}{n_p^2 + 2} - \frac{n_b^2 - 1}{n_b^2 + 2} \right]$$

where $\Delta\phi^m$ and $\Delta\phi^p$ are the change in volume fractions of monomer and polymer concentration respectively. It can be seen that the greater the difference between the refractive indices of the monomer or polymer and the binder, greater the change in the refractive index.

3.3.3 Diffusion model

As pointed out in the previous sections 3.3.1 and 3.3.2, hologram can be recorded in the photo polymer material in the form of the refractive index modulation between the bright and dark region. This results in the depletion of the monomer in bright regions and a concentration gradient of the monomer resulting in the monomer diffusion from the dark unexposed regions to the bright exposed regions. This section discusses the various diffusion models put forth for the hologram formation in dry photopolymer systems.

In 1994, Zhao and Mouroulis [18] solved a differential equation to describe the formation of first two order gratings in a dry photopolymer system using the one dimensional standard diffusion equation (Eq.3.1)

$$\frac{\partial u(x,t)}{\partial t} = \frac{\partial}{\partial x} \left[D(x,t) \frac{\partial u(x,t)}{\partial x} \right] - F(x,t)u(x,t) \quad [3.1]$$

where $u(x, t)$ is the monomer concentration, $F(x, t)$ is the polymerization rate, and $D(x, t)$ is the monomer diffusion coefficient. The ratio of diffusion rate to the polymerization rate is the key parameter that controls the hologram formation and it can be written as

$$\mathfrak{R} = \frac{D_0 k^2}{F_0} \quad [3.2]$$

where $k = 2\pi/d$ is the grating vector magnitude, d is the fringe spacing, D_0 is the diffusion constant and F_0 the polymerization rate constant. Numerical results showed that low recording intensities and smaller fringe spacing resulted in large \mathfrak{R} ($\gg 1$) values and qualitatively matched with the experimental results using the Du Pont HRF-600-10 film. The experiments were carried out at 514 nm for the spatial frequencies 666 lines/mm, 1000 lines/mm and 2000 lines/mm. Zhao and Mouroulis [19] extended the model by introducing the γ parameter representing the exponential relationship between recording intensity and the polymerization rate. This new parameter γ allowed the model to estimate diffusion in higher order gratings at low intensity. Later, the same group [20] examined the first and second order gratings strengths. This was done by measuring the diffraction efficiencies at first and second Bragg angles, recorded at difference intensities. It was found that high recording intensities resulted in weaker first order grating and stronger second order gratings in the DuPont photopolymers. Piazzolla and Jenkins [21] introduced a diffusion model

in which it was assumed that monomer diffusion was much faster than the grating formation. The model describes that the beam ratio controls the refractive index modulation at saturation. They confirmed their theoretical results by comparing the refractive index modulation at saturation with the experimental values. The experimental values were obtained from diffraction efficiency of the transmission gratings. Colvin et al., [22] extended Zhao and Mouroulis [18] work and showed the applicability of the diffusion modelling studies on the indigenously developed acrylate photosensitive polymer system. They extracted theoretical values of diffusion and polymerisation rate constants from the model and used them to obtain quantitative growth rate of the grating. Experimental values for the growth rate of the diffraction efficiencies were also obtained for the first and second order gratings. Their theoretical values fitted well with the experimental data, concluding that the model can be used for optimizing the performance of the materials and can be employed for other recording systems as well.

Loungnot et al [23] presented a theoretical model which correlated the variations in the monomer concentration with the efficiency of the grating. In their approach they introduced a diffusion parameter that depended on the local viscosity of the photopolymer recording material and also insisted that this parameter should be dependent on the space and time. This time dependence is related to the continuous conversion of the double bonds in to single bonds (during polymerisation) and the space dependence is related to the fringe spacing. Infra red spectroscopy can be used to study the presence of vibration modes in a molecule. Using this they obtained the experimental values of monomer percentage conversion with respect to time from the

optical density values of the recording material. An agreement between the theoretical calculations and the experimental results was obtained.

Karpov et al., [24] proposed a theoretical model for hologram recording using a bi-monomer photopolymer system. This model derived the rate equations, which is used to describe the sequence of chemical transformations in their photopolymers using appropriate wavelength. Based on the non linear nature of the diffusion process during polymerisation, they derived diffusion equations for the multi component system. The theoretical value of refractive index modulation thus obtained was compared with the experimental values.

Piazolla and Jenkins [25] further developed their previous model [21] to include free monomer diffusion in the photo polymerization mechanism. This model was validated by fitting the experimental results to the theoretical data in order to quantitatively predict the relationship between the recording intensity, (which they assumed constant) and the saturated diffraction efficiency. At higher recording intensity the free monomer diffusion rate is slow compared with the grating formation rate. They also discussed the variation in the refractive index modulation due to dark diffusion effects, which was not considered in their previous model [21].

To predict material behaviour at high spatial frequency, Sheridan and Lawrence [26] introduced a non-local material response function into the model proposed by Zhao and Mouroulis [18]. Non-local material response function represents the effect of monomer concentration at location x' and t' on the amount of material being polymerised at location x at time t . In this analysis [26], the non-local time dependent

effects were included and assumed to occur on a short timescale and therefore treated as instantaneous. They compared the theoretical solutions with the experimental diffraction efficiency growth curves and estimated parameters such as monomer diffusion constant and non local variance [27].

Moreau et al., [28] used the revised diffusion model proposed by Zhao and Mouroulis [18] to describe the combined photopolymerization and free monomer diffusion processes. Experimentally they determined the values of polymerization rate and diffusion coefficient of the DuPont photopolymer. To validate their model (Moreau et al.,) these experimental values were used in the quantitative simulation of the grating. From the simulation, they observed small delay during the growth of refractive index modulation (grating). This delay was concluded to be due to the presence of oxygen molecules in the material that prevented the photochemical reaction. Therefore the formation of polymerization chain will take place only after all the oxygen molecules have been consumed.

Blaya et al., [29] derived a set of analytical expressions for the temporal variation of the components of the photopolymer material assuming that the diffusion process at the time of recording process is negligible. They used the Lorentz–Lorenz relation, and determined the evolution of the refractive index modulation and the diffraction efficiency. From the theoretical studies, an estimation of the average chain length and kinetic parameters of the photo polymerization process can be obtained when intensity and concentrations (methylene blue, acrylamide and triethanolamine) were changed. Neipp et al., [30] used a first harmonic diffusion model to characterize an acrylamide based photopolymer material by analysing the effects of adding a cross-linking

monomer to this material and varying the material layer thickness. It was found that the addition of the cross linking monomer (N-N' methylene-bisacrylamide), increased the polymerization rate and slightly increased the refractive index modulation. The same authors showed [31] that the exact solutions for the first order of the monomer and polymer concentrations for the refractive index modulation can be obtained, provided the polymerization rate was constant. From the analysis, it was shown that the saturated refractive index modulation depends not only on the refractive index of the polymer but also on the refractive index of the binder.

Kelly et al., [32] revised the non-local polymer diffusion model in order to incorporate the non-ideal kinetic behaviour in which immobilized polymer chains were dominated by free radicals. They compared the extracted parameters of the polymerization process for the cases of two chain terminating mutually and termination by free radical. The experiments carried out in acrylamide based photopolymer were seemed to fit better with free radical termination model. Gallego et al., [33] proposed a three dimensional model to analyse the formation of refractive index profiles of acrylamide based photopolymers with different viscosities ranging from 2×10^{-13} cm²/s (high viscous systems) to 5×10^{-9} cm²/s (low viscous systems) and for different intensity attenuations inside the material (by varying the dye concentrations). This model showed that the recording materials with high viscosity provides greater uniformity in the refractive index profile, though resulting in lower index modulation and large amount of residual monomers. This type of high viscous photopolymer systems finds application in multiplex holographic recording.

Kelly et al., [34] further extended the non-local polymer diffusion model to examine the volume changes that occur in the photopolymer during the recording process. They examined the evolution of the refractive index modulation for short exposures and showed that for short exposures the influence of volume changes is negligible. Gallego et al., [35] presented a three dimensional model to analyse thick holographic gratings recorded in acrylamide based photopolymers. The diffraction efficiency in the first order was determined by using an algorithm based on rigorous coupled wave theory and analysed the diffraction efficiency of the gratings recorded at different intensities. They showed that the effective optical thickness increases with the increasing exposure intensity. Gleeson et al., [36] extended the polymer driven diffusion model by including effects of oxygen based inhibition and time varying absorption of the material during exposure. They experimentally observed that by exposing with high intensity the initial inhibition period can be reduced.

Gallego et al., [37] solved the equations of the model [33] using finite difference methods to analyse the monomer diffusion in thick photopolymer materials. Gleeson et al., revised [38] the non local diffusion model by including effects of non-steady state kinetics, spatial and temporal non local polymer chain growth, time-varying photon absorption, diffusion-controlled viscosity effects, multiple termination mechanisms, and inhibition. Then using the model they obtained the key parameters such as initiation, polymerization, termination rate and monomer diffusion rate constants. They validated this model [38] by applying the theoretical values thus obtained to the fit of experimental diffraction efficiency measurements for two different materials (acrylamide based photopolymer and epoxy resin based photopolymer). Zhai et al., [39] presented a model to estimate the effect of uniform

post exposure on existing holographic gratings, and experimentally verified that the refractive index modulation of the existing grating continues to increase under the influence of dark and uniform post exposure.

Experimental studies on diffusion processes in acrylamide based photopolymer were also carried out at the CIEO. Feely [40] conducted a study on the diffusion of dye molecules through amplitude gratings for various spatial frequencies. In 2004 Naydenova et al., [11] measured the kinetics of the refractive index modulation of the material after short exposure and were able to distinguish two diffusion processes – diffusion process 1 that occurs from dark fringe regions to bright fringe regions and diffusion process 2 that occurs from bright to dark fringe regions. They concluded that the diffusion process 1 was faster and led to an increase of the refractive-index modulation and was ascribed to monomer diffusion. The second diffusion process made a negative contribution to the refractive index modulation. It was responsible for the poor performance of the photopolymer at high spatial frequency of recording and was ascribed to short terminated and unterminated polymer chains. In 2005, Martin et al., [12] proposed a two way diffusion model that explained the fall off in diffraction efficiency in non cross linked gratings and observed that the cross linker contributed to high spatial frequency. Babeva et al., [41] presented a two-way diffusion model for short-exposure holographic grating formation in the acrylamide-based photopolymer. The model predicted that the experimentally observed drop in refractive-index modulation at high spatial frequency was due to both monomer and polymer diffusion. It also distinguished between short polymer chains capable of diffusing and long polymer chains that are immobile.

3.4 Scattering in the material

An important characteristic of the holographic recording material is its scattering at lower wavelength which can be measured as a bidirectional scattering distribution function BSDF. BSDF is the ratio of the intensity of the scattered light $P_{scatter}$ (as function of angle θ) to the incident intensity $P_{incident}$ per unit solid angle $\Omega_{detector}$ as shown in equation 3.3 [42, 43] and is measured using the scatterometer shown in figure 3.2.

$$BSDF(\theta) = \frac{P_{scatter}(\theta)}{P_{incident} \Omega_{detector}} \quad (3.3)$$

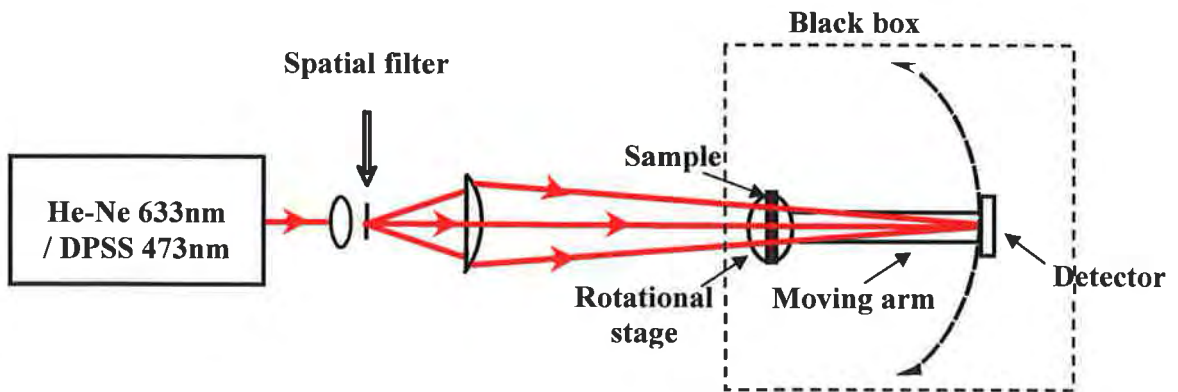


Figure 3.2 Scatterometer set up to measure BSDF

The BSDF was obtained by measuring the scattered light intensity as a function of angle using two laser wavelengths (at 473 nm and 633 nm) by illuminating the sample with a spatially filtered converging beam. The experiments were done at these two wavelengths so as to cover a wide range of the visible region. The intensity of the incident light on the sample placed on the rotational stage, was $0.8 \mu\text{W}$ and $0.65 \mu\text{W}$ for blue and red wavelengths respectively. The spot radius of the laser beam on the sample was 1 cm. The detector (Newport 1830C Optical Power Meter) was placed on

the moving arm to measure the angular dependence of the intensity. The rotational stage arm was controlled by a LabView programme. The distance from sample to the detector was 24.5 cm and an aperture of 1 mm diameter was placed in front of detector. This complete scatterometer setup was enclosed in a black box to minimize stray light reaching the detector.

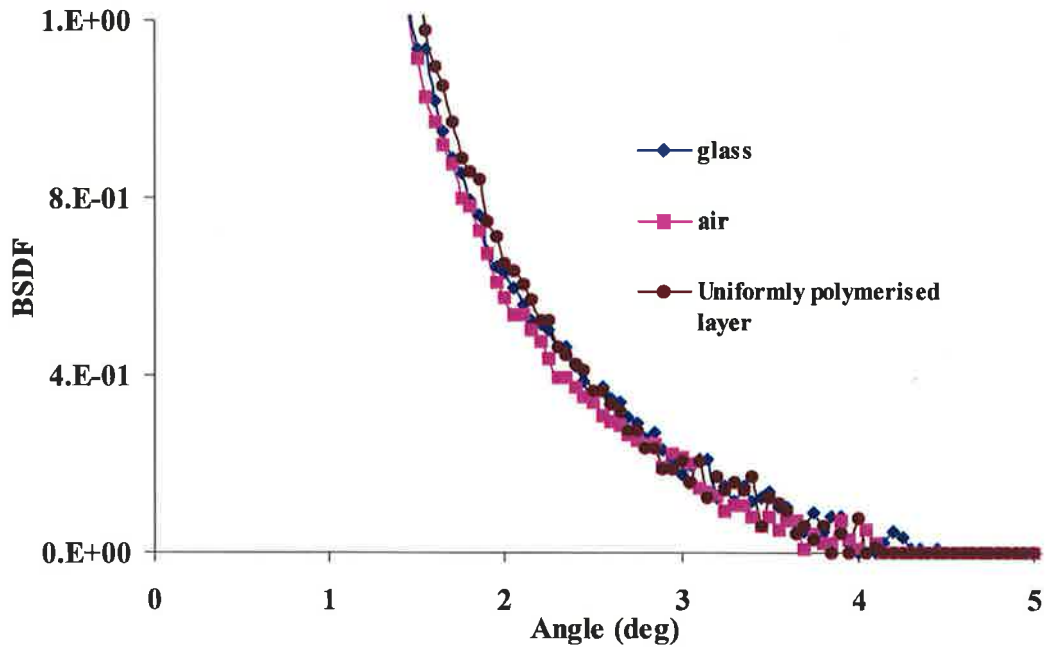


Figure 3.3 BSCDF data for the air (blue diamond), glass (pink square) and uniformly polymerised layer (brown diamond) measured at 473nm.

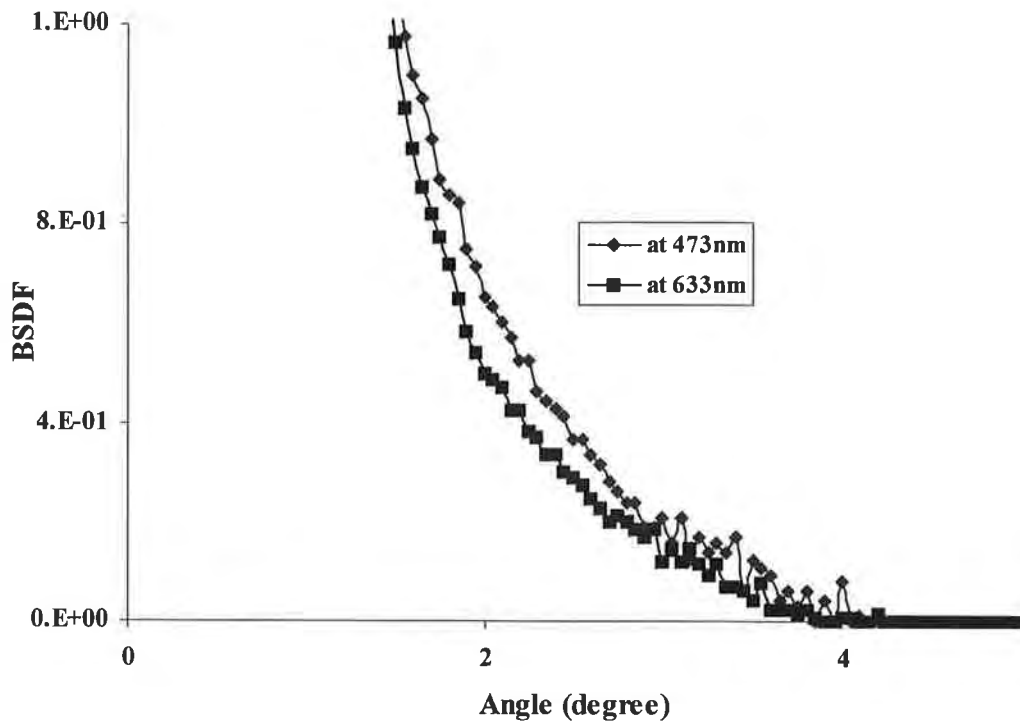


Figure 3.4 Shows the BSDF of the uniformly polymerised photopolymer layer measured at 633nm (black square) and 473nm (brown diamond).

The BSDF graphs for the air, glass and uniformly polymerised layer at 473nm are shown in figure 3.3. From the graph it can be observed that the scattering of the uniformly polymerised layer is close to that of the glass and air which indicates that the material is characterised by very low scattering. Figure 3.4 shows the BSDF data of the uniformly polymerised layer measured at 633 nm in comparison with data measured at 473 nm. As expected the scattering is greater at the shorter wavelength, 473 nm than at longer wavelength 633 nm. From these experiments it can be concluded that the total scattering of the layers with thickness of 60 μm is very low and negligible in the present composition of ABP. This is because the photopolymer material is grainless unlike silver halide photographic emulsions. From the above results we believe that this photopolymer material is suitable for reflection holographic recording.

Having understood the basic recording mechanism for the photopolymer the next target is the development of acrylamide based photopolymer full colour reflection holographic recording. The next chapters describe the recording of holographic gratings using CIEO developed photopolymer material at 633 nm, 473 nm as a part of developing the material for full colour reflection holographic recording.

References

1. D.H.Close, A.D.Jacobson, J.D.Margerum, R.G.Brault, and F.J.McClung, "Hologram Recording on Photopolymer Materials," *Appl. Phys. Lett.* 14, 159-160 (1969).
2. J.A.Jenny, "Holographic recording in photopolymers," *J. Opt. Soc. Am.* 60, 1155-1161 (1970).
3. R.L.Van Renesse, "Photopolymers in Holography," *Opt. Laser Technol.* 4, 24 (1972).
4. S.Sugawara, K. Murase, and T. Kitayama, "Holographic Recording by Dye-Sensitized Photopolymerization of Acrylamide," *Appl. Opt.* 14, 378-382 (1975).
5. N.Sadlej and B.Smolinska, "Stable photo-sensitive polymer layers for holography", *Opt. Laser Tech.* 175–179 (1975).
6. M.J.Jeudy and J.J.Robillard, "Spectral Sensitization of a Variable Index Material for Recording Phase Holograms with High Efficiency", *Opt. Comm.* 13, 25-28 (1975).
7. S.Calixto, "Dry polymer for holographic recording", *Appl. Opt.* 26, 3904–3909 (1987).
8. A.Fimia, N.Lopez and F.Mateos, "Acrylamide photopolymers for use in real time holography: Improving energetic sensitivity", *Proc. SPIE* 1732, 105–109 (1992).
9. S.Martin, P.Leclere, Y.Renotte, V.Toal and Y.Lion, "Characterisation of an acrylamide-based dry photopolymer holographic recording material", *Opt. Eng.* 33, 3942–3946 (1994).

10. R.Jallapuram, "Optimization of an acrylamide-based photopolymer for reflection holographic recording" Ph.D thesis, submitted to Dublin Institute of Technology (2005).
11. I.Naydenova, R.Jallapuram, R.Howard, S.Martin and V.Toal, "Investigation of the diffusion processes in a self-processing acrylamide-based photopolymer system", *Appl. Opt.*, 43, 2900-2905 (2004).
12. S.Martin, I.Naydenova, R.Jallapuram, R.Howard and V.Toal, "Two way diffusion model for the recording mechanism in a self developing dry acrylamide photopolymer", *Proc.SPIE*, 6252, 37-44 (2006).
13. I.Naydenova, H.Sherif, S.Martin, J.Raghavendra, V.Toal, "A Holographic sensor". Patent number: WO2007060648A3.
14. K.Matyjaszewski, T.P.Davis, "Handbook of Radical Polymerization", John Wiley and Sons (2002).
15. A.Reiser, "Photoreactive polymers". The science and technology of resists, John Wiley and Sons (1989).
16. W.Tomlinson and E.Chandross, "Organic photochemical refractive index image recording systems," in *Advances in Photochemistry*, T. N. Pitts, G. S. Hammond, K.Gallnik, and D.Grosjier, eds., Wiley Interscience, London (1980).
17. I.Aubrecht, M.Miler, I.Koudela, "Recording of holographic diffraction gratings in photopolymers: theoretical modelling and real-time monitoring of grating growth", *J.Mod.Opt*, 45, 1465-1477 (1998).
18. G.Zhao and P.Mouroulis, "Diffusion-model of hologram formation in dry photopolymer materials," *J. Mod. Opt.*41, 1929–1939 (1994).

19. G.Zhao and P.Mouroulis, "Extension of a diffusion-model for holographic photopolymers," *J. Mod. Opt.* 42, 2571–2573 (1995).
20. G.Zhao and P.Mouroulis, "Second-order grating formation in dry holographic photopolymers," *Opt. Commun.* 115, 528–532 (1995).
21. S.Piazzolla and B.K.Jenkins, "Holographic grating formation in photopolymers," *Opt. Lett.* 21, 1075–1077 (1996).
22. V.L.Colvin, R.G.Larson, A.L.Harris and M.L.Schilling "Quantitative model of volume hologram formation in photopolymers" *J. Appl. Phys.* 81, 5913–5923 (1997).
23. D.J.Loungnot. P.Jost and L.Lavielle, "Polymers for holographic recording. VI. Some basic ideas for modelling the kinetics of the recording process Pure," *Appl. Opt.* 6, 225–245 (1997).
24. G.M.Karpov, V.V.Obukhovsky, T.N.Smirnova and V.V.Lemeshko, "Spatial transfer of matter as a method of holographic recording in photoformers," *Opt. Commun.* 174, 391–404 (2000).
25. S.Piazzolla and B.K.Jenkins, "First-harmonic diffusion model for holographic grating formation in photopolymers," *J. Opt. Soc. Am. B* 17, 1147–1157 (2000).
26. J.T.Sheridan and J.R.Lawrence, "Nonlocal response diffusion model of holographic recording in photopolymer," *J. Opt. Soc. Am. A* 17, 1108–14 (2000).
27. J.R.Lawrence, F.T.O'Neill and J.T.Sheridan, "Photopolymer holographic recording material parameter estimation using a nonlocal diffusion based model," *J. Appl. Phys.* 90, 3142–3148 (2001).

28. V.Moreau, Y.Renotte and Y.Lion, "Characterization of DuPont photopolymer: determination of kinetic parameters in a diffusion model," *Appl. Opt.* 41, 3427–3435 (2002).
29. S.Blaya, L.Carretero, R.F.Madrigal, M.Ulibarrena, P.Acebal and A.Fimia, "Photopolymerization model for holographic gratings formation in photopolymers," *Appl. Phys. B* 77, 639–662 (2003)
30. C.Neipp, S.Gallego, M.Ortuno, A.Marquez, A.Belendez and I.Pascual, "Characterization of a PVA/acrylamide photopolymer. Influence of a cross-linking monomer in the final characteristics of the hologram," *Opt. Commun.* 224, 27–34 (2003)
31. C.Neipp, S.Gallego, M.Ortuno, A.Marquez, M.L.Pascual, A.Belendez and I.Pascual, "First-harmonic diffusion-based model applied to a polyvinyl-alcohol–acrylamide-based photopolymer" *J. Opt. Soc. Am. B* 20 2052–2060 (2003)
32. J.V.Kelly, F.T.O'Neill, J.T.Sheridan, C.Neipp, S.Gallego and M.Ortuno, "Holographic photopolymer materials: nonlocal polymerization-driven diffusion under non ideal kinetic conditions," *J. Opt. Soc. Am. B* 22 407–16 (2005).
33. S.Gallego, M.Ortuno, C.Neipp, A.Marquez, A.Belendez, I.Pascual, J.V.Kelly and J.T.Sheridan, "Three dimensional analysis of holographic photopolymers based memories," *Opt. Express* 13 3543–3557 (2005)
34. J.V.Kelly, M.R.Gleeson, C.E.Close F.T.O'Neill, J.T.Sheridan, S. Gallego and C. Neipp, "Temporal analysis of grating formation in photopolymer using the nonlocal polymerization-driven diffusion model" *Opt. Express* 13 6990–7004 (2006).

35. S.Gallego, M.Ortuno, C.Neipp, A.Marquez, A.Belendez, E.Fernandez and I.Pascual, "Three-dimensional characterization of thick grating formation in PVA/AA based photopolymer," *Opt. Express* 14, 5121–5128 (2006).
36. M.R.Gleeson, J.V.Kelly, C.E.Close, F.T.O'Neill and J.T.Sheridan, "Effects of absorption and inhibition during grating formation in photopolymer materials," *J. Opt. Soc. Am. B* 23, 2079–2088 (2006).
37. S.Gallego, C.Neipp, M.Ortuno, A.Belendez, E.Fernandez and I.Pascual, "Analysis of monomer diffusion in depth in photopolymer materials," *Opt. Commun.* 274, 43–49 (2007).
38. M.R.Gleeson, S.Liu, R.R.McLeod, and J.T.Sheridan, "Nonlocal photopolymerization kinetics including multiple termination mechanisms and dark reactions. Part II. Experimental validation," *JOSA B*, Vol. 26, 1746-1754 (2009).
39. Q.Zhai, S.Tao, T.Zhang, X.Song and D.Wang, "Investigation on mechanism of multiple holographic recording with uniform diffraction efficiency in photopolymers," *Optics Express*, Vol. 17, 10871-10880 (2009).
40. C.A.Feely, "Development and characterisation of red sensitized photopolymer holographic recording material" Ph.D thesis, University of Dublin, 1998.
41. T.Babeva, I.Naydenova, D.Mackey, S.Martin, and V.Toal, "Two-way diffusion model for short-exposure holographic grating formation in acrylamide based photopolymer," *J. Opt. Soc. Am. B* , Vol. 27, (197-203) 2010.
42. J.C.Stover, "Optical scattering: measurement and analysis" second edition, SPIE Press (1995).

43. Á.Kerekes, E.Lőrincz, P. S. Ramanujam and S. Hvilsted, "Light scattering of thin azobenzene side-chain polyester layers", Opt. Comm. 206, 57-65 (2002).

CHAPTER 4

HOLOGRAPHIC RECORDING AT 633 NM IN AN ACRYLAMIDE BASED PHOTOPOLYMER

4.1 Introduction

The main objective of this work as mentioned in the previous chapters is to develop a self processing acrylamide based photopolymer to record full colour reflection holograms for display applications. Previously this photopolymer was well established for recording reflection holograms at 532 nm wavelength [1]. A considerable amount of work was done by Feely et al., [2, 3] to record transmission gratings using this photopolymer composition, at 633 nm wavelength. Here, as a first step towards reaching the goal, the same photopolymer composition [1] with a photosensitive dye absorbing at 633 nm was used to record high spatial frequency (4200 lines/mm) reflection holographic gratings at 633 nm using He-Ne laser. The influence of nanoparticles on the diffraction efficiency of the gratings was also studied.

The work described in this chapter is aimed at

1. Revisiting the sensitisation of this self processing acrylamide based photopolymer at 633 nm and record holographic transmission gratings.
2. Recording reflection holographic gratings at this wavelength using the same composition.
3. Enhancing the diffraction efficiency of the reflection holographic gratings by doping the photopolymer with Si- MFI zeolite nanoparticles.

4. Spectral characterization of both doped and undoped nanoparticle photopolymer compositions.

4.2 Sample preparation

The photosensitive material consists of acrylamide (monomer), N-N' methylene bisacrylamide (co-monomer), polyvinyl alcohol (binder), triethanolamine (electron donor) and methylene blue (photosensitive dye). The composition is shown in table-4.1. The photopolymer solution was prepared by adding 0.25 g of N-N' methylene bisacrylamide, 0.8 g of acrylamide and 2 ml of triethanolamine to 17.5 ml of 10 % w/v polyvinyl alcohol (PVA) stock solution. The solution was thoroughly mixed using a magnetic stirrer to make sure that the acrylamide and bisacrylamide were completely dissolved in the PVA stock solution. 3 ml of photosensitive dye stock solution (0.11 g / 100 ml) was then added to the above solution and mixed thoroughly to obtain a homogenous photopolymer solution.

Table 4.1 Photopolymer composition

10 % w/v PVA aqueous solution	Acrylamide	N-N'methylene bisacrylamide	Triethanolamine	0.11 % w/v of MB dye
17.5 ml	0.8 g	0.25 g	2 ml	3 ml

Two separate volumes 0.6 ml and 0.3 ml of this photopolymer solution was gravity settled on thin optically transparent glass plates of size 2.5 cm x 7.5 cm. The samples were left to dry for 6 to 7 hours in a dark room. The thicknesses of the corresponding layers after drying were $60 \pm 5 \mu\text{m}$ and $30 \pm 5 \mu\text{m}$ respectively, was measured using a white light surface profilometer ADE Phase Shift MicroXAM 100. Figure 4.1 shows the absorption spectrum of the dry photopolymer layer confirms good absorption in

the red wavelength region. The absorption was measured using a Perkin-Elmer Lambda 900 UV-VIS-NIR absorption spectrometer.

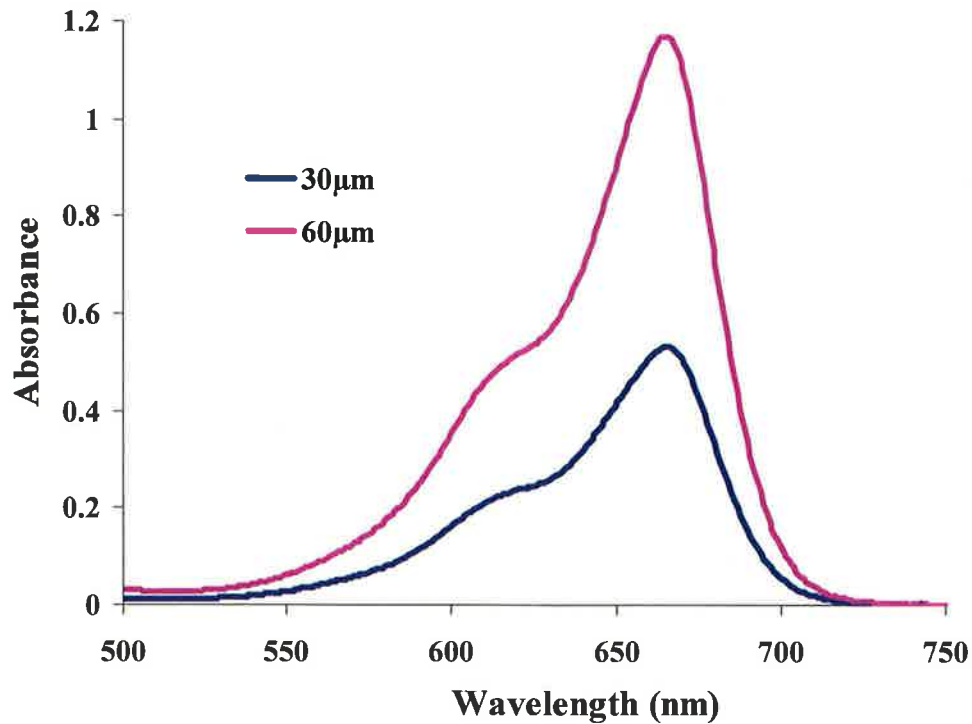


Figure 4.1 Absorption spectrum of dry photopolymer layer sensitized to record at 633 nm

4.3 Recording of transmission gratings at 633 nm

Recording of transmission gratings at 633 nm was revisited so as to confirm the reproducibility of results obtained by Feely et al., [2]. This was done by repeating the experiments to measure diffraction efficiency of transmission gratings with fringe spacing (d) of 1 μm and 0.5 μm , which correspond to spatial frequencies of 1000 lines/mm and 2000 lines/mm respectively. The experimental setup for recording transmission gratings is shown in figure 4.2.

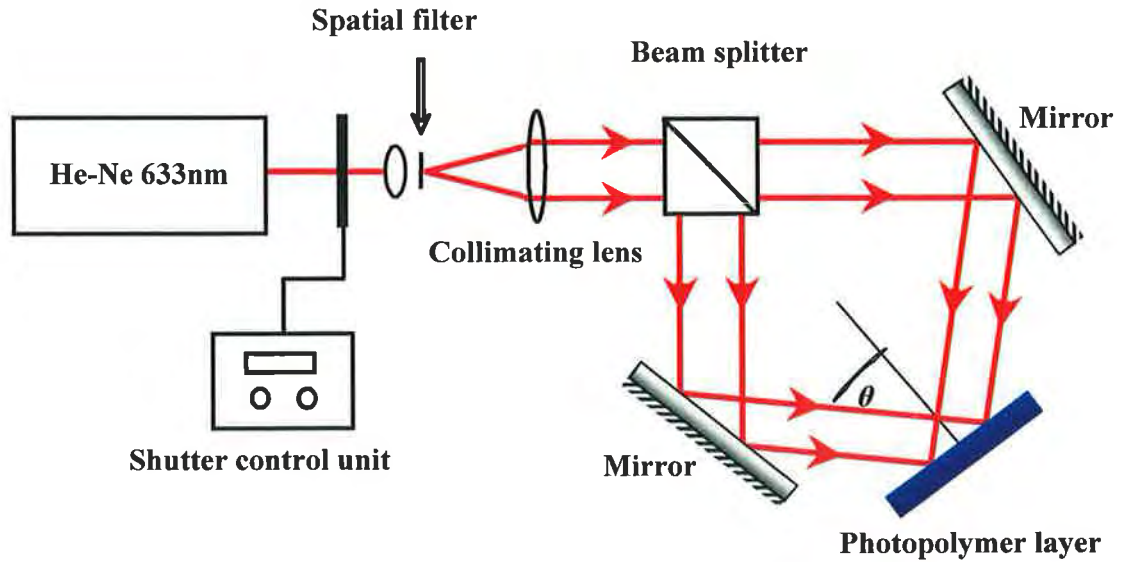


Figure 4.2 Experimental setup for recording transmission gratings

The light from the He-Ne laser ($\lambda=633$ nm) was spatially filtered and collimated. The collimated beam was then split into two beams using a beam splitter (60:40). Better visibility is possible with the 50:50 beam splitter which in turn will improve diffraction efficiency, which was unavailable in lab. The two beams were then directed onto the photosensitive plate using two adjustable mirrors. These beams make an angle θ_B with the plate, calculated using the Bragg equation 2.2.

Transmission gratings were recorded using different exposure times with an intensity of 3 mW/cm^2 in $60 \text{ }\mu\text{m}$ thick photopolymer layers. The corresponding diffraction efficiency was measured in the first order beam by using a 532 nm green laser. As the material is less sensitive at 532 nm, exposure at this wavelength using a very low probe beam intensity ($100 \text{ }\mu\text{W/cm}^2$) for few seconds should not greatly affect the diffraction efficiency of the grating. The diffraction efficiency (η) is defined as the ratio of the light intensity diffracted in the first order (I_1) to the incident reading beam intensity (I_0). The η % is given as

$$\eta\% = \frac{I_1}{I_0} \times 100 \quad (4.1)$$

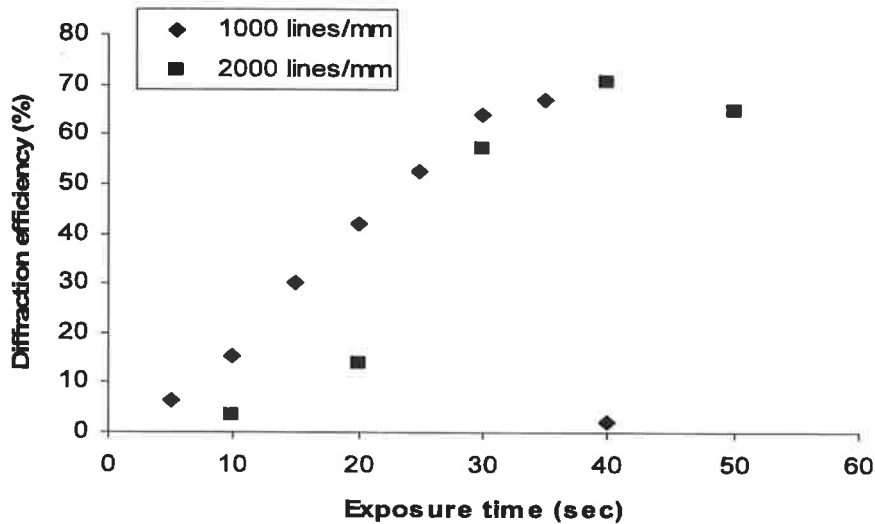


Figure 4.3 Diffraction efficiency as a function of exposure time for transmission gratings recorded at 1000 lines/mm and 2000 lines/mm spatial frequency for 633nm.

Figure 4.3 shows the graph of the diffraction efficiency as a function of exposure time. The diffraction efficiency increases with exposure time. Maximum efficiencies of 65% and 70% were obtained for gratings with spatial frequency of 1000 lines/mm and 2000 lines/mm respectively.

4.4 Reflection gratings recorded at 633 nm

This section discusses the best recording conditions for recording reflection holograms to achieve the highest possible diffraction efficiency in this photopolymer system. The experimental set up for recording the reflection holographic gratings at higher spatial frequency (4200 lines/mm) is shown in figure 4.4. The spatially filtered laser beam (He-Ne laser) was collimated and split into two beams using a beam

splitter. The two beams were then diverted using two adjustable mirrors onto the photopolymer layer from opposite sides to record the reflection holographic gratings.

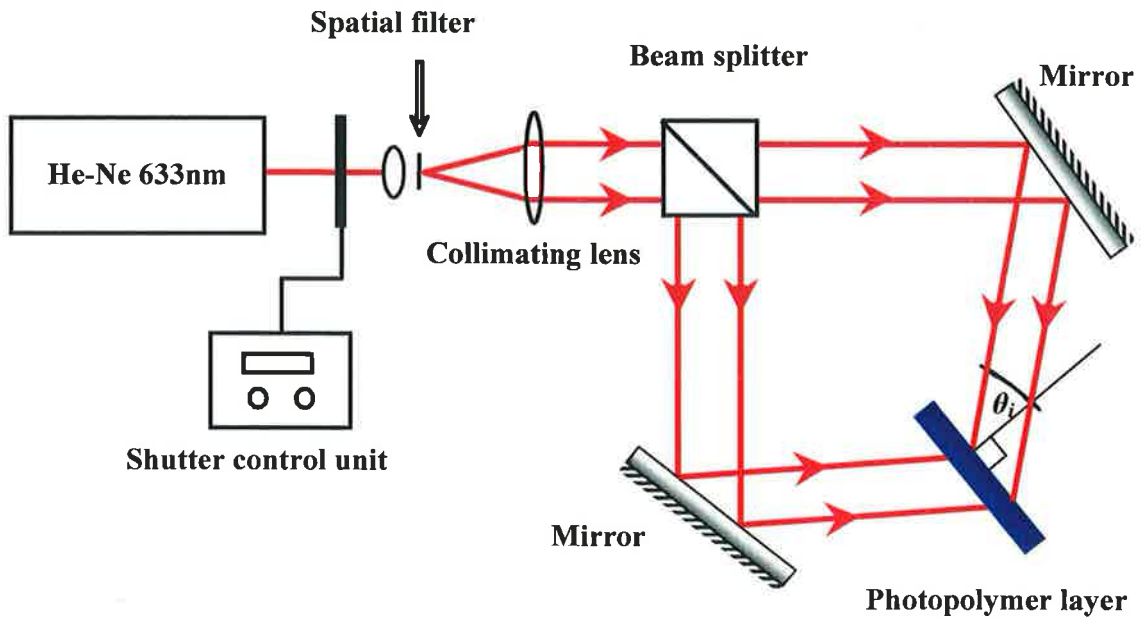


Figure 4.4 Experimental setup for recording reflection grating

The angle inside the photopolymer layer between these two beams is calculated using Bragg's diffraction equation (Eq. 2.2).

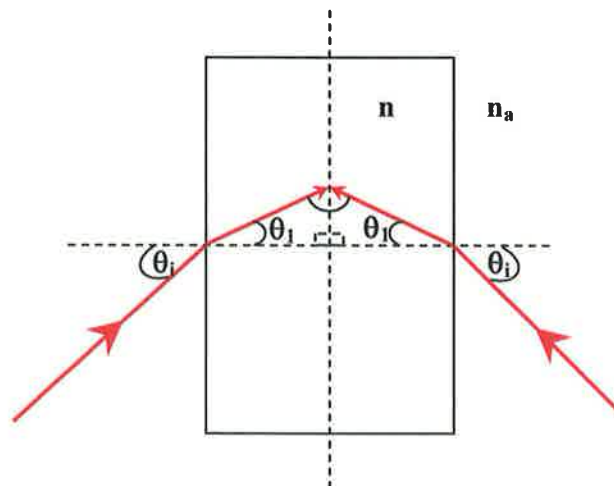


Figure 4.5 Recording geometry (cross section view) of reflection gratings.

The inter beam angle inside the photopolymer layer can be determined using Snell's law. Figure 4.5 shows the cross sectional view of the recording geometry, where n_a is the refractive index of air, θ_i is the incident angle outside the material, θ_l is corresponding refraction angle of the light in the material.

In this experiment, the incident angle 40° was chosen to illuminate the photopolymer layer from outside and this angle corresponds to half of the recording inter beam angle which is $\theta = 64.62^\circ$ inside the photopolymer layer. This value corresponds to a spatial frequency of 4200 lines/mm for a wavelength of 633 nm.

The photopolymer layers used for recording reflection gratings were prepared as explained in section 4.2. Gratings were recorded for different exposure times with intensities of 3 mW/cm^2 and 1.5 mW/cm^2 on layers of thickness $60 \text{ }\mu\text{m}$ and $30 \text{ }\mu\text{m}$. The experiments were done at two intensities only, due to the limited laser power available. The diffraction efficiencies of the reflection gratings, measured by exposing the grating to one of the recording beams are shown in figures 4.6 and 4.7. The percentage diffraction efficiency ($\eta\%$) was calculated using equation 4.1.

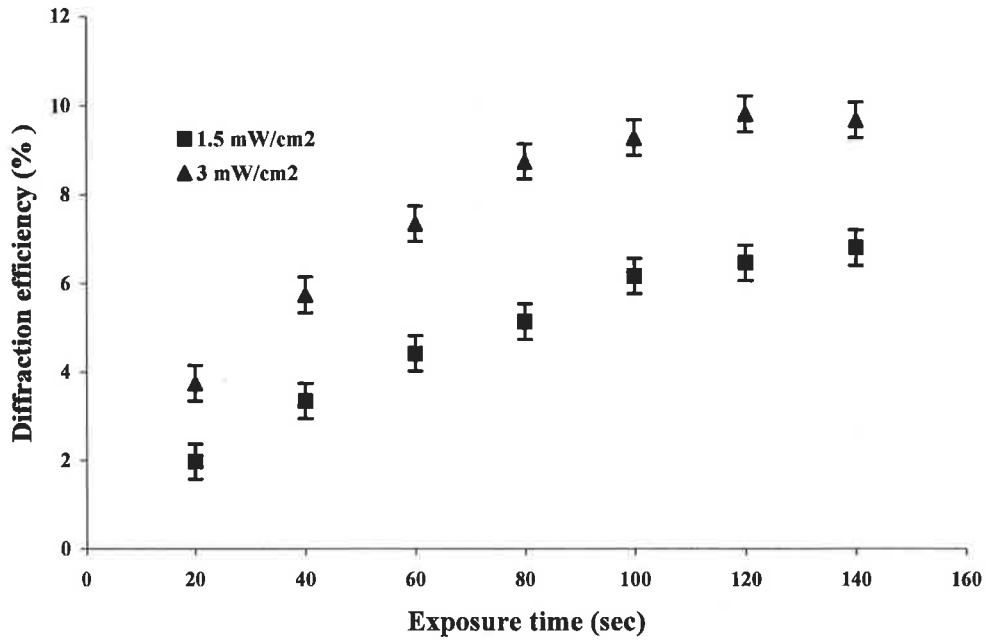


Figure 4.6 Diffraction efficiency (%) of reflection gratings (4200 lines/mm) as a function of exposure time (sec) for layer thickness of 60 μm at two intensities (3 mW/cm^2 and 1.5 mW/cm^2).

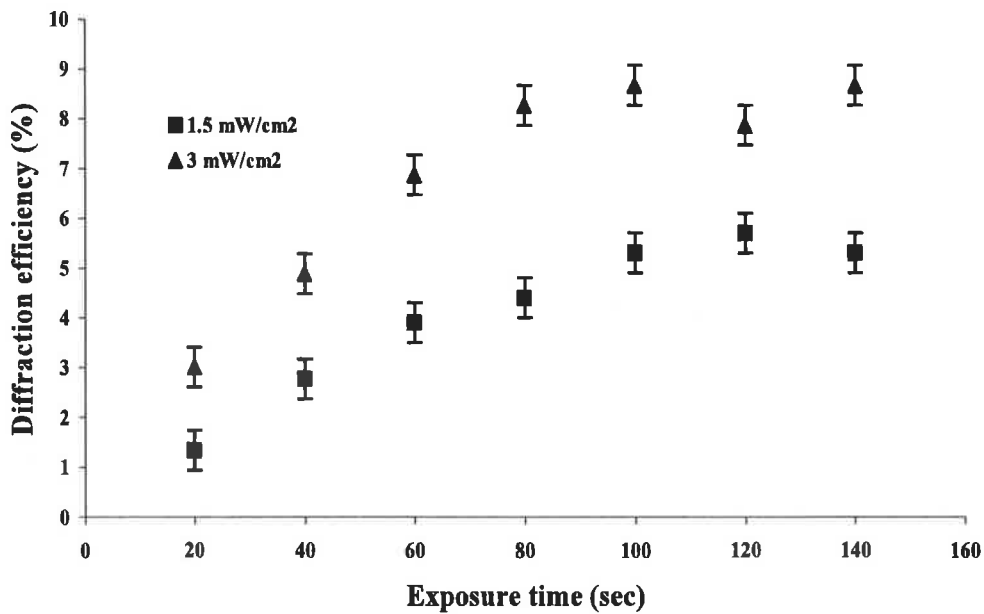


Figure 4.7 Diffraction efficiency (%) of reflection gratings (4200 lines/mm) as a function of exposure time (sec) for a 30 μm thick layer at two recording intensities (3 mW/cm^2 and 1.5 mW/cm^2).

Figures 4.6 and 4.7 show that in both cases (30 μm and 60 μm) the diffraction efficiency of the gratings increases with time of exposure, and reaches a maximum of 9.8 % and 6.5 % for 60 μm thick layer for recording intensities of 3 mW/cm^2 and 1.5 mW/cm^2 respectively; For a 30 μm thick layer, diffraction efficiencies of 8.6 % and 5.7 % were achieved for 3 mW/cm^2 and 1.5 mW/cm^2 respectively. It can be observed that there is not much difference between the two thicknesses in the trend of growth of diffraction efficiency. However there is a small increase in the final diffraction efficiency for the gratings recorded at higher recording intensities (3 mW/cm^2) compared to lower recording intensity (1.5 mW/cm^2).

To conclude finally, from these experiments the best conditions within the available range of laser power for recording the highest possible diffraction efficiency gratings were determined. The possibility for improving the diffraction efficiency by doping with zeolite Si-MFI nanoparticles was investigated and will be discussed in the following section.

4.5 Doping with nanoparticles

The main reason for doping the photopolymer with nanoparticles was to increase the refractive index modulation, which in turn increases the diffraction efficiency of recorded holographic gratings [4-5]. Zeolites are microporous crystalline materials with uniform pore size distribution and well defined ordered structure. They are compatible with acrylamide based photopolymer, and layers with good optical quality are easy to produce [6]. Here in this study the photopolymer was doped with 1.8 % w/v aqueous solution (stock solution) of 30 nm size Si-MFI zeolite nanoparticles. Figure 4.8 shows the schematic representation of Si-MFI nanoparticle [7]. Naydenova

et al., improved the diffraction efficiency of the grating by increasing the refractive index modulation using these nanoparticles [8].



Figure 4.8 Schematic representation of Si MFI nanoparticle [7].

The optical properties of an acrylamide-based photopolymer doped with Si-MFI zeolites were studied by Babeva et al., [9]. Studies using spatially resolved Raman spectroscopy and AFM on the redistribution of Si-MFI zeolite nanoparticles within a photopolymer layer during recording of holographic gratings at a spatial frequency of 200 lines/mm were also reported [10]. The concentration 2.5 %, 5 %, and 7.5 % of the nanoparticles is calculated with respect to the mass of the photopolymer to obtain three different Si-MFI concentrations in the photopolymer layers. The holographic recording setup shown in figure 4.4 was used to record reflection gratings at a spatial frequency of 4200 lines/mm at an intensity of 3 mW/cm². The dry photopolymer layer thicknesses was maintained to be 30 μ m at all nanoparticle doped concentrations in order to have a common thickness, and was confirmed by measuring with white light

interferometer. The measured diffraction efficiencies of the gratings recorded in doped and undoped layers are shown in figure 4.9.

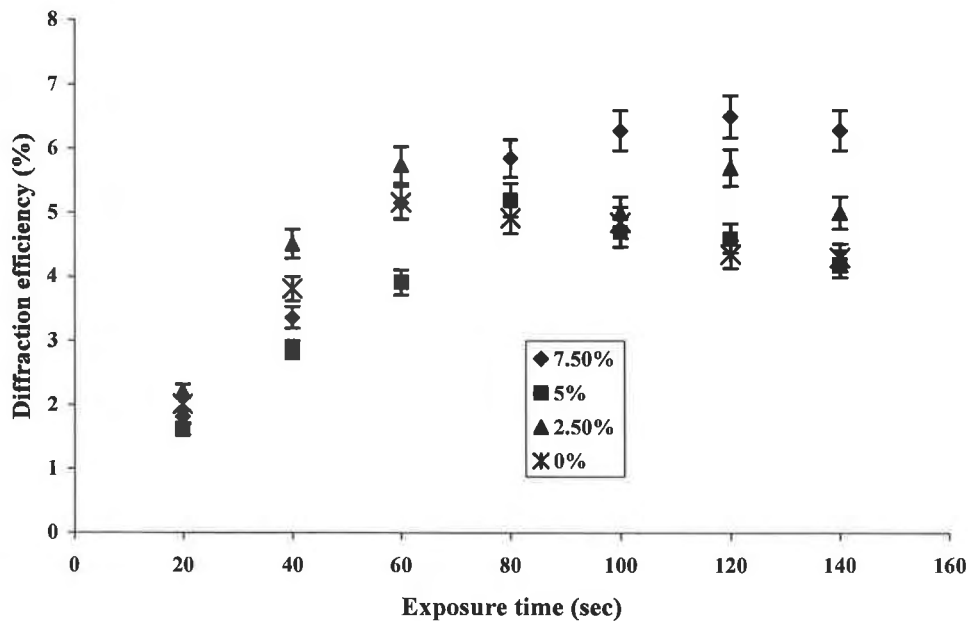


Figure 4.9 Comparison of diffraction efficiency growth profiles for the reflection gratings recorded at 633nm for four different concentrations of zeolite nanoparticles (Si-MFI).

From figure 4.9 it can be observed that the diffraction efficiency for the recorded gratings for undoped photopolymer composition (0 %) reaches a maximum of 5 % and saturates at about 4.5% as time of exposure increases. The nanoparticle doped composition (2.5 %, 5 % and 7.5 %) show little improvement in maximum diffraction efficiency. In these cases the diffraction efficiency was little higher, with a maximum of approximately 6 %, and saturates as time of exposure increases.

The reconstructed wavelengths may differ from the recorded wavelengths in holographic gratings due to the dimensional changes (swelling and shrinkage), so the spectral characteristics of the doped and undoped gratings were determined, as discussed in following section.

4.6 Spectral characterisation

In this section the holographic gratings that were recorded in photopolymer with the four different concentrations of Si-MFI (0%, 2.5%, 5%, and 7.5%) were measured using the experimental setup shown in figure 4.10. A halogen white light (Avantes, AvaLight-HAL [10]) was coupled into an optical fibre and collimated using a collimating lens. The collimated beam is made to incident on the recorded grating approximately at Bragg angle. The diffracted light from the grating was coupled into a second optical fibre connected to an Avantes AvaSpec-2048 spectrum analyser. The spectral characterization of the diffracted beam was measured as a function of the nanoparticle concentrations and is shown in figure 4.11.

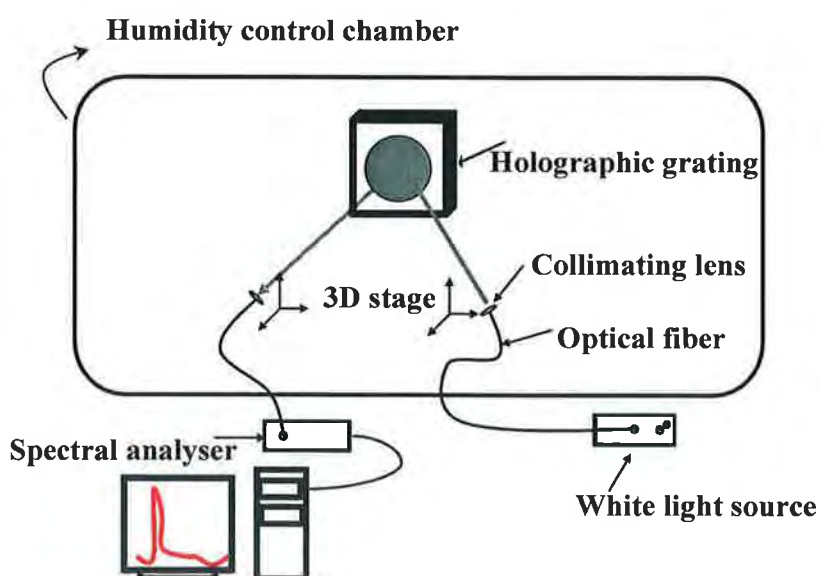


Figure 4.10 Experimental setup used for spectral characterisation of the reflection gratings.

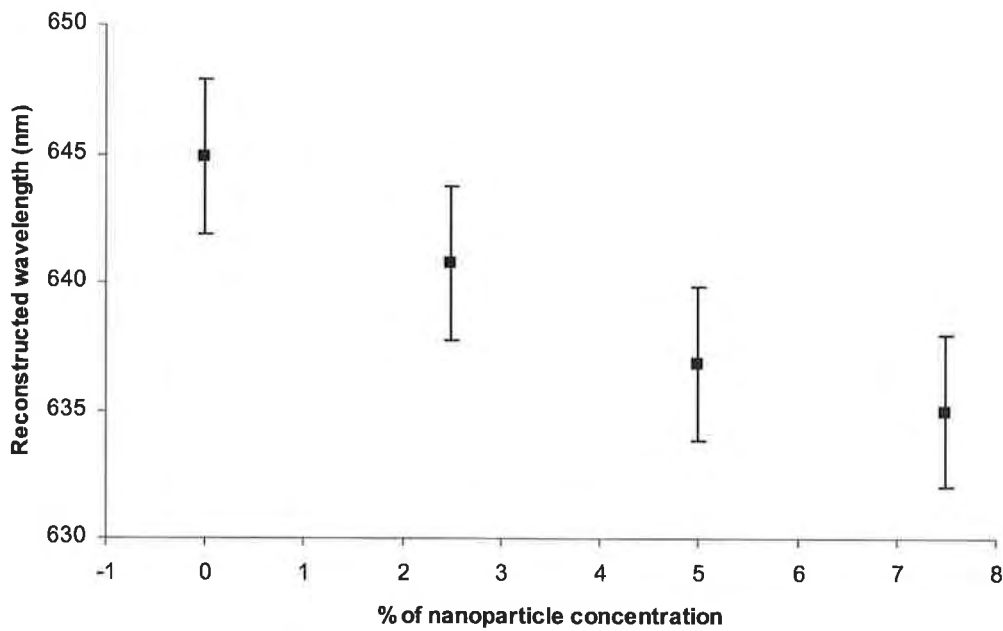


Figure 4.11 Bragg peak wavelengths as function of nanoparticle concentration for the gratings recorded at 633nm wavelength.

In figure 4.11 it can be seen that for the undoped photopolymer composition (0%) the Bragg peak wavelength of the diffracted beam was 644.9 nm. This shows a swelling of the material which is the dimensional changes in recorded holographic gratings that correspond to 1.88%. This value is obtained by calculating the unit increment of the Bragg peak wavelength. Bragg peak wavelengths of 640.7 nm, 636.8 nm and 635 nm are obtained for 2.5%, 5% and 7.5% nano-particle concentrations in the photopolymer which correspond to swelling of 1.21%, 0.6% and 0.3% respectively.

4.7 Reflection holograms

Reflection holograms were recorded in 30 μm thick photopolymer layer with an intensity of 3 mW/cm^2 using Denisyuk recording geometry. Figures 4.12 shows the photographs of the reconstructed reflection holographic images of the recorded object when illuminated using a white light (spot lamp).

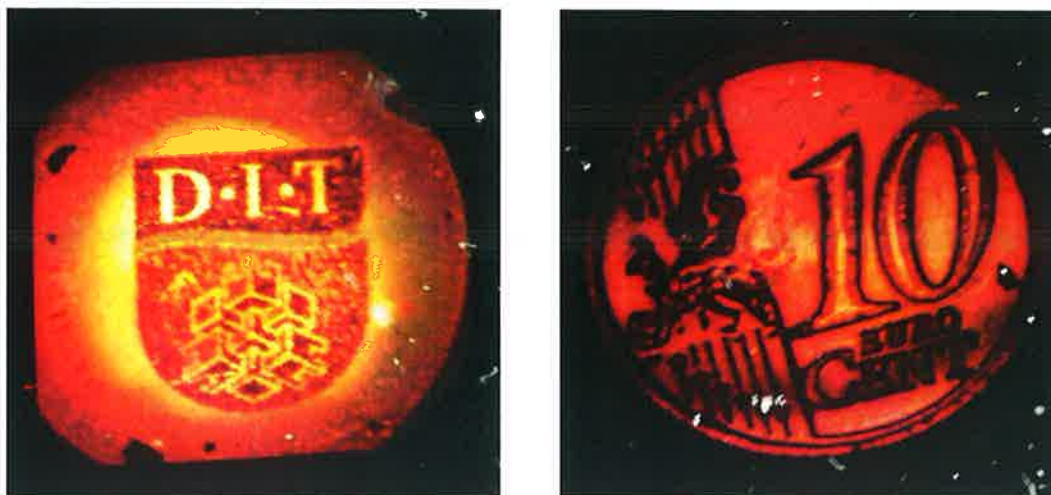


Figure 4.12. Photographs of white light holographic reconstructions after recording with a red laser at 633nm.

4.8 Conclusion

To summarise, the sensitisation of self processing acrylamide based photopolymer at 633 nm has been revisited by recording transmission gratings. With good results from the recording of the transmission gratings the same composition was used to record reflection holographic gratings at the same wavelength. A diffraction efficiency of the reflections gratings increased with time of exposure. An efficiency of 9.8 % and 6.5 % was achieved for 60 μm thick layer, at intensities 3 mW/cm^2 and 1.5 mW/cm^2 respectively. For 30 μm thick layer and at the same intensities, a diffraction efficiency of 8.6 % and 5.7 % was achieved. The diffraction efficiency of the reflection holographic gratings was only slightly improved by doping the photopolymer with Si-MFI zeolite nanoparticles. Finally from the spectral characterization studies of both doped and undoped nanoparticle photopolymer composition it can be concluded that even though there is very small improvement in the diffraction efficiency with available intensity, swelling can be reduced from 1.21 % to 0.3 % with a concentration of 7.5 % nanoparticle doping.

The next chapter explains sensitisation of the photopolymer at 473 nm, recording transmission and reflection gratings at this wavelength. It also includes spectral characterisation of the diffracted beam from the reflection gratings for both doped and undoped photopolymer composition.

References

1. R.Jallapuram, "Optimization of an acrylamide-based photopolymer for reflection holographic recording" Ph.D thesis, Dublin Institute of Technology, 2005.
2. C.A.Feely, "Development and characterisation of red sensitized photopolymer holographic recording material" Ph.D thesis, University of Dublin, 1998.
3. C.A.Feely, S.Martin, V.Toal, A.Fimia, F.Mateos, "Optimization of a red sensitive photopolymer" Holographic Materials III, Proc. SPIE, Vol. 2688 (1995).
4. N.Suzuki, Y.Tomita, K.Ohmori, M.Hidaka and K.Chikama, "Highly transparent ZrO₂ nanoparticle-dispersed acrylate photopolymers for volume holographic recording," Opt. Express 14 12712-12719 (2006).
5. Y.Tomita, K.Chikama, Y.Nohara, N.Suzuki, K.Furushima and Y.Endoh, "Two-dimensional imaging of atomic distribution morphology created by holographically induced mass transfer of monomer molecules and nanoparticles in a silica-nanoparticle-dispersed photopolymer film" Opt. Lett. 31 1402-1404 (2006).
6. I.Naydenova and V.Toal, "Nanoparticle doped photopolymers for holographic applications Ordered Porous Solids," (Amsterdam: Elsevier) (2008).
7. [http://izasc.ethz.ch/fmi/xsl/IZA-SC/ftc_fw.xsl?-db=Atlas_main&-lay=fw&-max=25&STC=MFI&-find \(25-08-2010\)](http://izasc.ethz.ch/fmi/xsl/IZA-SC/ftc_fw.xsl?-db=Atlas_main&-lay=fw&-max=25&STC=MFI&-find (25-08-2010)).
8. I.Naydenova, T.Babeva, E.Leite, T.Baron, S.Martin, V.Toal, and S.Mintova, "Organic/Inorganic Nanocomposites with Improved Optical Properties" to be submitted to Langmuir.

9. T.Babeva , R.Todorov , S.Mintova , T.Yovcheva , I.Naydenova and V.Toal,
“Optical properties of silica MFI doped acrylamide-based photopolymer” J.
Opt. A: Pure Appl. Opt, Vol. 11, 024015 (2009).
10. A.M.Ostrowski, I.Naydenova and V.Toal, "Light-induced redistribution of Si-
MFI zeolite nanoparticles in acrylamide-based photopolymer holographic
gratings" J. Opt. A: Pure Appl. Opt. 11, 034004 (2009).
11. [http://www.avantes.com/Chemistry/AvaLight-HAL-Tungsten-Halogen-Light-
Source/Detailed-product-flyer.html](http://www.avantes.com/Chemistry/AvaLight-HAL-Tungsten-Halogen-Light-Source/Detailed-product-flyer.html).

CHAPTER 5

HOLOGRAPHIC RECORDING AT 473 NM IN AN ACRYLAMIDE BASED PHOTOPOLYMER

5.1 Introduction

This chapter reports on the sensitisation of the photopolymer material in the blue region of the visible spectrum, the recording of transmission and reflection gratings at this wavelength and the spectral characterisation of gratings recorded in both doped and undoped photopolymer.

Briefly this chapter covers the following:

1. Sensitisation of self processing acrylamide based photopolymer at 473 nm and recording holographic transmission gratings.
2. Recording of reflection holographic gratings at this wavelength.
3. Dye optimization to increase the diffraction efficiency of reflection gratings.
4. Improvement of the diffraction efficiency of the reflection holographic gratings by doping the photopolymer with Si-MFI zeolite nanoparticles.
5. Spectral characterization of both doped (nanoparticles) and undoped photopolymer compositions.

5.2 Recording transmission gratings at 473 nm

Initially dyes such as congo red, fast green, erythrosin B, eosin Y and Acriflavine was checked for their sensitisation at 473 nm. With congo red and fast green gratings were

unable to be recorded. Although erythrosin B and eosin Y can be used, their absorbance at blue wavelength was relatively low. Apart from that, these dyes have a broad absorbance dominating in the green region. So when it comes to recording of full colour holograms using erythrosine B/eosin Y, these dye cannot be recommended to be used for sensitising at blue wavelength. DCPVA showed a shift towards the UV region, when mixed with the acrylamide based photopolymer composition for full colour application. Finally acriflavine was chosen for the following experiments through out this thesis. Acriflavine showed good absorption in blue region, mixed well with the acrylamide based photopolymer and also had compatibility with other dyes for full colour holographic recording applications.

The photopolymer layers were prepared with the same composition as in section 4.2. The layer thicknesses were 15 μm , 30 μm and 60 μm . Transmission holographic gratings were recorded at a spatial frequency of 2000 lines/mm and the corresponding diffraction efficiency was measured in real time. Figure 5.1 shows the absorption spectrum of a $30 \pm 5 \mu\text{m}$ thick dry photopolymer layer with composition as given in table 4.1. The photosensitive dye using in this case was acriflavine.

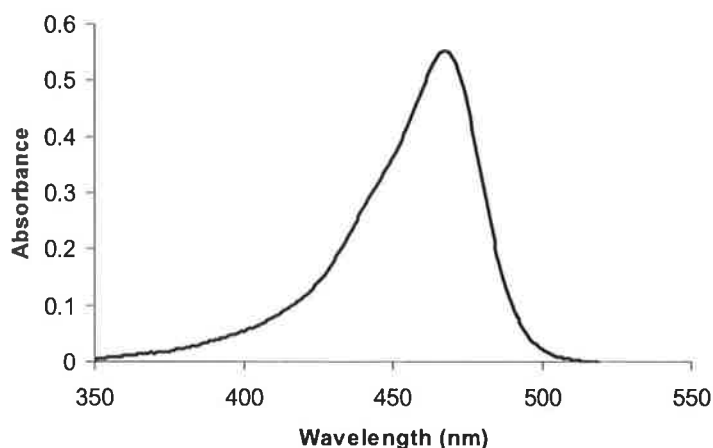


Figure 5.1 Absorption spectrum of dry photopolymer layer sensitized with acriflavine

The experimental setup for recording transmission gratings (2000 lines/mm) at 473 nm and measuring diffraction efficiency in the real time is shown in figure 5.2. The angle between the two beams was chosen in such way that the spatial frequency of the recorded transmission grating was 2000 lines/mm (calculated using the Bragg equation 2.2). Exposure times up to 250 sec were used and the diffraction efficiency was measured in real time using a 633 nm He-Ne laser.

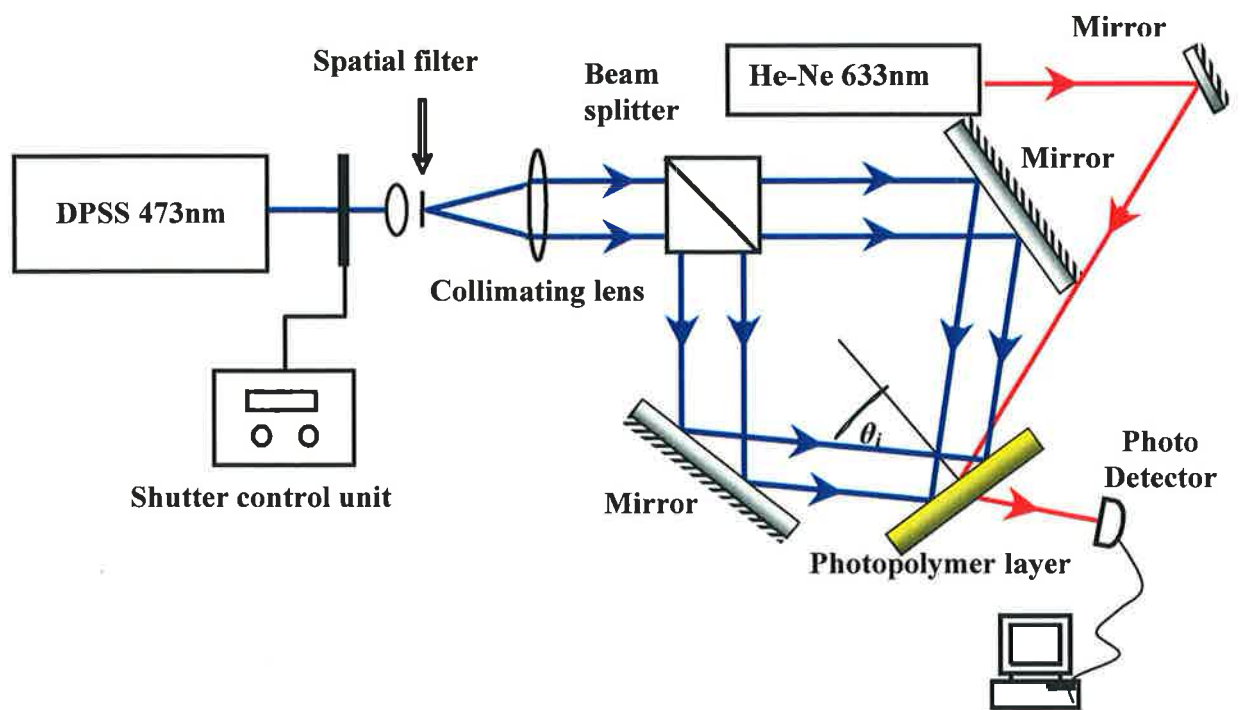


Figure 5.2 Experimental setup for recording transmission grating and to measure the diffraction efficiency in real time

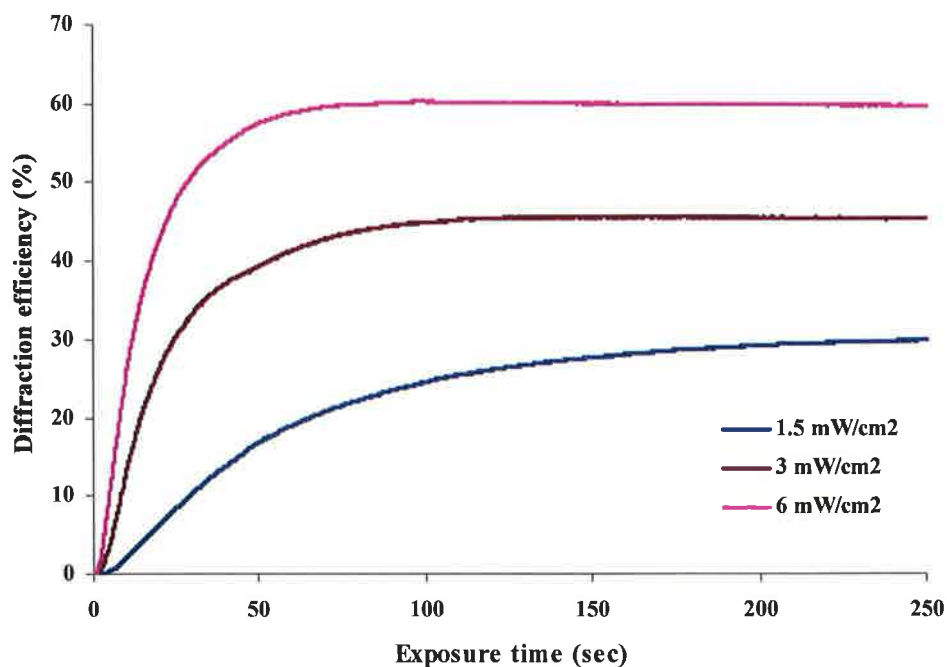


Figure 5.3 Diffraction efficiency (%) of transmission gratings (2000lines/mm) as a function of exposure time (sec) recorded at 473 nm for layer thickness 15μm at three different intensities (1.5 mW/cm², 3 mW/cm² and 6 mW/cm²).

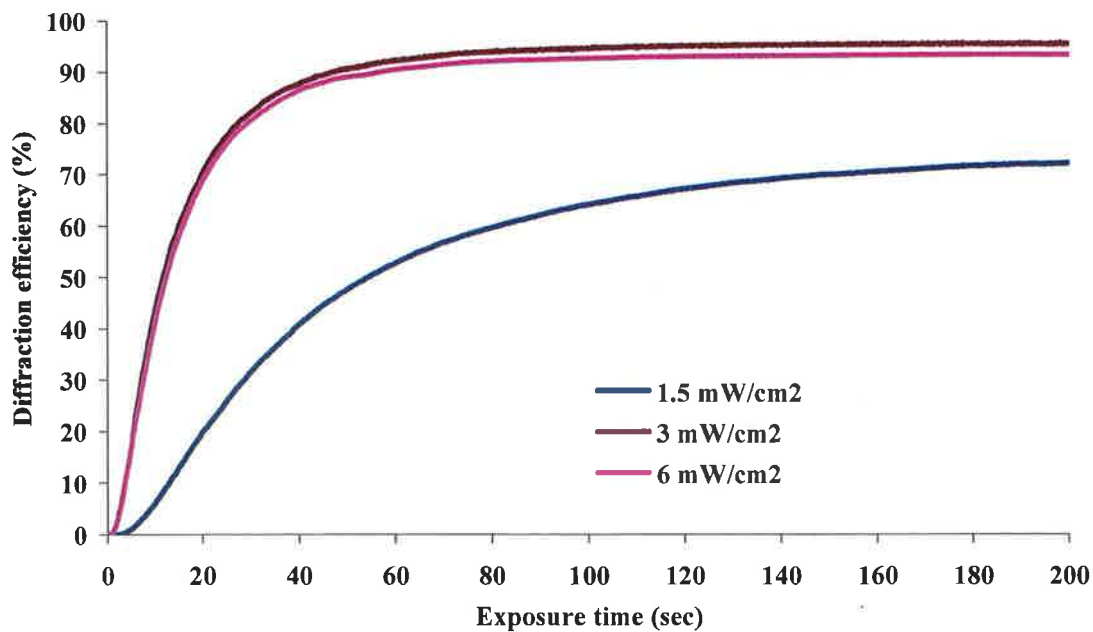


Figure 5.4 Diffraction efficiency (%) of transmission gratings (2000 lines/mm) as a function of exposure time (sec) recorded at 473 nm for layer thickness 30 μm at three intensities (1.5 mW/cm², 3 mW/cm² and 6 mW/cm²).

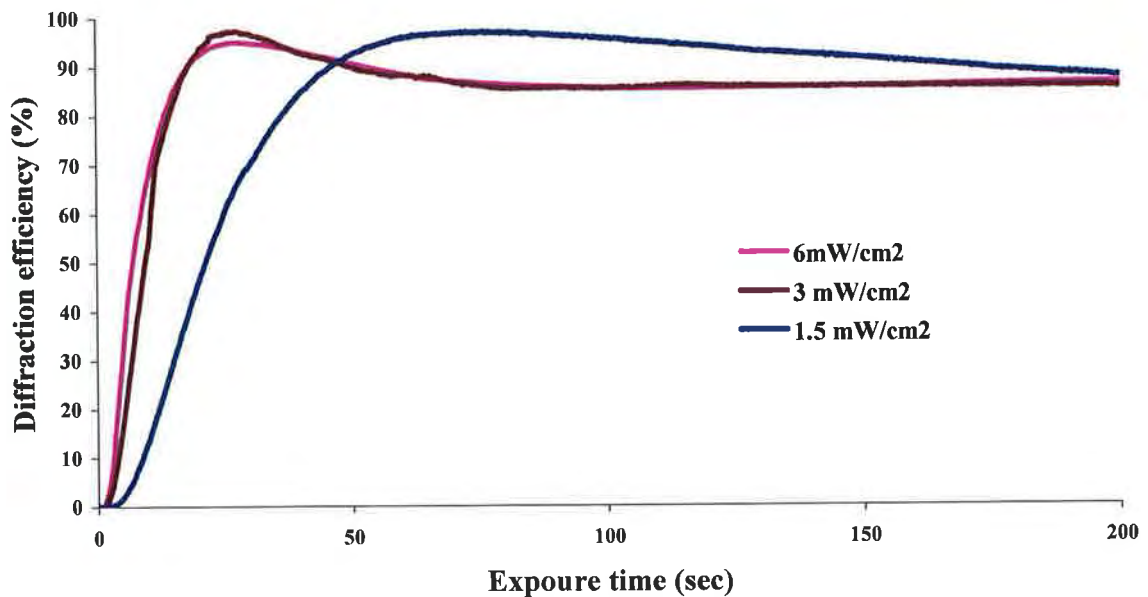


Figure 5.5 Diffraction efficiency (%) of transmission gratings (2000 lines/mm) as a function of exposure time (sec) recorded at 473 nm for a layer thickness 60 μ m at three intensities (1.5 mW/cm², 3 mW/cm² and 6 mW/cm²).

Figures 5.3, 5.4 and 5.5 show graphs of the diffraction efficiency as a function of exposure time for the grating recorded in 15 μ m, 30 μ m and 60 μ m thick photopolymer layers respectively. From figure 5.5 it can be observed that the maximum diffraction efficiency achieved in a 60 μ m thick photopolymer layer is 100 % for the three different intensities (1.5 mW/cm², 3 mW/cm² and 6 mW/cm²). The maximum diffraction efficiency that was achieved in a 30 μ m layer is 70% for the intensity 1.5 mW/cm² and 90% for both 3 mW/cm² and 6mW/cm² (figure 5.4). The growth of the diffraction efficiency is slower at lower intensity 1.5 mW/cm² compared to the higher recording intensities. The gratings recorded at higher intensity saturated much quicker than those recorded using the lower intensity. In particular there is not much difference in the growth profiles for the two recording intensities 3mW/cm² and 6 mW/cm² in both 30 μ m and 60 μ m thick layers.

In the case of 15 μm thick photopolymer layer the maximum diffraction efficiency that could be achieved was 30 %, 45 % and 60 % for the intensities 1.5 mW/cm^2 , 3 mW/cm^2 and 6 mW/cm^2 (shown in figure 5.3). This can be explained as due to insufficient monomers being polymerized as the refractive index modulation is lower in thinner layers (15 μm); also the diffraction efficiency reaches saturation (below 60 %) even at higher intensity and longer exposure times (more than 300 sec). In addition, in 30 μm layers the efficiency of the gratings for the lower intensity (1.5 mW/cm^2) reached saturation at 70 %. In the case of 60 μm thick layers at an intensity of 1.5 mW/cm^2 , 100 % diffraction efficiency was obtained with slow growth.

From these results it can be concluded that the self processing acrylamide based photopolymer material sensitized at blue wavelength region can be used for holographic recording. The best conditions for the holographic recording, to obtain a diffraction efficiency of 100 %, are 60 μm and 30 μm photopolymer layer thickness with intensities of 6 mW/cm^2 and 3 mW/cm^2 for both thicknesses with an exposure time of 50 sec. This study was further extended to investigate if the same material can be used for recording reflection gratings and also to find the best possible conditions to make display holograms at 473 nm.

5.3 Reflection gratings at 473 nm

Reflection gratings were recorded at 5700 lines/mm using the experimental setup shown in figure 4.4 with the same composition that was used for recording transmission gratings (section 5.2). The methodology followed was the same as explained in section 4.4. Figures 5.6 and 5.7 show the diffraction efficiency growth curves for the reflection gratings in layers of two different thicknesses (30 μm , 60 μm) with recording intensities 3 mW/cm^2 and 6 mW/cm^2 . From figure 5.6 it can be

observed that the maximum diffraction efficiency achieved for a thickness of 30 μm photopolymer layer was 1.5 % for intensities of 3 mW/cm^2 and 6 mW/cm^2 . Whereas in the case of 60 μm thick photopolymer layers the maximum diffraction efficiencies achieved were 1.5 % for an intensity of 6 mW/cm^2 and 1.2 % for intensity of 3 mW/cm^2 as shown in figure 5.7.

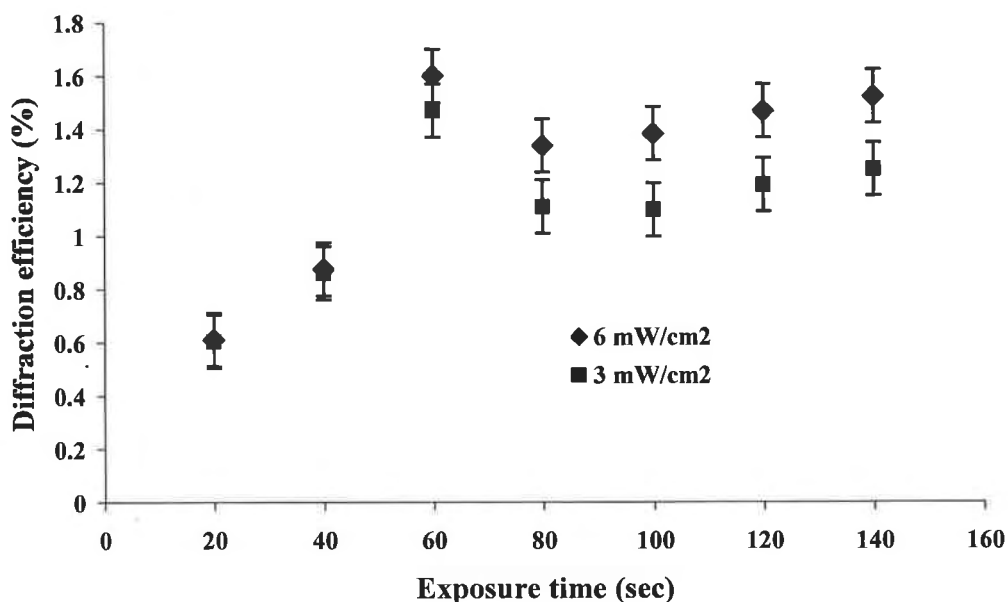


Figure 5.6 Diffraction efficiency (%) of reflection gratings (5700 lines/mm) as a function of exposure time (sec) recorded at 473 nm for layer thickness of 30 μm at two intensities (3 mW/cm^2 and 6 mW/cm^2).

In the case of 30 μm thick photopolymer layer, the diffraction efficiency increases with exposure time, and it can be observed that there is a slight improvement in the diffraction efficiency when the intensity of recording beam was increased from 3 mW/cm^2 to 6 mW/cm^2 . From the growth curves of two different thicknesses of the photopolymer layers (30 μm and 60 μm) it can also be seen that the rate of increase in the diffraction efficiency with respect to time of exposure is lower for 60 μm thick layers than for the 30 μm layers and this could be due to the higher optical density of

60 μm thick photopolymer layers. However, the overall diffraction efficiency is higher for the gratings recorded in a 60 μm photopolymer layers compared to 30 μm (figure 5.7).

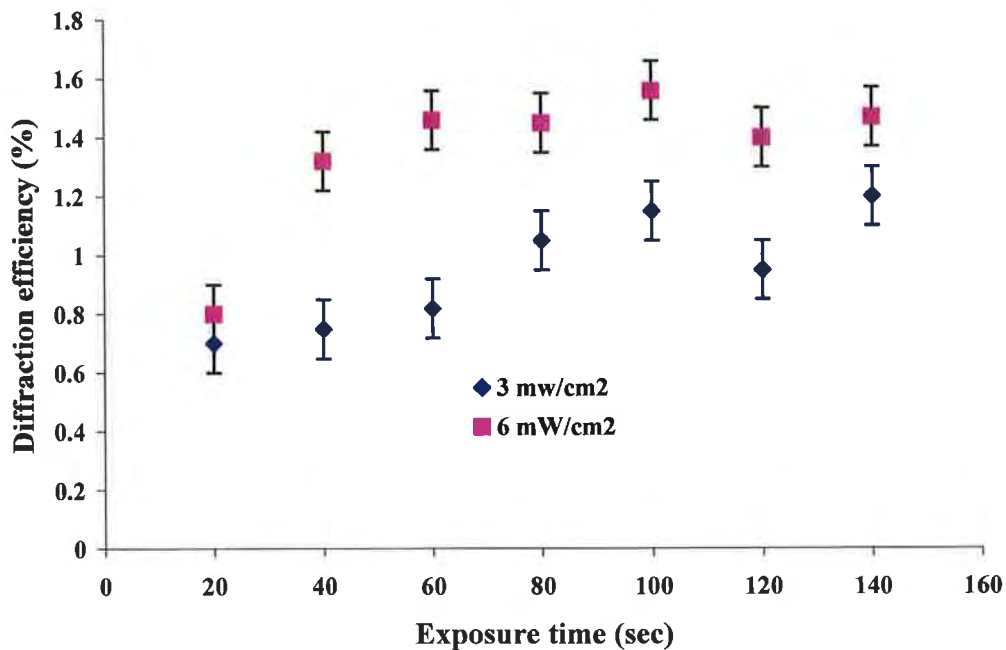


Figure 5.7 Diffraction efficiency (%) of reflection gratings (5700 lines/mm) as a function of exposure time (sec) recorded at 473 nm for a layer thickness 60 μm at two intensities (3 mW/cm² and 6 mW/cm²).

To further understand the behaviour of the material at lower thickness and higher intensity, recording of the reflection holographic gratings were performed with 15 μm thick photopolymer layers and illuminating at 6 mW/cm². As expected the diffraction efficiency increased with increase of exposure time and reached saturation with a maximum diffraction efficiency of 0.7 %, as shown in figure 5.8.

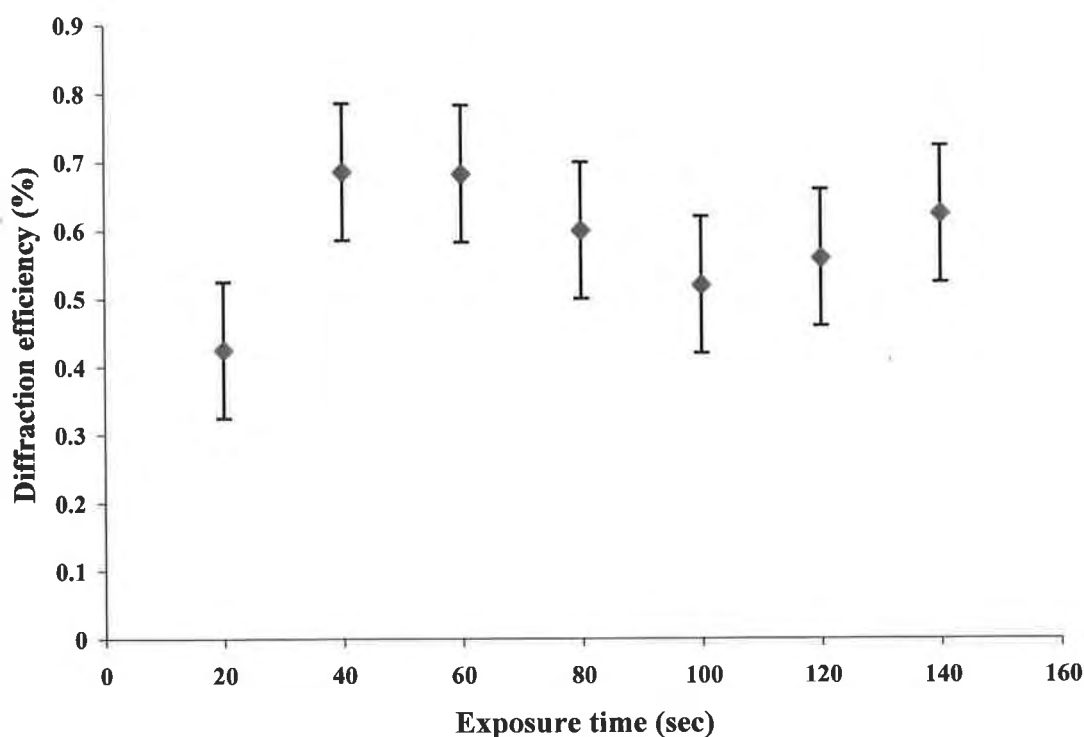


Figure 5.8 Diffraction efficiency (%) of reflection gratings (5700 lines/mm) as a function of exposure time (sec) recorded for a layer thickness 15 μm at 6 mW/cm^2 intensity.

At this point it can be concluded that the maximum diffraction efficiency that was achieved is 1.7 %, in a 30 μm thick layer with an intensity of 6 mW/cm^2 for the photopolymer composition shown in table 5.1. One of the possible reasons for this low diffraction efficiency is the inability of the material to record high spatial frequency holographic gratings (less than 0.2 μm fringe spacing) because the photopolymer chains formed in the bright regions might be diffusing into the dark regions, which affects the refractive index difference between dark and bright regions [Chapter 3, see reference 11, 12]. The other reason for obtaining low diffraction efficiency could be insufficient numbers of free radicals available to initiate the polymerisation. This problem can be minimized by varying the dye concentrations. Further experiments were carried out varying the dye concentrations, and the experimental results are discussed in the following section 5.4.

5.4 Optimizing dye concentration at 473 nm

The new composition was prepared by taking the same number of molecules of acriflavine as that of erythrosine B dye that is used for the recording reflection holograms at green wavelength. The molecular weights of erythrosine B and acriflavine are 879.84 g/mol, 259.73 g/mol respectively. The concentration of stock solution of acriflavine dye was decreased from 0.11 g/100ml to 0.08 g/100ml. This might help to improve the diffraction efficiency since decreasing the concentration improves the transmittance of the recording material ensuring enough dye molecules for photo initiating process. The photopolymer composition for this is shown in table 5.1. Figure 5.9 shows the absorption spectra of 30 μm thick dry photopolymer layer for all the photopolymer compositions shown in table 5.1, in comparison with the dye concentration (0.11 % w/v of acriflavine). Figure 5.10 shows the measured diffraction efficiency of recorded reflection holographic gratings for these three new compositions.

10% w/v PVA aqueous solution	Acrylamide	NN'methylene bisacrylamide	Triethanolamine	0.08% w/v of ACF dye
17.5 ml	0.8 g	0.25 g	2 ml	2 ml
17.5 ml	0.8 g	0.25 g	2 ml	3 ml
17.5 ml	0.8 g	0.25 g	2 ml	4 ml
10% w/v PVA aqueous solution	Acrylamide	NN'methylene bisacrylamide	Triethanolamine	0.11% w/v of ACF dye
17.5 ml	0.8 g	0.25 g	2 ml	3 ml

Table 5.1 Photopolymer compositions with four different concentrations of the acriflavine dye.

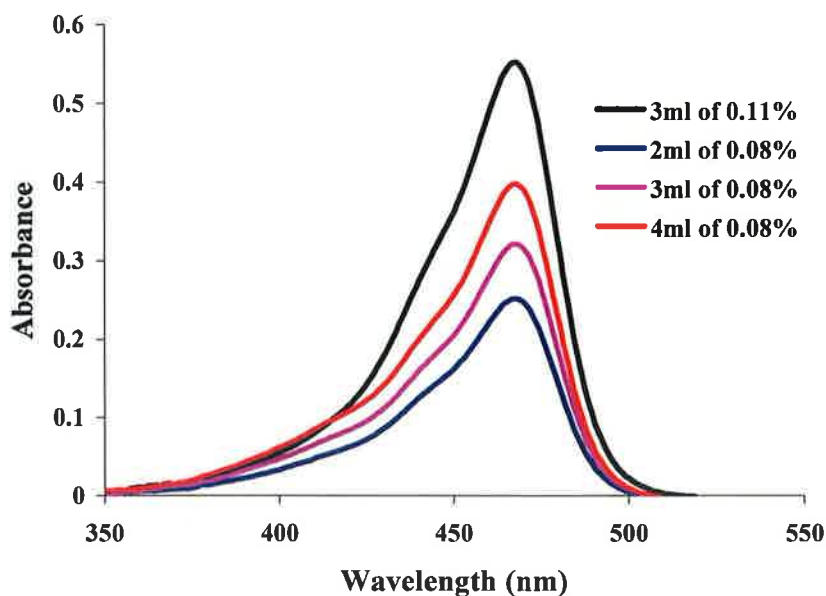


Figure 5.9 Absorption spectra of four different concentrations of the acriflavine dye shown in table 5.1 .

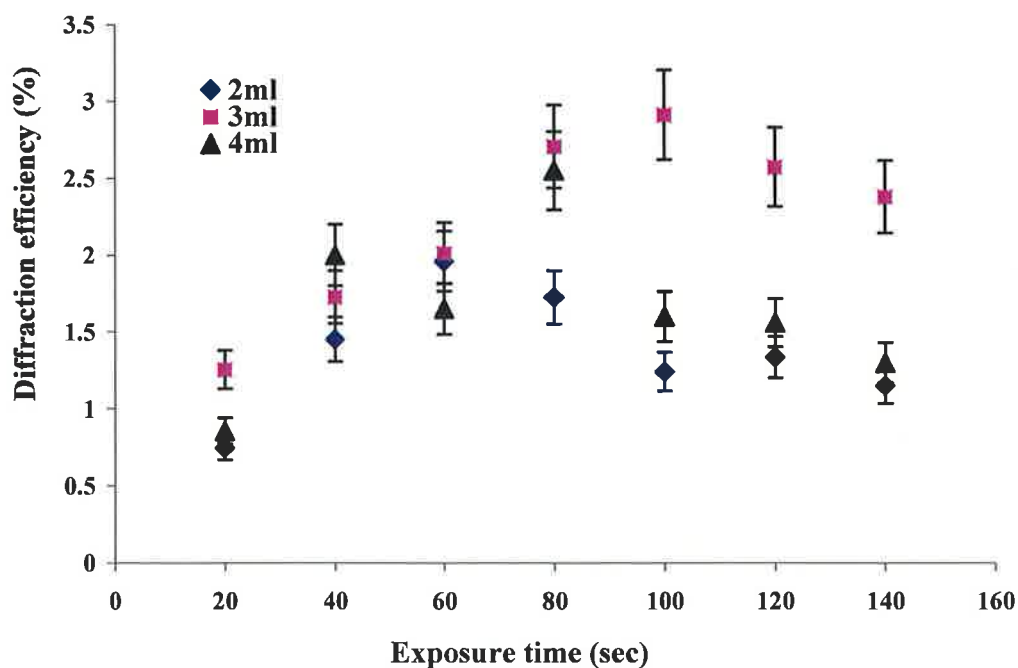


Figure 5.10 Comparison of diffraction efficiency growth profiles for the gratings recorded at 473nm for different concentrations of the acriflavine dye.

The diffraction efficiency of the reflections gratings containing 2 ml of 0.08% dye solution rises to a maximum of 2 % and then reaches saturation at 1.5 %. In the case

of 3 ml and 4 ml dye composition the maximum efficiency achieved was 3 % and 2.5 % respectively. From figure 5.6 it can be seen that the maximum diffraction efficiency of 1.6 % was achieved for 3 ml of 0.11% w/v Acriflavine dye concentration. It can be concluded that the 3 ml of 0.08% dye solution gives better diffraction efficiency than the 4 ml and 2 ml of 0.08% and also 3 ml of 0.11% stock dye solutions. This might be due to, in 0.11% stock dye solution, the number of dye molecules are more than the requirement and the material was optically very dense causing inefficient penetration of light.

Further experiments were conducted by doping the material with Si-MFI zeolite nanoparticles. This was done to check the possibility of controlling the spectral position of the Bragg peak of the diffracted beam and to improve diffraction efficiency of recorded gratings. Experimental results are given in the following section 5.5.

5.5 Doping with nanoparticles

Here the photopolymer material was doped with a solution of 1.8 % w/v of Si-MFI zeolite nanoparticles of 30 nm in size. Three different concentrations of 2.5 %, 5 %, and 7.5 % nanoparticle doped photopolymer solution were made. Holographic reflection gratings were recorded at a spatial frequency of 5700 lines/mm using a DPSS 473 nm wavelength laser with an intensity of 6 mW/cm². The diffraction efficiencies of the recorded gratings as a function of time of exposure are shown in figure 5.11. The dry photopolymer layer thickness was 30 μm.

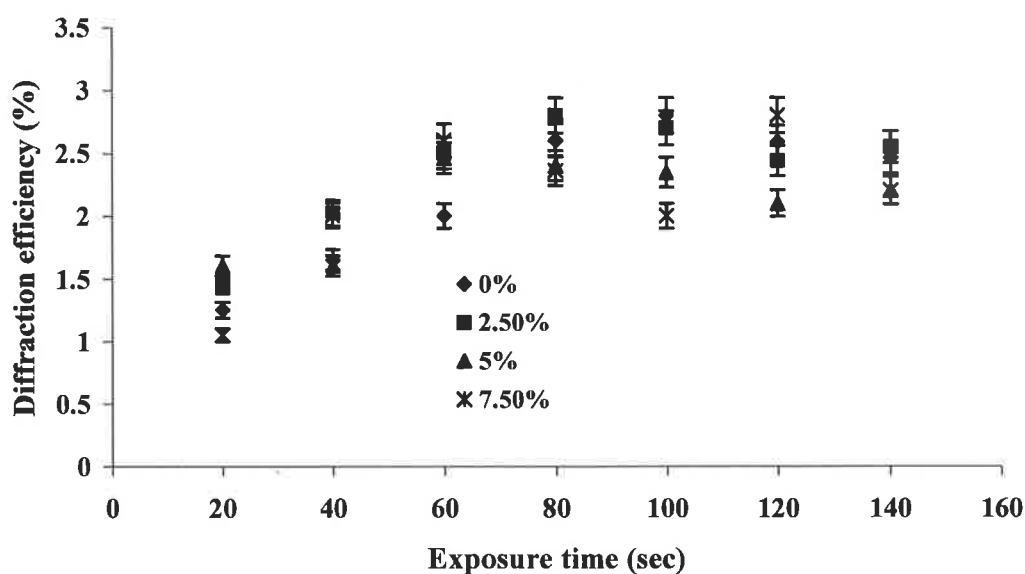


Figure 5.11 Diffraction efficiency growth profiles for the reflection gratings recorded at 473nm for four different concentrations of Si-MFI zeolite nanoparticles.

The diffraction efficiency of the material doped with nanoparticles slightly increased in comparison with undoped material (0%). Over all there was not much difference in maximum diffraction efficiency between doped and undoped photopolymer gratings. In the next step the recorded gratings were spectrally characterized using a spectrophotometer in order to measure the Bragg peak wavelength of the diffracted beam.

5.6 Spectral characterisation

Figure 4.9 in section 4.6, shows the experimental setup used for measuring the wavelength of diffracted light. The gratings recorded at 80 sec exposure time in section 5.5 were used. This exposure time is considered to be suitable for all the four nanoparticle compositions (0%, 2.5%, 5% and 7.5%) because it can be seen that the diffraction efficiency starts saturating from 80 sec. Figure 5.12 shows the Bragg peak of the diffracted beam as a function of nanoparticle concentration. The results show

that there is a shift in the position of the Bragg peak in the undoped photopolymer from a recording wavelength of 473 nm to 464 nm which implies shrinkage of 1.9 %.

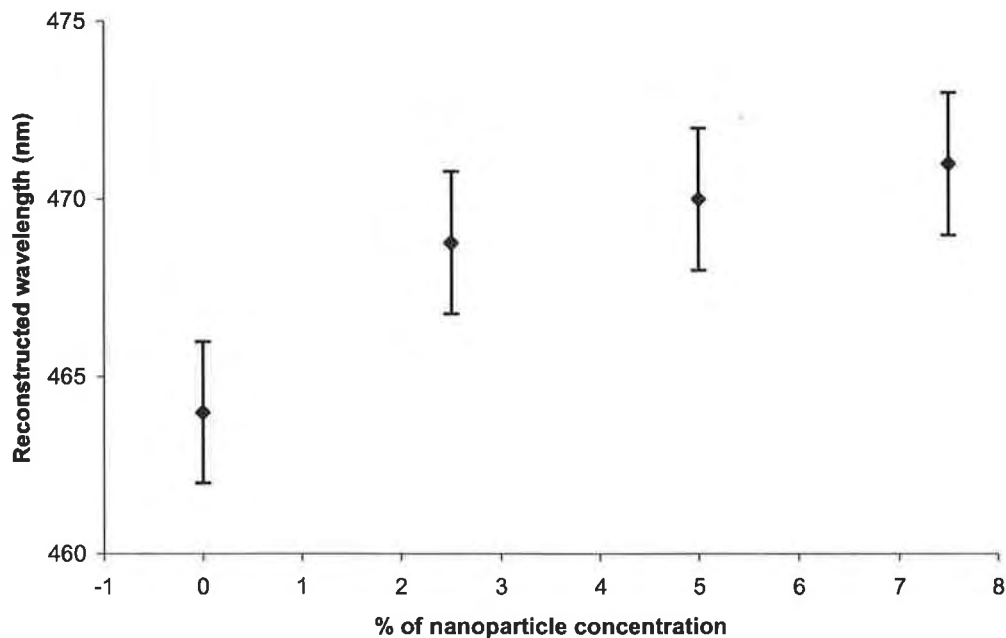


Figure 5.12 Shows the wavelength of the Bragg peak for a recorded grating at 473 nm as a function of concentration of nanoparticles in the photopolymer.

The wavelengths of the Bragg peak of the diffracted beam obtained for the nanoparticle concentrations of 2.5 %, 5 % and 7.5 % are 468.8 nm, 470.3 nm and 471 nm, implying shrinkages of 0.89 %, 0.57 %, and 0.4 % respectively. Therefore increasing the nanoparticle concentration controls the dimensional changes in the material and in turn the Bragg peak of the diffracted beam is obtained near the recording wavelength.

5.7 Reflection holograms

Reflection holograms were recorded in 30 μm thick photopolymer layers with an intensity of 6 mW/cm^2 using the Denisyuk recording geometry. Figures 5.13 shows photographs of the reconstructed reflection holographic images of the object when illuminated using a white light (spot lamp).



Figure 5.13. Photograph of white light holographic reconstructions recorded with a blue laser at 473 nm.

5.8 Conclusion

The self processing acrylamide based photopolymer was sensitised to record at 473 nm using acriflavine dye. Transmission gratings were recorded at this wavelength with a spatial frequency of 2000 lines/mm for three different intensities (1.5 mW/cm^2 , 3 mW/cm^2 , and 6 mW/cm^2) and for three thicknesses ($15 \text{ }\mu\text{m}$, $30 \text{ }\mu\text{m}$, and $60 \text{ }\mu\text{m}$). Diffraction efficiency of 100 % was obtained for the transmission gratings recorded in photopolymer layers of $60 \text{ }\mu\text{m}$ thickness. The same photopolymer composition was used to record reflection holographic gratings. The diffraction efficiency of the reflection holographic gratings was improved from 1.7 % to 3 % by varying the dye concentration in the photopolymer composition. Overall, doping with nanoparticles did not result in a considerable improvement in the diffraction efficiency of the reflection gratings. From spectral characterization studies it can be concluded that by doping the photopolymer with Si-MFI zeolite nanoparticles the dimensional changes has been reduced from 1.9 % to 0.4 %.

In order to find the maximum possible diffraction efficiency in the reflection holographic gratings, the diffraction efficiency was calculated theoretically using Kogelnik's theory. The refractive index modulation was calculated for the experimental values (for transmission holographic gratings) of the thickness 15 μm , 30 μm and 60 μm for the intensity of 6 mW/cm^2 using equation 2.20. The values obtained were 15.37×10^{-3} , 6.49×10^{-3} , 4.08×10^{-3} for thickness 15 μm , 30 μm and 60 μm respectively. By taking these, as maximum refractive index modulation values for the corresponding thicknesses, the maximum diffraction efficiency has been calculated theoretically (using equation 2.25) in reflection holographic gratings which is 100%.

CHAPTER 6

HOLOGRAPHIC RECORDING IN PANCHROMATIC ACRYLAMIDE BASED PHOTOPOLYMER

6.1 Introduction

The experiments described in this chapter are aimed towards determining the recording capability of the panchromatic acrylamide based photopolymer material sensitized at three selected primary wavelengths, red (633 nm), green (532 nm) and blue (473 nm) for white light viewable colour holographic display applications. For this purpose reflection holographic gratings were recorded in different thickness photopolymer layers at different intensities and the corresponding diffraction efficiency was measured at each recording wavelength. Further the photopolymer material was doped with zeolite nanoparticles (Si-MFI) to improve the diffraction efficiency of the reflection gratings.

This chapter describes the following work:

1. Sensitising self processing acrylamide based photopolymer at all three primary wavelengths and establishing the optical setup for recording full colour hologram by combining the beams from the lasers operating at the three selected primary wavelengths.
2. Recording of reflection holographic gratings individually at each recording wavelength and measurement of the corresponding diffraction efficiencies.
3. Study of the influence of the Si-MFI zeolite nanoparticle dopants on the diffraction efficiency of the reflection holographic gratings.

4. Spectral characterization of reflection holographic gratings.
5. Recording of full colour transmission and reflection holograms.

6.2 Recording material and experimental setup

Acrylamide based photopolymer is sensitized at three laser wavelengths, red (He-Ne 633 nm), green (Verdi 532 nm) and blue (DPSS 473 nm) by using three dyes methylene blue (MB), erythrosine B (EB) and acriflavine (ACF) for holographic recording. The photopolymer composition used here is specified in Table 4.1, and also contains 3 ml of each of three dye stock solutions (0.11% w/v) instead of a single dye. The photopolymer layer preparation procedure was similar to that explained in section 4.2. The absorption spectrum of a 60 ± 5 μm thick photopolymer layer containing all three photosensitive dyes is shown in figure 6.1. From this spectrum, it can be observed that the material has well defined peaks of absorption at 473 nm, 532 nm and near 633 nm wavelengths. Each dye species is clearly distinguishable, which is clear evidence that there is no interaction between the dye molecules.

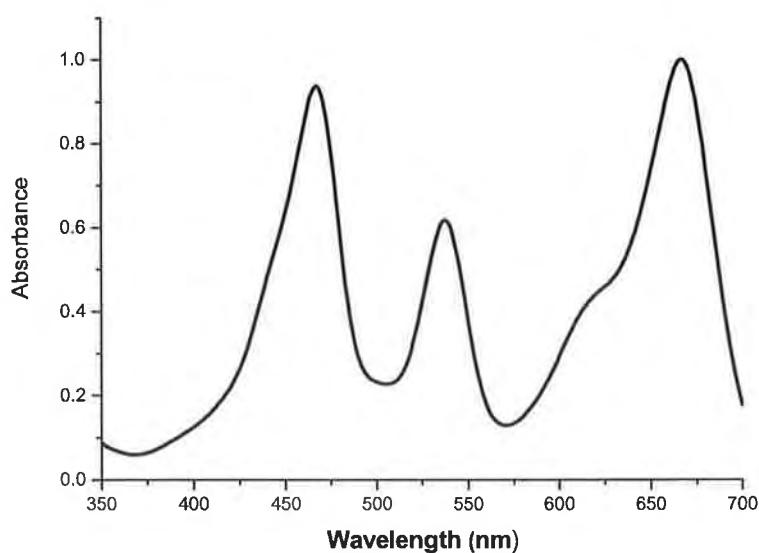


Figure 6.1 Normalised absorption spectrum of panchromatic acrylamide based photopolymer recording material.

Reflection holographic gratings were recorded in this panchromatic photopolymer layer using the experimental setup shown in Figure 6.2. The optical set up consists of three lasers whose beams were combined using a mirror and two dichroic mirrors (DM). The combined laser beams were spatially filtered using a single spatial filter and then collimated. The collimated beam was split into two beams using a beam splitter. The two beams were then diverted onto the photopolymer layer using two adjustable mirrors to record the holographic gratings.

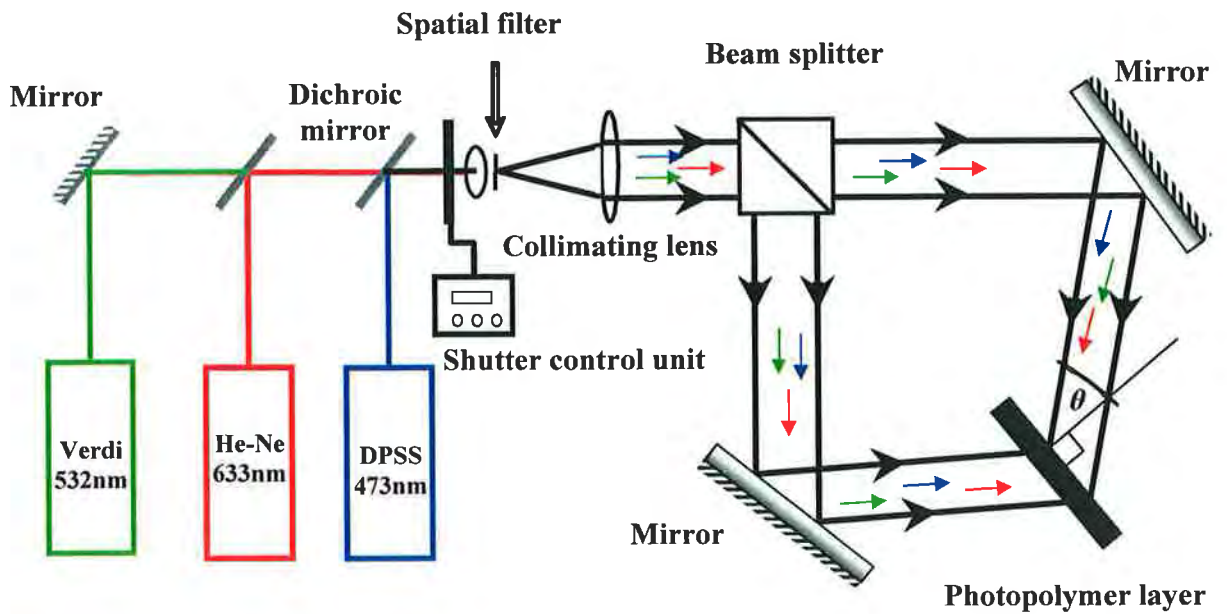


Figure 6.2 Experimental setup for recording multicolour reflection holographic grating.

The spatial frequencies that were selected for recording holographic reflection gratings at three wavelengths 633 nm, 532 nm and 473 nm were 4200 lines/mm, 5000 lines/mm and 5700 lines/mm respectively, and were calculated using the Bragg equation (Equation 2.2).

6.3 Recording reflection gratings

Initial experiments were carried out by recording reflection gratings at 633 nm with an intensity of 1.8 mW/cm^2 in the photopolymer layers with thickness $60 \pm 5 \text{ }\mu\text{m}$, exposed for different exposure times ranging from 20 sec to 120 sec with an increment of 20 sec for each new recording. The diffraction efficiency of each reflection grating was then measured by exposing the grating to one of the recording beams. The intensity in the diffracted beam was measured using a photo detector. The experiments were repeated for green (532 nm) and blue (473 nm) wavelengths on separate sets of photopolymer layers. The recording intensities for the green and blue wavelengths were 3 mW/cm^2 and 4 mW/cm^2 respectively. The percentage of diffraction efficiency was calculated using equation 4.1.

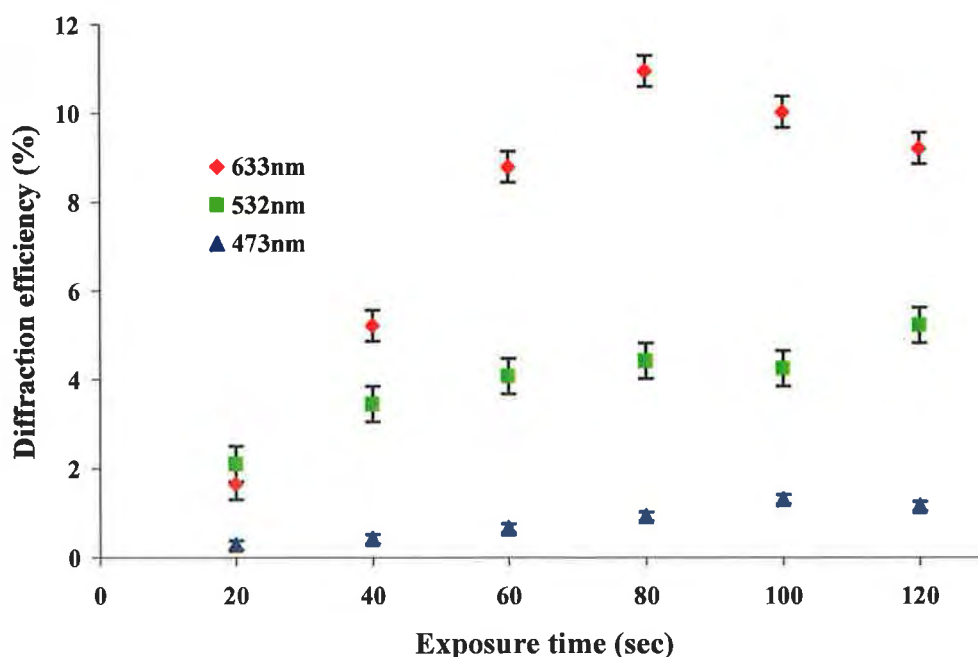


Figure 6.3 Diffraction efficiency (%) as a function of time of exposure for the reflection gratings recorded at red, green and blue wavelengths in a $60 \text{ }\mu\text{m}$ thick photopolymer layer.

From figure 6.3 it can be seen that, as the exposure time increases, diffraction efficiency increases. The recording time for maximum diffraction efficiency for the three wavelengths is between 80 sec and 100 sec. However, the maximum diffraction efficiencies are different for the three wavelengths. The maximum diffraction efficiency for the gratings recorded at 633 nm, 532 nm and 473 nm wavelengths are 11.5 %, 6 %, and 1.6 % respectively. These differences in the diffraction efficiency of the recording material at different wavelengths are at least partly due to the fact that the spatial frequencies increase with the decrease in wavelength. Another possible reason could be that the quantum yield of free radicals is different for the three dyes which is an important parameter which drives the polymerization process and results in the refractive index modulation between the bright and dark regions.

6.4 Optimization of dye composition

For the monochromatic photopolymer composition sensitised at 473 nm, the optimum dye concentration was 3 ml of 0.08% of the Acriflavine dye (section 5.4). As this concentration showed an improvement in the diffraction efficiency, the same concentration has been used in the panchromatic composition. For red and green wavelengths, the dye concentration mentioned in section 6.2 is used. Absorption spectra of the corresponding photopolymer composition with two different (30 μm and 60 μm) layer thicknesses are shown in figure 6.4.

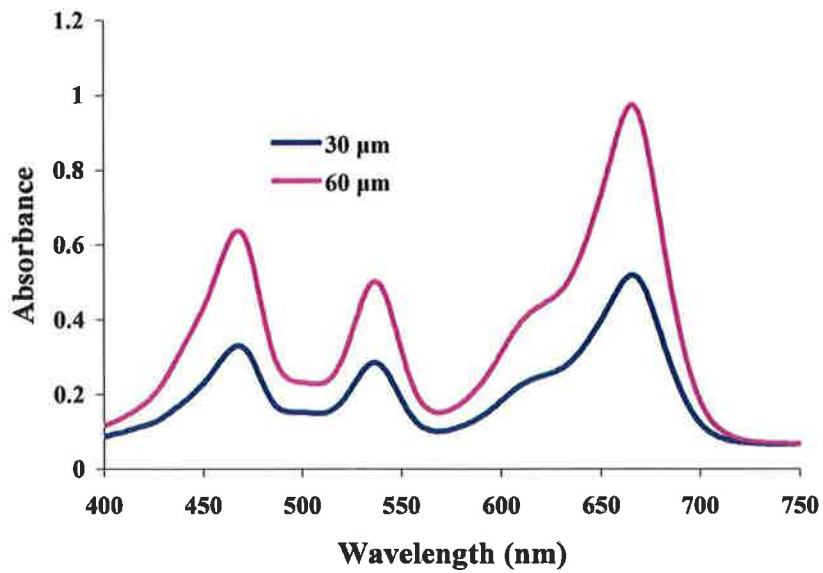


Figure 6.4 Absorption spectra of panchromatic acrylamide based photopolymer recording material for two different thicknesses (30 μm and 60 μm).

6.4.1 Recording at wavelength 633nm

Reflection holographic gratings were recorded using the composition mentioned in the above section 6.4 for two different layer thickness 30 μm and 60 μm at intensities of 1.5 mW/cm² and 3 mW/cm². The corresponding diffraction efficiencies were measured and are shown in figures 6.5 and 6.6.

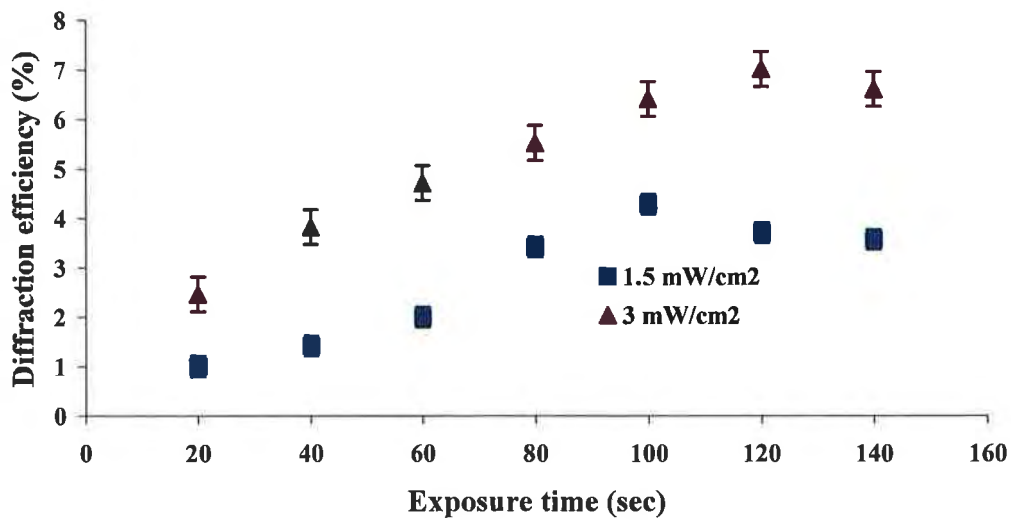


Figure 6.5 Diffraction efficiency of reflection gratings recorded at 4200 lines/mm spatial frequency as a function of exposure time (sec) in a 30 μm layers for 3 mW/cm^2 and 1.5 mW/cm^2 recording intensities at 633nm.

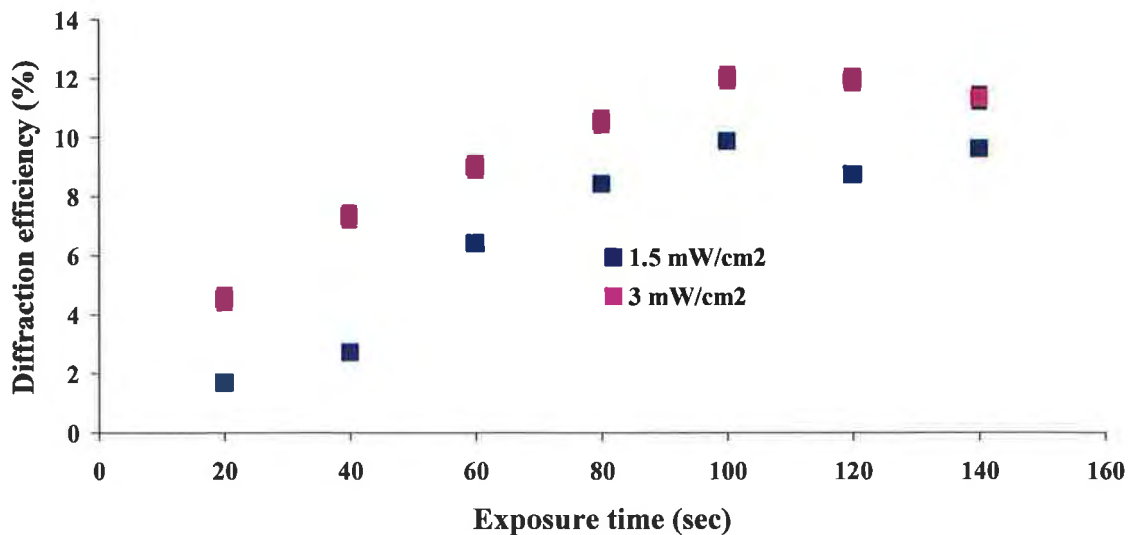


Figure 6.6 Diffraction efficiency of reflection gratings recorded at 4200 lines/mm spatial frequency as a function of exposure time (sec) in a 60 μm layers for 3 mW/cm^2 and 1.5 mW/cm^2 recording intensities at 633nm.

From figure 6.5 it can be seen that the maximum diffraction efficiencies were 6.7 %, and 4 % for intensities of 1.5 mW/cm^2 and 3 mW/cm^2 respectively for the reflection gratings recorded in 30 μm thick photopolymer layers. In the case of 60 μm thick

photopolymer layers a maximum diffraction efficiency of 12 % and 9.8 % was achieved for intensities of 1.5 mW/cm^2 and 3 mW/cm^2 respectively. In both thicknesses the diffraction efficiency of the material increases with time of exposure, reaching a maximum between 100 -120 sec. In $60 \text{ }\mu\text{m}$ thick layers the diffraction efficiency of the material was higher in comparison with $30 \text{ }\mu\text{m}$ thick layers. Previously for the monochromatic photopolymer composition at 633 nm wavelength (chapter-4, section 4.2), the diffraction efficiencies were observed to be 9.8 % and 6.5 % for a $60 \text{ }\mu\text{m}$ thick layer at intensity 3 mW/cm^2 and 1.5 mW/cm^2 respectively, while for the thickness of $30 \text{ }\mu\text{m}$, 8.6 % and 5.7 % efficiencies were achieved. There is a difference of 2 % between diffraction efficiencies obtained using the monochromatic and panchromatic compositions at this wavelength, which might be due to the small variation in thickness of the layers. Moreover it is clear that there is no difficulty in holographic recording due to the presence of the other photosensitive dyes.

6.4.2 Recording at wavelength 532nm

Reflection gratings with a spatial frequency of 5000 lines/mm were recorded at 532 nm wavelength. Again the gratings were recorded in two different thickness ($30 \text{ }\mu\text{m}$ and $60 \text{ }\mu\text{m}$) layers with intensities 3 mW/cm^2 and 1.5 mW/cm^2 . Figures 6.7 and 6.8 show the diffraction efficiencies obtained in these layers as a function of the exposure time.

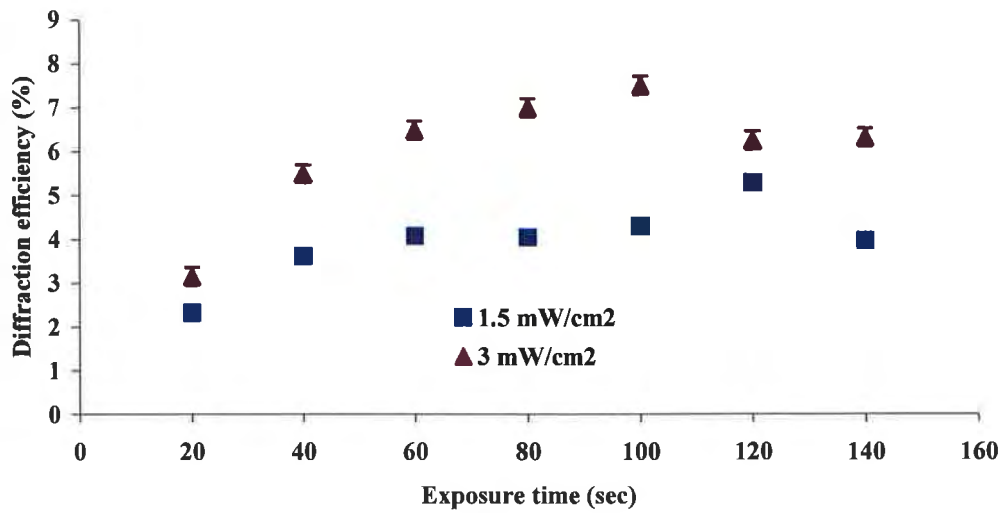


Figure 6.7 Diffraction efficiency (%) of reflection gratings recorded in 30 μm layers (5000 lines/mm) as a function of exposure time (sec) for 3 mW/cm² and 1.5 mW/cm² recording intensities at 532nm.

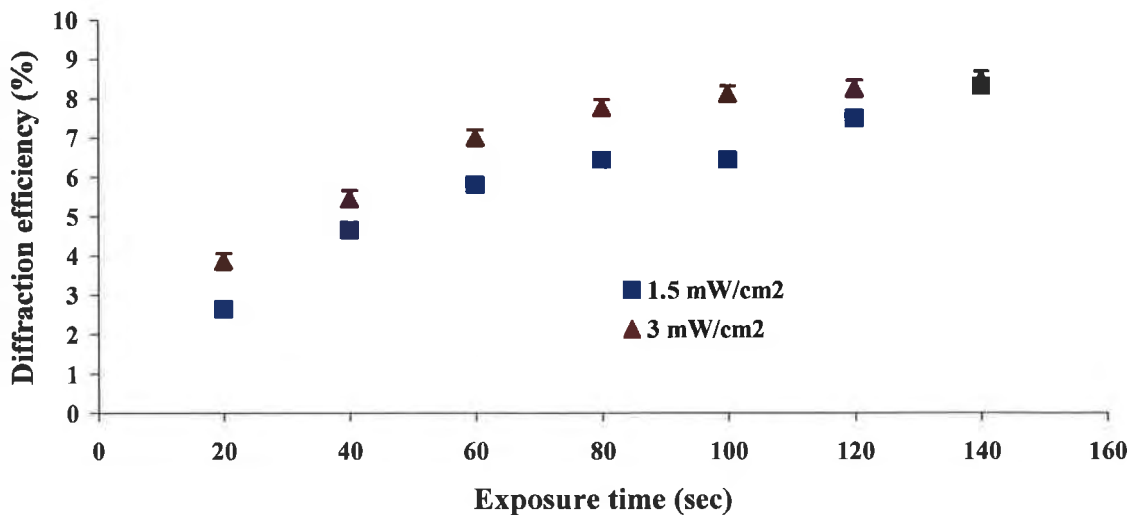


Figure 6.8 Diffraction efficiencies (%) of reflection gratings (5000 lines/mm) recorded in 60 μm layers as a function of exposure of time (sec) for 3 mW/cm² and 1.5 mW/cm² recording intensities at 532nm.

Maximum diffraction efficiencies of 7.5 % and 5 % were obtained in the 30 μm thick layers for intensities of 3 mW/cm² and 1.5 mW/cm² respectively. In case of 60 μm thick layers a maximum diffraction efficiency of 8 % was achieved for both

intensities. The maximum diffraction efficiency that was achieved for 60 μ m thick layer is slightly higher than that of the 30 μ m thick layer.

6.4.3 Recording at wavelength 473 nm

In the case of monochromatic photopolymer sensitive at 473 nm, although recording was done at low intensity (1.5 mW/cm²) (See chapter 5.3, Figure 5.8) the results showed that this material required rather higher recording intensities. Now in the panchromatic version of the material, holographic gratings were recorded at 473nm with a spatial frequency of 5700 lines/mm in two different thicknesses (30 μ m and 60 μ m) of layer using intensities of 3 mW/cm² and 6 mW/cm². The diffraction efficiency as a function of exposure time is shown in figures 6.9 and 6.10.

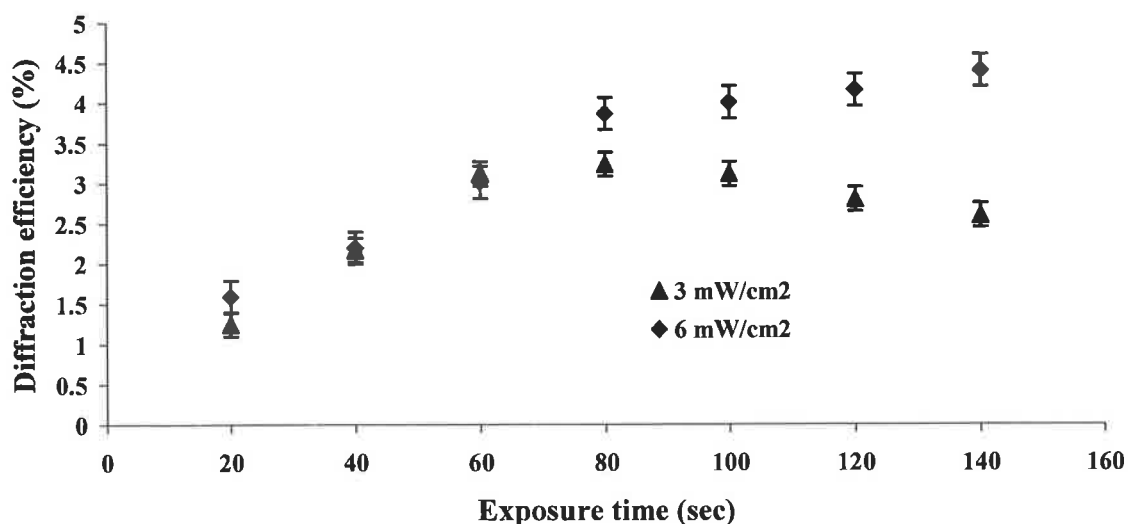


Figure 6.9 Diffraction efficiency (%) of reflection gratings (5700 lines/mm) as a function of exposure time (sec) recorded in 30 μ m layers for two intensities 3 mW/cm² and 6 mW/cm² at 473nm.

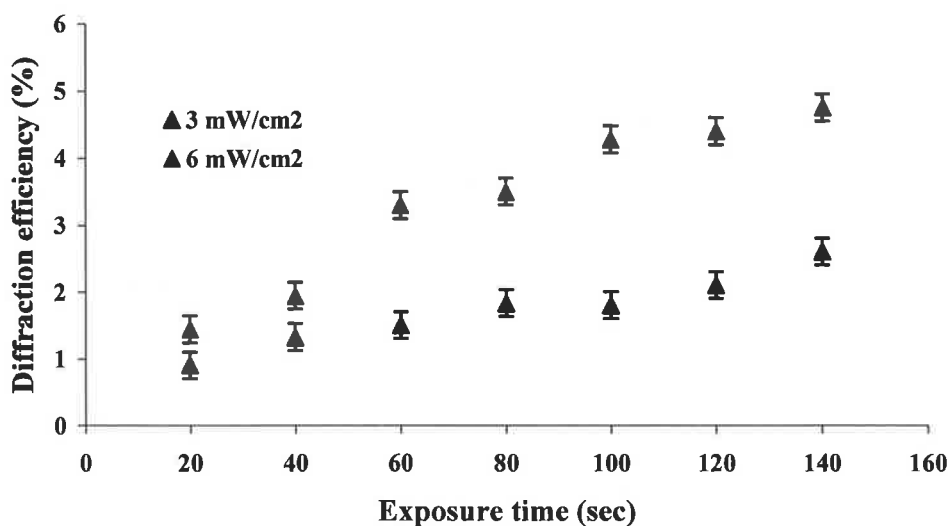


Figure 6.10 Diffraction efficiency (%) of reflection gratings (5700 lines/mm) as a function of exposure time (sec) recorded in 60 μm layers for intensities of 3 mW/cm^2 and 6 mW/cm^2 at 473nm.

From Figure 6.9 it can be seen that diffraction efficiency of the holographic gratings increases with recording time and reaches saturation after 100 sec. Maximum diffraction efficiencies of 4 % and 3.2 % were obtained in 30 μm thick layers for intensities of 6 mW/cm^2 and 3 mW/cm^2 respectively. In the case of 60 μm thick layers, growth of diffraction efficiency (shown in figure 6.10) was low in comparison with 30 μm thick layers and reached a maximum diffraction efficiency of 4.5 % and 2.6 % for intensities of 6 mW/cm^2 and 3 mW/cm^2 respectively.

6.5 Reflection gratings in nanoparticle doped material

With the aim of improving the diffraction efficiency of the recorded gratings and obtaining better control over the Bragg peak of the diffracted beam, the photopolymer material was doped using zeolite Si-MFI nanoparticles with concentrations of 2.5 % and 5 %. These concentrations were used since it was observed from the previous results (Sections 4.5 and 5.5) that the diffracted wavelength could be controlled in this

way. Holographic gratings were recorded at each wavelength to compare the efficiencies of gratings in nanoparticle doped material with those of gratings in the undoped material.

The photopolymer composition that was used for recording purposes is the same as described in section 6.4. 30 μm thick photopolymer layers were prepared and gratings were recorded at a spatial frequency of 4200 lines/mm with an intensity of 4.5 mW/cm^2 using a He-Ne laser of wavelength 633 nm. The reason for using higher intensity of 4.5 mW/cm^2 (than 3 mW/cm^2 -section 6.4.1) was, firstly, to see if there is any improvement in the diffraction efficiency of the material at this intensity and secondly to check for redistribution of nanoparticles from the bright regions to the dark regions at higher intensities. The diffraction efficiencies of the recorded gratings were plotted against time of exposure, as shown in figure 6.11. Here 0 % represents the undoped photopolymer composition.

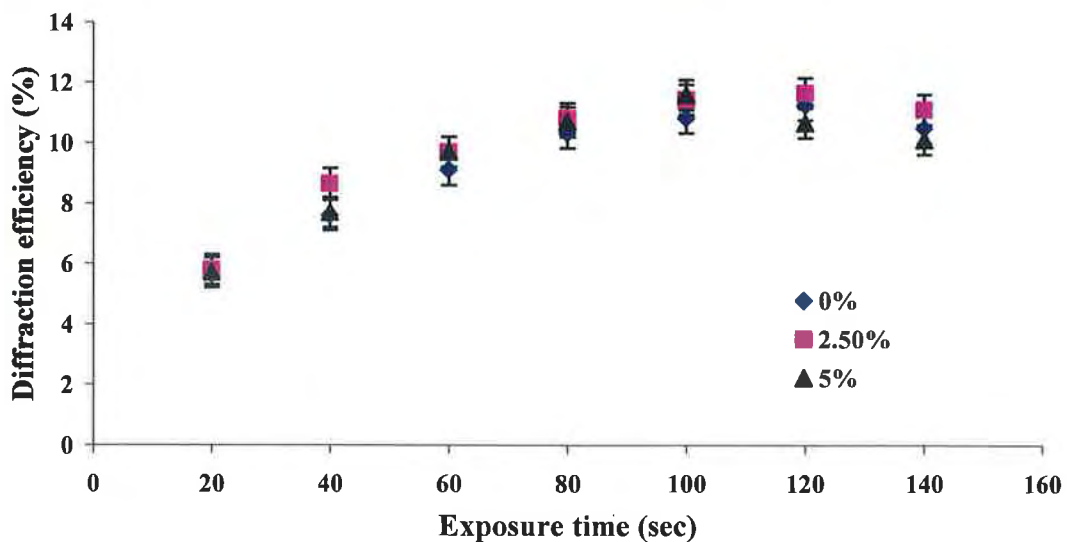


Figure 6.11 Diffraction efficiency (%) of reflection gratings (4200 lines/mm, $\lambda=633\text{nm}$) as a function of exposure time (sec) recorded in layers of thickness 30 μm at an intensity of 4.5 mW/cm^2 .

In figure 6.11 comparison of the diffraction efficiency of the gratings recorded in layers with three nanoparticle concentrations (0 %, 2.5 % and 5 %) are shown. The diffraction efficiency growth of the recorded gratings with respect to the time of exposure is same for all three concentrations. The maximum diffraction that was obtained was 11 % at 100 sec exposure time.

Experiments were carried out to measure the diffraction efficiencies of gratings recorded at 532 nm and 473 nm with a spatial frequency of 5000 lines/mm and 5700 lines/mm respectively. The diffraction efficiencies plotted against exposure time are shown in figures 6.12 (for 532 nm) and 6.13 (for 473 nm)

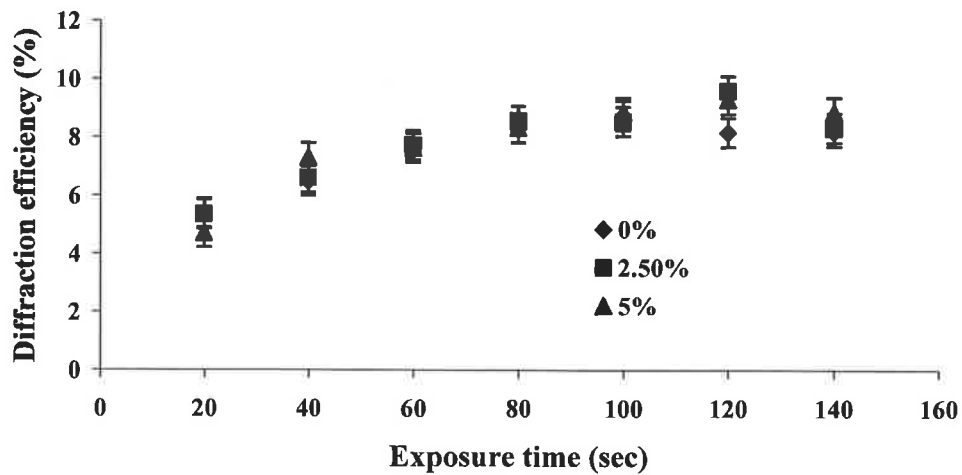


Figure 6.12 Diffraction efficiencies (%) of reflection gratings (5000 lines/mm, $\lambda=532\text{nm}$) as a function of exposure time (sec) recorded in layers of thickness $30\ \mu\text{m}$ at an intensity of $4.5\ \text{mW/cm}^2$.

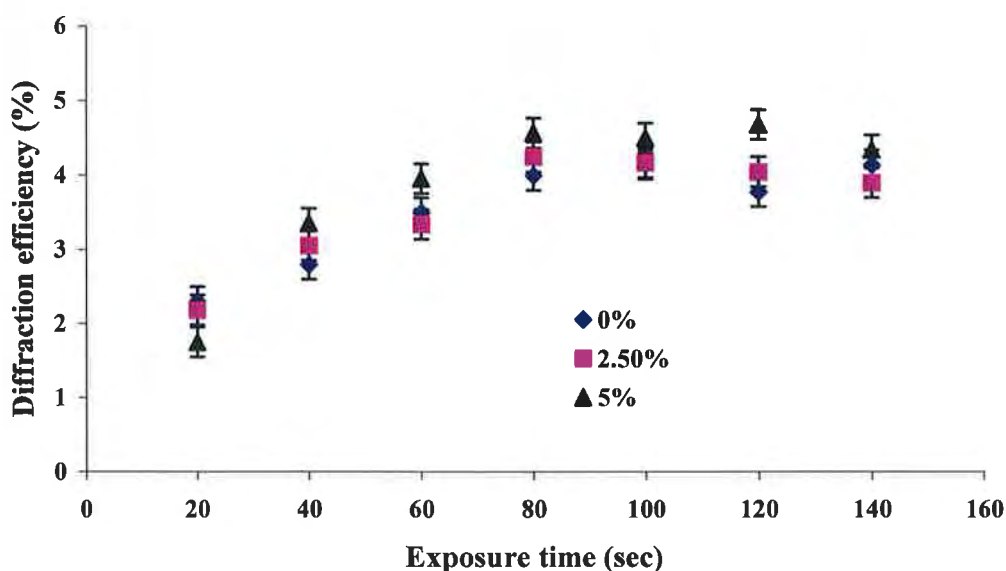


Figure 6.13 Diffraction efficiency (%) of reflection gratings (5700 lines/mm, $\lambda=473$ nm) as a function of exposure time (sec) recorded in layers of thickness $30 \mu\text{m}$ at an intensity of 7.5 mW/cm^2 .

In the undoped photopolymer composition the diffraction efficiency reaches a maximum of 9 %. In doped photopolymer compositions with nanoparticle concentrations of 2.5 % and 5 %, the maximum diffraction efficiency was similar and there is not much difference due to the doping of nanoparticle. Similarly, in the case of gratings recorded at 473 nm with an intensity of 7.5 mW/cm^2 , the maximum diffraction efficiency obtained for undoped photopolymer composition was 4.5%, while in the case of 2.5% and 5% nanoparticle concentrations the efficiency of the gratings increased with time of exposure, reached to a maximum of 4.5% and then saturated. It was observed that nanoparticle doped photopolymer showed no improvement in the grating efficiency in comparison to the undoped photopolymer composition.

6.6 Spectral characterisation

This section deals with the spectral characterisation of the reflection gratings recorded in the panchromatic photopolymer composition. The gratings were also recorded in the photopolymer compositions with nanoparticle concentrations of 2.5% and 5%. The photopolymer composition doped with 7.5% nanoparticle concentration was not used, because as can be seen from sections 4.6 and 5.6, the percentage of swelling and shrinking is within the error range of the preceding value of 5 %. The experimental setup for measuring the spectral response of the diffracted light to determine the Bragg peak wavelength and the methodology is explained in section 4.6. Spectral characterisation of the reflection gratings were recorded at individual primary wavelengths and also with combined RGB laser beam in the panchromatic acrylamide based photopolymer.

6.6.1 Spectral characterization of reflection gratings recorded at 633 nm

Figure 6.14 shows the spectral response curve for the reflection grating recorded in an undoped panchromatic photopolymer composition. From the graph, it can be observed that the peak of the Bragg wavelength selectivity curve for the grating recorded at 633 nm shift from 633 nm to 644.6 nm which shows a swelling of 1.83 %. To control the wavelength shift due to the swelling of the material, the photopolymer was doped with nanoparticles with 2.5 % and 5 % concentrations and the corresponding peaks of the Bragg wavelength selectivity curves were compared with those obtained from gratings recorded in the undoped photopolymer composition. Figure 6.15 shows the wavelength of the peak of the Bragg selectivity curve plotted with respect to the nanoparticle concentration. It can be seen that by doping the photopolymer with 5 %

nanoparticles, the shift in the wavelength of the peak of the Bragg selectivity curve lowered from 644.6 nm to 636 nm.

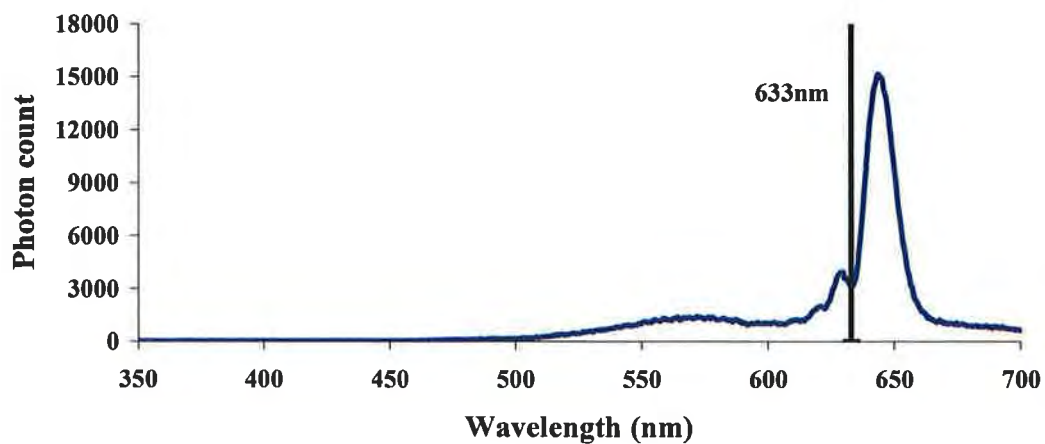


Figure 6.14 Bragg spectral selectivity curve of the reflection grating recorded at 633nm in panchromatic photopolymer.

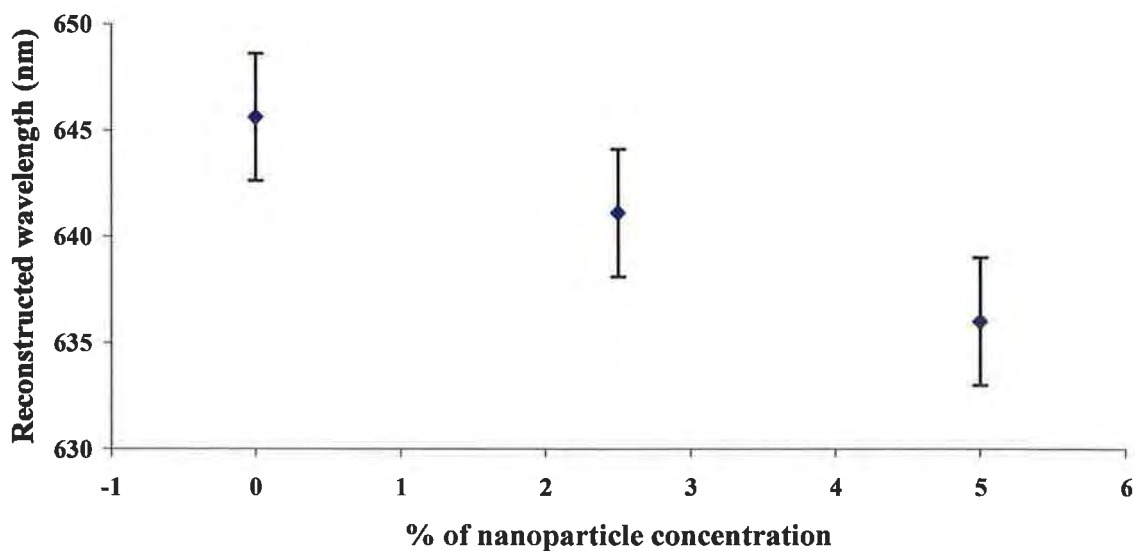


Figure 6.15 Peak wavelength of the Bragg spectral selectivity curve for the gratings recorded at 633nm plotted against nanoparticle concentration in the photopolymer.

6.8.2 Spectral characterization of reflection gratings recorded at 532nm

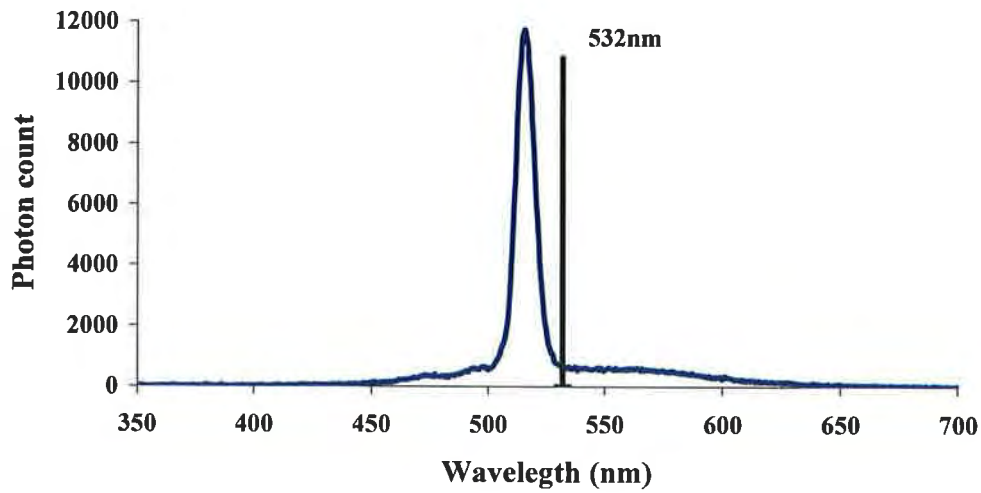


Figure 6.16 Bragg spectral selectivity curve of a reflection grating recorded at 532nm in panchromatic photopolymer.

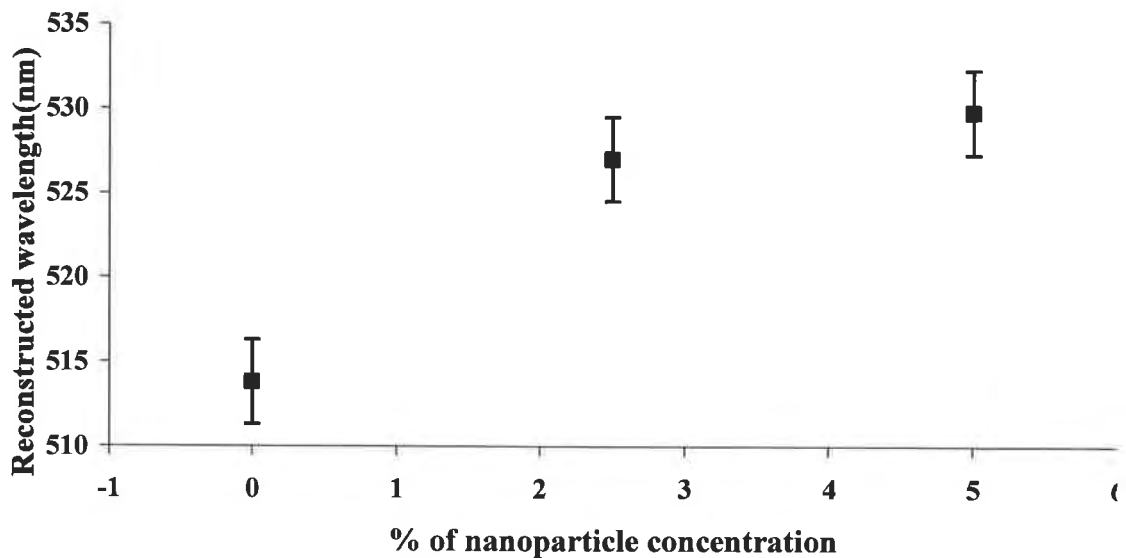


Figure 6.17 Peak wavelength of Bragg spectral selectivity curves of gratings recorded at 532 nm as a function of nanoparticle concentration in the photopolymer.

The Bragg spectral selectivity curve of a grating recorded at 532 nm is shown in figure 6.16. The peak is at 515.7 nm, which shows shrinkage of 3.2%. Wavelengths corresponding to the peaks of the Bragg spectral selectivity curves of the photopolymer doped with nanoparticles are shown in figure 6.17. The peaks of the

Bragg spectral selectivity curves of the recorded gratings were shifted from 515.7 nm to 529 nm when doped with 5 % nanoparticle concentrations. This corresponds to a reduction in shrinkage to 0.5%.

6.8.3 Spectral characterization of reflection gratings recorded at 473nm

Figure 6.18 shows the Bragg spectral selectivity curve of a grating recorded at 473 nm of undoped panchromatic photopolymer. The peak of the Bragg selectivity curve shifts to 464.8nm from 473nm indicating a shrinkage of 1.7 %. As shown in Figure 6.19, doping with 5% nanoparticle concentration results in the reduction of shrinkage to 0.52%.

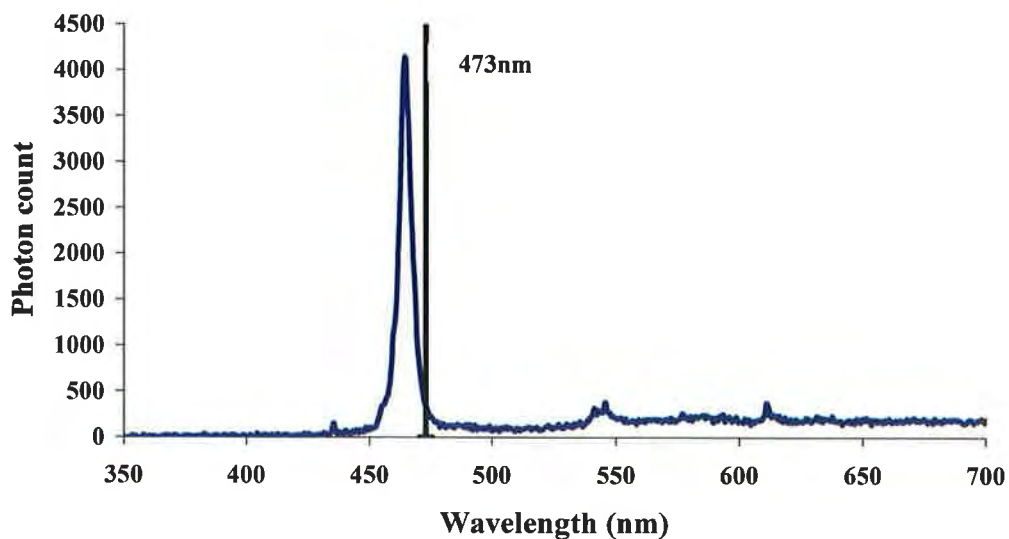


Figure 6.18 Spectral response curve of the reflection grating recorded at 473nm in panchromatic photopolymer.

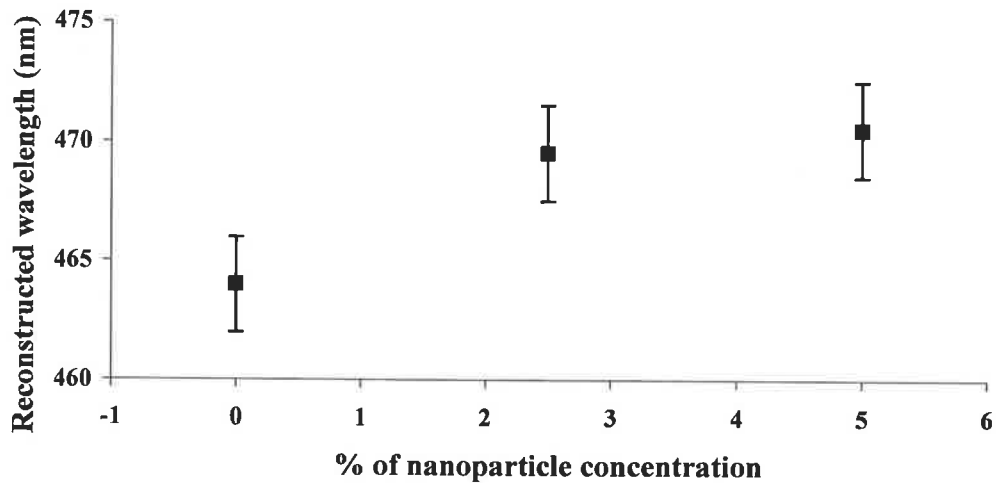


Figure 6.19 Reconstructed wavelengths of gratings recorded at 473nm as a function of nanoparticle concentration in the photopolymer.

6.8.4 Spectral characterization of multicolour reflection gratings

The spectral characterisation of three wavelength multiplexed holographic gratings recorded in an undoped panchromatic photopolymer (0%) using combined RGB beams is shown in figure 6.20. The peaks of the Bragg spectral selectivity curve of the grating are at 469.5nm, 528.7nm and 628.6nm which are shifted towards the lower wavelength region. The corresponding shrinkage for individual wavelengths is 0.74 %, 0.62 % and 0.69 % respectively.

Doping the photopolymer with 2.5 % and 5 % nanoparticle concentrations made negligible difference in the wavelength of the peak of the Bragg spectral selectivity curve. The Bragg spectral selectivity curves for the gratings recorded in both undoped and nanoparticle doped panchromatic photopolymer composition are shown in figure 6.20.

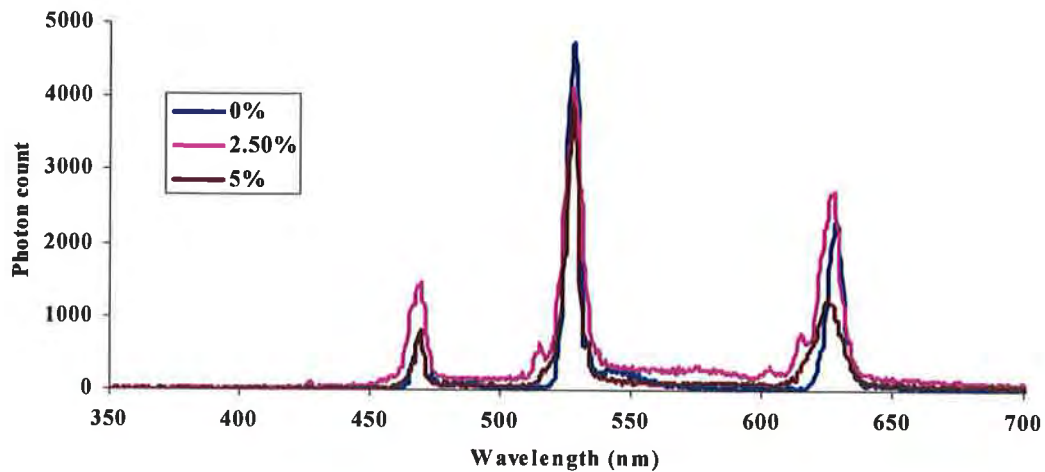


Figure 6.20 Bragg spectral selectivity curves of a reflection grating recorded using combined RGB beams in undoped and 2.5% and 5% nanoparticle doped panchromatic photopolymer composition.

From the figure 6.20 it can be clearly seen that the doping of nanoparticles did not result in the improvements in the positions of the peaks of the Bragg spectral selectivity curves for the gratings recorded on the panchromatic photopolymer composition. Therefore multicolour holograms were recorded using the undoped photopolymer composition as explained in the next section.

6.7 Transmission holograms

Transmission holograms were recorded in the acrylamide based panchromatic photopolymer by illuminating with the three laser beams simultaneously. The experimental setup is shown in Figure 6.21.

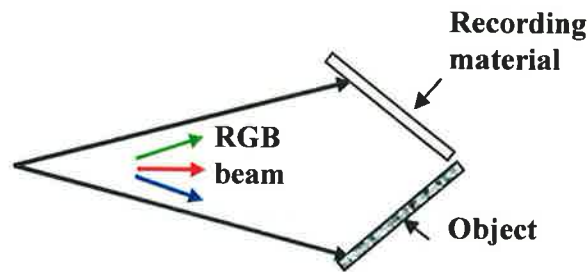


Figure 6.21 Optical setup for recording transmission hologram

A euro 10 cent coin was selected as the object. The combined RGB beam was spatially filtered and expanded to illuminate both the recording material and the object. Interference fringes are formed in the photopolymer layer by the light reflected from the object and light which directly illuminates the photopolymer layer to record a transmission hologram as the two beams illuminate the photopolymer layer from the same side. The recording intensities were 6 mW/cm^2 for 473 nm wavelength and 3 mW/cm^2 for 633 nm and 532 nm wavelengths. The thickness of photopolymer layer was $60 \pm 5 \text{ }\mu\text{m}$. A photograph of the reconstructed image from the transmission hologram, when illuminated with the combined RGB beam is shown in Figure 6.22.

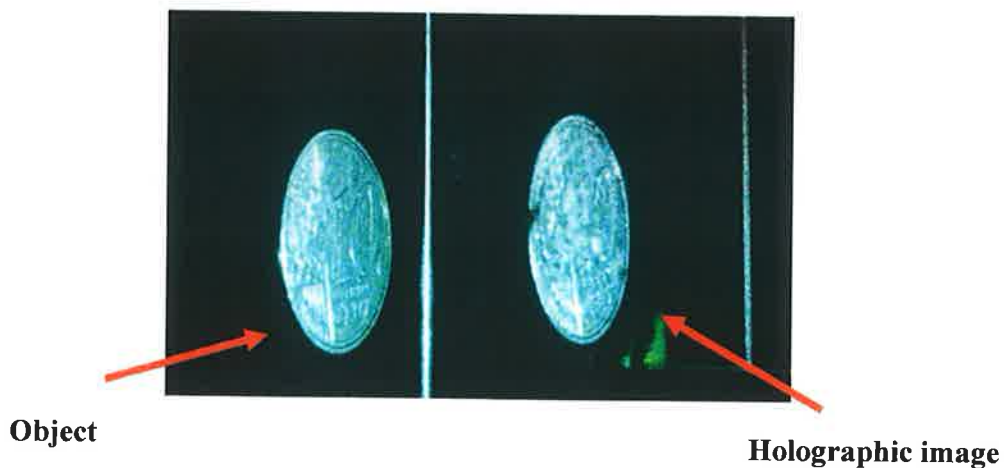


Figure 6.22 Photographic image of holographic reconstruction from the colour transmission hologram in comparison with object

6.8 Reflection holograms

Reflection holograms of a 10 cent coin were recorded at 633nm, 473nm, and 532nm wavelengths at separate locations on the same 30 μ m thick photopolymer layer using Denisyuk single beam geometry. The reconstructed images are shown in Figure 6.23



Figure 6.23 Photograph of white light holographic reconstructions from holograms recorded at the three primary wavelengths. The object used was a 10 euro cent coin.

Further to prove that the material is suitable for full colour holographic display application, more holograms were recorded using Denisyuk recording geometry. For this purpose, the objects were made by taking a print of a coloured object on a transparency and sticking them on a mirror surface. Photopolymer layer of 30 μ m thickness was illuminated with the combined RGB beams for an exposure time of 80 sec. Photographs of the images reconstructed from the reflection holograms when illuminated with a white light source are shown in Figures 6.24b and 6.25.

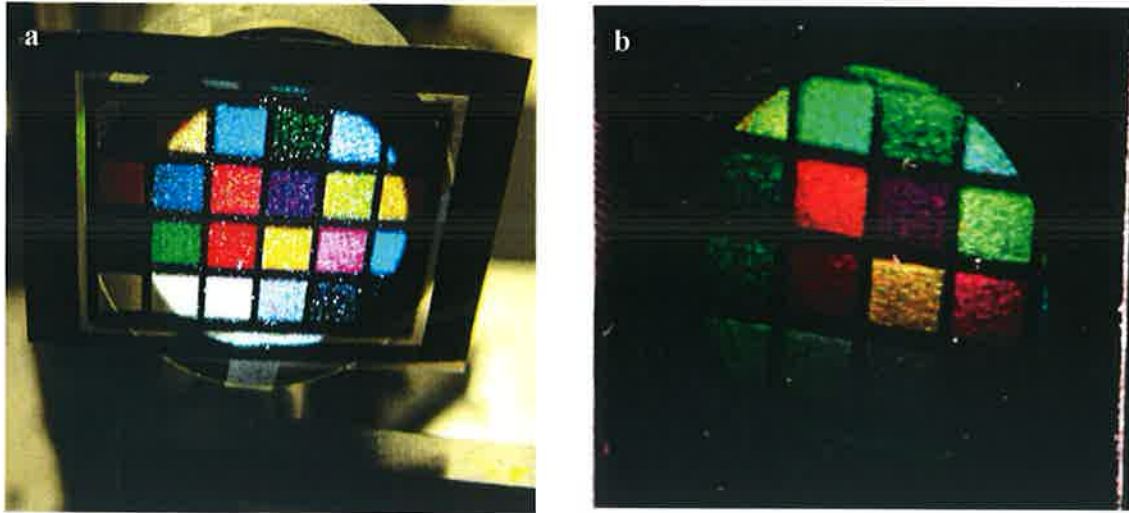


Figure 6.24 Photograph of (a) object and (b) reconstructed holographic image.

Figure 6.24(a) is a photograph of the object that was illuminated by the RGB combined white light beam. It can be seen from the photograph that the colour balance is appropriate with respect to the human eye, which in turn indicates that the combined RGB beam incident on the object, is balanced resulting in white light. The colour balance in the RGB incident beam plays a very important role in producing the reconstructed light with wavelengths nearest to the recording wavelengths. Figure 6.24 (b) shows the photograph of the reconstructed image when the hologram is illuminated with an incandescent spot lamp. A number of colour holograms were recorded with different colour objects using the same geometry. The photographs of the holographic reconstruction when illuminated with an incandescent spot lamp are shown in Figure 6.25. Photographs of the original objects are shown for comparison on the right side corners in Figure 6.25 (a), (b), (c) and (d). In the reconstructed images it can be observed the green colour domination. This might be due to high sensitivity material at green wavelength in comparison with other wavelength region.

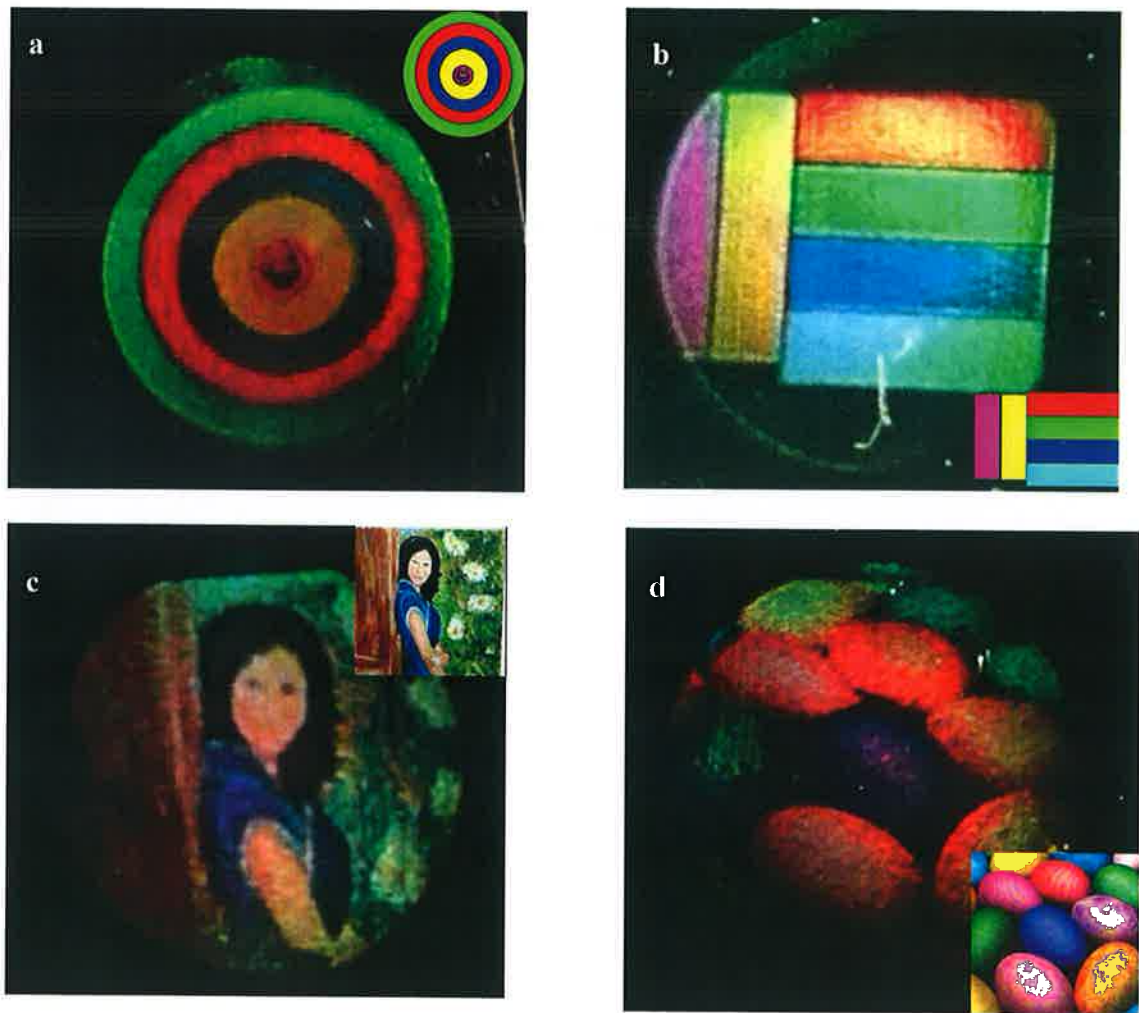


Figure 6.25 shows photographs of the images reconstructed from the holograms with the objects shown in the insets.

6.9 Conclusion

A self processing acrylamide based photopolymer has been sensitised at three primary wavelengths and an optical system for recording full colour holograms by combining the three selected primary wavelength laser beams has been set up. Reflection holographic gratings were recorded individually at each recording wavelength and the corresponding diffraction efficiencies were measured. The influence of Si- MFI Zeolite nano-particles on the diffraction efficiency of the recorded reflection gratings and on the dimensional changes (shrinkage and swelling) was studied. Although the

doping produced no improvement in the diffraction efficiency of both the single and multicolour reflection gratings, there was a control over the dimensional changes in the reflection gratings recorded using single wavelength, at the same time there was no control over the dimensional changes in the multicolour reflection gratings. Beyond doubt, all the experiments have ultimately led to successful development of panchromatic photopolymer composition.

Full colour transmission and reflection holograms were successfully recorded in the panchromatic acrylamide based photopolymer developed in IEO Centre. In Figure 6.23 one can observe the blue colour to be weak. This is due to the low diffraction efficiency of the material in this wavelength region (Figure 6.9 and 6.10). The reason for the low diffraction efficiency could be due to high spatial frequency at the blue recording wavelength and strong absorption of the blue light during the recording. By optimisation of the material composition (monomers, co initiator and binder) and dye concentrations, the diffraction efficiency can be improved.

Figure 6.24(b) and 6.25 show the reconstructed images of holograms recorded with the combined RGB beam (which was colour balanced with respect to the visual eye). These holograms are dominated by green colour, which suggests that by decreasing the intensity of green wavelength with respect to the other two wavelengths (red and blue) one can achieve, better colour balanced holograms. Additionally the material shrinkage (see figure 6.20) affects the colour rendering of the hologram.

CHAPTER 7

CONCLUSION

The main objective of this work was to develop a self-processing photopolymer suitable for full colour reflection holography.

To meet this objective the following steps were necessary.

- Determine the transmission and reflection holographic characteristics of various formulations of photopolymer at 633 nm and 473 nm.
- Sensitize self processing acrylamide based photopolymer at all three primary wavelengths to record reflection holographic gratings.
- Record full colour transmission and reflection holograms.

Self processing acrylamide based photopolymer was already sensitized at 633 nm using methylene blue photosensitive dye. So, firstly as explained in Chapter 4, this photopolymer composition was successfully used to record transmission gratings at 633 nm. The diffraction efficiencies obtained for the gratings recorded at spatial frequencies 1000 lines/mm and 2000 lines/mm were 65 % and 70 % respectively for a recording intensity of 4 mW/cm² for a 30 μm thickness photopolymer layer (section 4.3). Secondly, the same photopolymer and dye combination was used to record reflection holographic gratings at the same wavelength. The diffraction efficiencies for the reflection gratings recorded at 4200 lines/mm spatial frequency were 9.8 % and 6.5 % at intensities of 3 mW/cm² and 1.5 mW/cm² respectively for a 60 μm thick layer, while for a thickness of 30 μm, 8.6 % and 5.7 % efficiencies were achieved at intensities of 3 mW/cm² and 1.5 mW/cm² respectively (section 4.4). With the aim of

improving the diffraction efficiencies of the reflection gratings, the photopolymer was doped with Si-MFI zeolite nanoparticles. Although the diffraction efficiency of the reflection gratings was only slightly improved (section 4.5), spectral characterization studies showed a reduced swelling of the photopolymer material from 1.88 % to 0.6 % which means that this material is more suitable for reflection holography where reconstruction at the original recording wavelength is essential (section 4.6). Reflection holograms were recorded successfully at 633 nm (section 4.7)

The acrylamide based photopolymer was sensitised at 473 nm using acriflavine dye and both transmission and reflection gratings were recorded. Diffraction efficiency of 100 % was obtained for the transmission gratings (2000 lines/mm) in 60 μm thick layers with exposure energy of 100 mJ/cm^2 (section 5.2). Therefore, the same photopolymer composition was also used to record reflection holographic gratings (5700 lines/mm) at 473 nm wavelength (section 5.3). The diffraction efficiency of the reflection holographic gratings recorded in a 30 μm thick layer using a recording intensity of 6 mW/cm^2 was 1.7 %. The diffraction efficiency was improved from 1.7 % to 3 % by varying the dye concentration in the photopolymer composition (section 5.4). Doping the photopolymer composition with Si-MFI zeolite nanoparticles did not result in significant increase in the diffraction efficiency of the reflection holographic gratings. From the spectral characterisation studies, it was shown that the shrinkage of 1.9 % was reduced to 0.4 % by doping the photopolymer with 7.5 % by weight of 1.8 % w/v water dispersed nanoparticle solution (section 5.5).

The photopolymer was sensitised at all three primary wavelengths with three photosensitive dyes (methylene blue, erythrosine B and acriflavine). Reflection holographic gratings were recorded individually at each wavelength and the corresponding diffraction efficiencies were measured (section 6.4). The maximum diffraction efficiency of 12 % and 9.8 % was obtained in 60 μm thick layers, while 6.7 % and 4 % efficiencies were obtained in 30 μm thick layers at 633 nm at intensities 1.5 mW/cm^2 and 3 mW/cm^2 respectively. Maximum diffraction efficiencies of 7.5 % and 5 % were obtained for intensities of 1.5 mW/cm^2 and 3 mW/cm^2 respectively in 30 μm thick layer, while in the case of a 60 μm thick layer a maximum diffraction efficiency of 8 % was achieved with both intensities at 532 nm. A maximum diffraction efficiency of 4 % and 3.2 % was achieved for the gratings recorded in a 30 μm thick photopolymer layer for intensities 3 mW/cm^2 and 6 mW/cm^2 respectively, while the maximum efficiencies of 4.5 % and 2.6 % were obtained at these intensities respectively for a 60 μm thick photopolymer layer at 473 nm wavelength. In the same way as for the monochromatically sensitive materials, in order to improve the diffraction efficiency of the reflection holographic gratings, the photopolymer was doped with Si-MFI zeolite nanoparticles. Spectral characterisation of the reflection gratings (multiplexed reflection gratings) recorded by using the combined RGB beams simultaneously was carried out. The peak of the Bragg selectivity curves of these gratings recorded at 473 nm, 532 nm and 633 nm were at 469.5 nm, 528.7 nm and 628.6 nm respectively (section 6.6). For the panchromatic system, the doping process showed no improvement in the diffraction efficiency (section 6.5) and also no control over the dimensional changes in the multicolour reflection gratings. For this reason, full colour reflection and the

transmission holograms were recorded in a photopolymer without nanoparticle dopants.

Finally, it was demonstrated that acrylamide based photopolymer can be sensitised at three primary wavelengths and full colour reflection holograms can be recorded successfully.

In the above experiments, depending upon the recording intensity and the layer thickness, 100% diffraction efficiency was achieved in the transmission holographic gratings, while in reflection holographic gratings it was limited. This could be due to the two way diffusion of the material which in turn decreases the refractive index modulation at high spatial frequency (Ref. Page-67). The material was doped with nanoparticles to control the dimensional changes and also to improve the diffraction efficiency. However there was no improvement in the diffraction efficiency in this case. The reason might be due to the aggregation of nanoparticles and the availability of low intensity laser beams (for recording). Naydenova et al., [Chapter -4, Ref-8] explains the possibility of improving the refractive index modulation at high recording intensity for the nanoparticle doped material, as the higher intensity improves the nanoparticles diffusion.

For future studies the photopolymer material can be further investigated for high quality display hologram recording. The performance of the recording material could be improved by varying the concentrations of monomers, co-initiator and by using different binders. This should be done systematically by monitoring the grating

growth during recording at each wavelength and at different spatial frequencies and using different compositions of the photopolymer recording material.

Given its sensitivity at all three primary wavelengths, the material can also be used for wavelength multiplexed holographic data storage. Moreover, this panchromatic material can also be used for the display applications including art holograms as well as for application in security and authentication.

Publications and Presentations

Journal and Conference papers

1. C.Meka, R.Jallapuram, S.Martin, I.Naydenova, V.Toal, "Development of panchromatic acrylamide based photopolymer for multicolour reflection holography" Applied Optics Vol. 49, Issue 8, pp. 1400-1405 , 2010.
2. M.Chakrapani, J.Raghavendra, S.Martin, I.Naydenova, V.Toal, "Acrylamide based photopolymer for multicolour holographic recording" 8th International Symoisum on Display Holography, 2009.
3. V. Sainov, E. Stoykova, B. Ivanov, M.Chakrapani, V.Toal, T.Petrova, "Exposure and spectral characteristics of bulgarian silver-halide materials for multicolor holographic recording" 8th International Symoisum on Display Holography, 2009.

Oral Presentation

1. M.Chakrapani, J.Raghavendra, S. Martin, I.Naydenova, V. Toal, "Acrylamide based photopolymer for multicolour holographic recording" 8th International Symoisum on Display Holography, 2009.
2. V.Sainov, E.Stoykova, B.Ivanov, M.Chakrapani, V.Toal, T.Petrova, "Exposure and spectral characteristics of bulgarian silver-halide materials for multicolor holographic recording" 8th International Symoisum on Display Holography, 2009.

Poster Presentation

1. M.Chakrapani, J.Raghavendra, S.Martin, V.Toal, "Colour holography in an acrylamide based photopolymer" Photonics North-West 2008, 8th May 2008, Manchester, United Kingdom.
2. M.Chakrapani, J.Raghavendra, S.Martin, V.Toal, "A step towards full colour holography in an acrylamide based photopolymer", Photonics Ireland 2007 conference, 24th to 26th September 2007 at Galway Bay Hotel, Galway.
3. M.Chakrapani, J.Raghavendra, S.Martin, V.Toal, "Two colour reflection holograms in an acrylamide based photopolymer", IOP spring weekend meeting, 30th March to 1st April 2007 in the County Arms Hotel, Birr, Co. Offaly.

